Ph.D. DISSERTATION

An Investigation for Strain–Response in Inkjet–Printed Ag Thin Films and Their Uses for Stretchable Applications

잉크젯 프린팅 공정 기반 은 박막 필름의 인장에 따른 특성 분석과 스트레쳐블 응용

February 2020

DEPARTMENT OF ELECTRICAL ENGINEERING
AND COMPUTER SCIENCE
COLLEGE OF ENGINEERING
SEOUL NATIONAL UNIVERSITY

SEONGDAE CHOI

An Investigation for Strain-Response in Inkjet-Printed Ag Thin Films and Their Uses for Stretchable Applications

잉크젯 프린팅 공정 기반 은 박막 필름의 인장에 따른 특성 분석과 스트레쳐블 응용

지도 교수 홍 용 택

이 논문을 공학박사 학위논문으로 제출함
2020 년 2 월

서울대학교 대학원
전기 · 컴퓨터 공학부
최 성 대

최성대의 공학박사 학위논문을 인준함
2020 년 2 월

위 원 장	정 윤 찬	(인)
부위원장	홍 용 택	(인)
위 원	이 수 연	(인)
위 원	김 도 환	(인)
위 원	Steve Park	(인)

Abstract

An Investigation for Strain-response in Inkjet-printed Ag Thin Films and their Uses for Stretchable Applications

SEONGDAE CHOI

DEPARTMENT OF ELECTRICAL ENGINEERING AND COMPUTER SCIENCE

COLLEGE OF ENGINEERING

SEOUL NATIONAL UNIVERSITY

As the recently developed electronic devices have been mostly aimed to the wellness and comfort for human-being, many researches have been devoted to flexible or stretchable devices that offer higher efficiency of human-machine interactions. The flexibility of the device has enabled high compatibility with human body, which gave rise to the developments of wearable, patchable, and implantable devices. For the wearable devices to be capable of detecting human motions or examining disease, skin-like sensors with high performance are needed to precisely sense the minute vital signs or high-level elongation of human body. Meanwhile, the advanced technologies on flexible and stretchable devices have brought many

opportunities for the users to more conveniently interact with electronic devices than conventional user interface method. Accordingly, the foldable smartphone has already been commercialized to the users, which offers unprecedented way of manipulating devices by enlarging display screen. Sooner or later, stretchable device including stretchable display will be introduced to create much more opportunities in various user interfaces. In addition, although the most commercialized devices are still rigid, some technologies such as force touch sensor have already been embodied in the devices, utilizing the advantages of flexible display beyond the current way of operating transparent touch screen panel on the screen. Thus, in flexible and stretchable electronic devices, it is important to measure the extent of small flexibility of rigid display screen and stretchability of the device for the feedback functionality of user interface operation.

For the aforementioned applications that are related to the interactions between users and devices, flexible strain sensor has been a candidate due to its high sensitivity and stretchability. For that, there has been a lot of research about conductive films that can be utilized for strain sensors in stretchable electronics. Among the various transducers for detecting stretchability, resistive strain sensor has the merit of facile fabrication and high sensitivity. The conductive materials with stretchable substrate form complex percolated conductive networks which are connected and disconnected by stretching and releasing the composite to determine electrical conductivity change. To obtain high strain-sensitivity of the sensor, crack-generated phenomenon on conductive thin films has widely been reported.

In this Ph. D. dissertation, I fabricated crack-generated metal nano particles based thin films for strain sensing device by inkjet-printing metal ink onto the elastomeric substrate in the application to the low-cost and facile future flexible and

stretchable electronics. The intrinsically brittle nature of metal nano particle causes the cracks on the film to be easily propagated and the electrical resistance abruptly increased under tensile strain. Taking advantage of the stretchable characteristic, some morphological strategies such as inkjet-printed vertical patterns were utilized to obtain further increased sensitivity of the strain sensor to measure slight stimuli (< 1% strain) of the device or human body. On the contrary, As the metal thin film is too vulnerable to external strain, instability of the film causes exponential increase in resistance and entire rupture of channel even at small strain loading. Therefore, other strategies such as wrinkle structure were needed for the film to be utilized as a strain sensor that is capable of working under wide range of strain. From the combination of wrinkle structure and thickness-gradient metal film, both sensitivity and durability of the strain sensor could be obtained. Furthermore, by asymmetrically pre-stretching the substrate, 2 dimensional strains were selectively detected by the strain sensor without interferences. The primary purpose of this dissertation is to investigate the intrinsic strain-response and micro-structural changes of the metal thin film, and apply morphological strategies on the film to enhance stretchable properties according to the applications. Moreover, I expect this easy and low-cost fabricating procedures will have an impact on the commercialization of the large-area stretchable electronics.

Keyword : Stretchable electronics, Wearable device, User interface , Inkjet-printing process, Crack-generated strain sensor, Morphological strategies

Student Number : 2013-23143

Contents

Chapter 1

Introduction

1.1. Stretchable electronics

Stretchable electronics [1-6] covers all the electronic devices or circuits that are embedded or deposited on the soft and stretchable substrate. The soft platform for electronic device has enabled countless applications regarding stretchable electronics, as surrounding environments in real life are mostly comprised with curvilinear surfaces including human skin. [7-10] Although many efforts on stretchable electronics have been devoted to maintaining electrical and mechanical properties of the electronic devices under high mechanical strain, [11-13] I need to focus on the additional applications that I can investigate such as wearable devices [14-22] and advanced user interface technology [20, 23-25]. Contrary to the conventional one-sided interaction between electronic device and human, close relationship has been made between human and machine as more intuitive and direct interface became possible. Thus, to more efficiently realize the human-to-machine or machine-to-human interactions in stretchable electronics, sensing system that can transduce mechanical stimulation into electrical value is needed for the feedback functionality.

1.1.1. Wearable electronics

Recently, a lot of research about wearable electronic device has been investigated to satisfy the needs of human being such as wellness, safety, rehabilitation, and predicting/managing diseases. To realize them, all the developments regarding wearable devices are aimed to several areas: health-monitoring, human-machine interaction, human motion detection, and electronic skin for prosthesis. Previously, the conventional wearable devices were electrograms such as electrocardiography (ECG), electromyography (EMG), and electroencephalography (EEG), which measures vital signals from the heart, muscles, and brain. However, use of the devices was limited due to their bulky and rigid structure. With the rise of flexible and stretchable electronics, conformable and skin-mountable wearable devices could be developed to more directly and exactly detect the signals from human body in daily life. For the wearable devices to precisely detect the state of human body, sensors that transduce mechanical deformations into electrical signals are needed. If the mechanical deformations on human body from arterial pulse to joint flexion are transformed to the degree of strain, the elongation ranges from very small value (< 1%) to fairly large strain (~50 %). Thus, the development of the sensor with excellent properties and flexibility is imperative in wearable electronics. Thus, among the various transducers such as pressure, strain, and temperature sensors, flexible strain sensor is the most promising candidate due to its high sensitivity and stretchability.

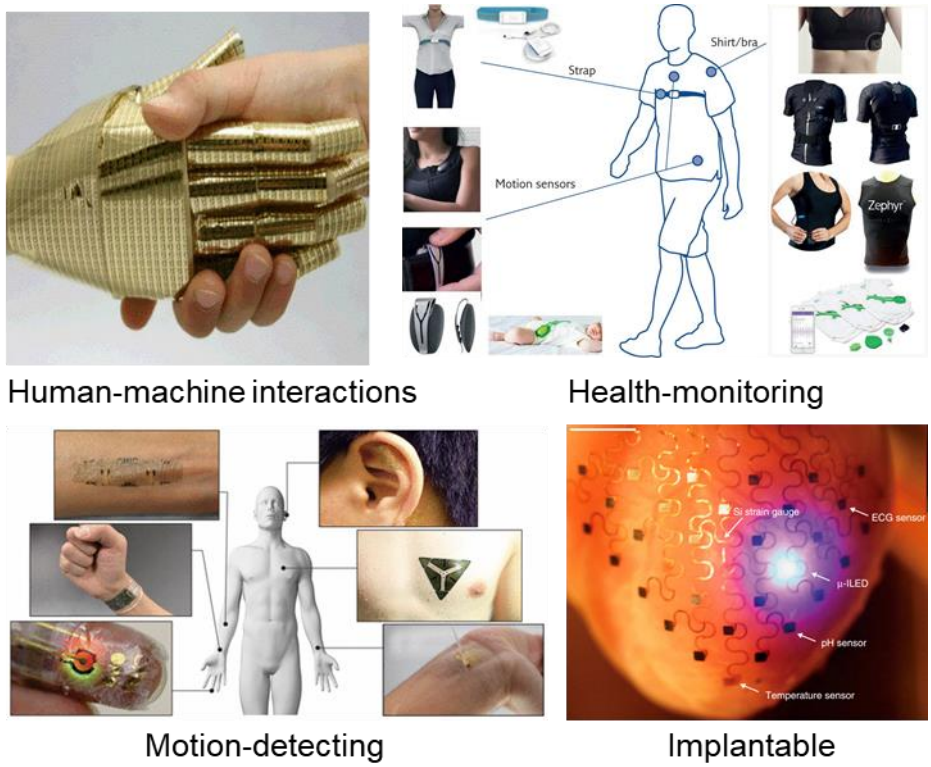

Figure 1.1. Applications of wearable electronics [26-29]

1.1.2. User interface technology

Nowadays, the foldable smartphone has already been commercialized, and the dimensionally switchable device let the users easily carry the device and watch the screen with enlarged screen, simultaneously. In other words, the rise of soft (flexible, rollable, and stretchable) electronics has suggested an inexperienced way of manipulating electronic devices including foldable smartphone. [14, 20, 23-25] Conventional electronic devices include some type of user input device, including, for example, buttons, slides, scroll wheels, and similar devices or user-input elements. However, as the flexible display has been developed and implemented on the device, some devices may include a touch sensor that is integrated or incorporated with a display screen to measure the flexure of display screen to provide non-binary touch input. The touch sensor may allow a user to interact directly with user-interface elements that are presented on the display screen, in contrast to some traditional touch sensors that may only provide a location of a touch on the device. To efficiently realize force touch user interface, it is imperative to accurately measure the force of a touch that is applied to the surface. For that, a lot of force sensing mechanisms such as capacitive, resistive, strain gauge, and ultrasound type/Frustrated total internal reflection (FTIR) have been introduced. (Figure 1.2) Among them capacitive pressure sensor was primitively embedded in the smartphone device by measuring the changed capacitance from the distance change between two electrodes, but the for sensor based on the capacitance principle requires a two-layer design. On the contrary, strain gauge is also widely used in industrial applications, as it only requires a single-layer pattern and shows high sensitivity under applied force.

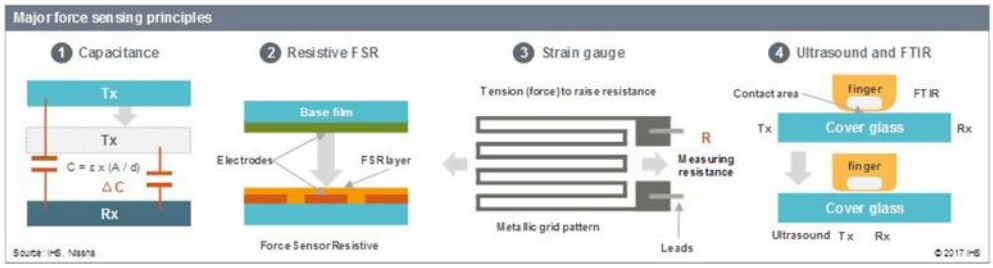

Figure 1.2. Various types of force sensing principles

Figure 1.3. Advanced user interface technology

Thus, if I simulate the strategy that have been used in force sensing technology of industrial applications (Figure 1.3), development of flexible strain sensing device with great sensitivity can be a key to future user interface electronics.

Likewise, stretchable display is expected to be actualized in some days, as many efforts are being aimed to protecting brittle and rigid devices and circuits from mechanical deformations or creating intrinsically stretchable devices and circuits. In stretchable electronics, I insist that it should not be limited to the benefits from the widened screen. Thus, more creative methods to interact with the devices might be implemented according to the expansion of the device. Moreover, there have been a few researches to complement the inevitable decrease in pixel resolution of stretchable display by elongated platform by selectively operating hidden pixels at certain degree of applied strain. (Figure 1.4) For those, measuring multi-dimensional and large strain is primary issue that I need solve, so the flexible strain sensors with excellent dimensional feasibility are expected to play a critical role in user interface of future stretchable electronics.

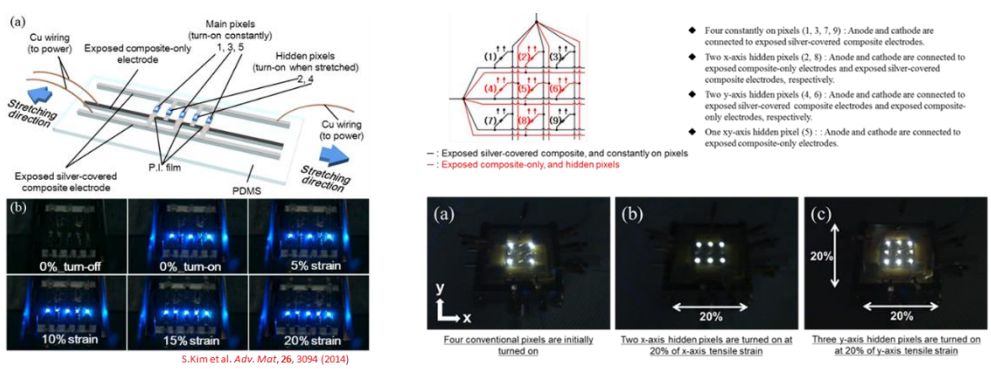

Figure 1.4. Previous strategies to sustain constant image resolution in stretchable electronics

1.2. Stretchable strain sensor

A strain sensor is a device that converts mechanical deformation into output signals based on changes in electrical signals such as resistance and capacitance. Conventional strain sensors are currently used in various applications, however, the brittle and rigid nature of materials present limitations in stretchability and stability. [30-33] On the contrary, recent progress in devices focusing on wearable and stretchable electronics requires flexible and stretchable strain sensor that can function at over 30 % strain. (Figure 1.5) Flexible and stretchable strain sensors could mainly be classified into resistive-type and capacitive-type sensors. Those sensors require relatively simple read-out systems and offer high flexibility and stretchability. Capacitive sensors employ a highly compliant dielectric layer sandwiched between a pair of electrodes, and the change in capacitance is resulted from the distance of electrodes under external strain.[34-36] On the other hand, resistive sensors are typically composed of electrically conductive sensing films combined with flexible substrates. When the composite is stretched, microstructural changes in the sensing films lead to the change of electrical resistance as a function of the applied strain. The choice of suitable materials and methods for fabricating strain sensor is also important to satisfy the requirements of low-cost, scalable, large-area and facile process. Thus, various conductive materials have been proposed with carbon blacks, carbon nanotubes (CNT) [36-38], and graphene, nanowire (NWs) [34, 39], nanoparticles (NPs) [17, 18, 21, 22, 40, 41]. And silicon-based polymers (polydimethylsiloxane (PDMS), Ecoflex, and Dragon skin) have been commonly chosen as flexible substrate materials.

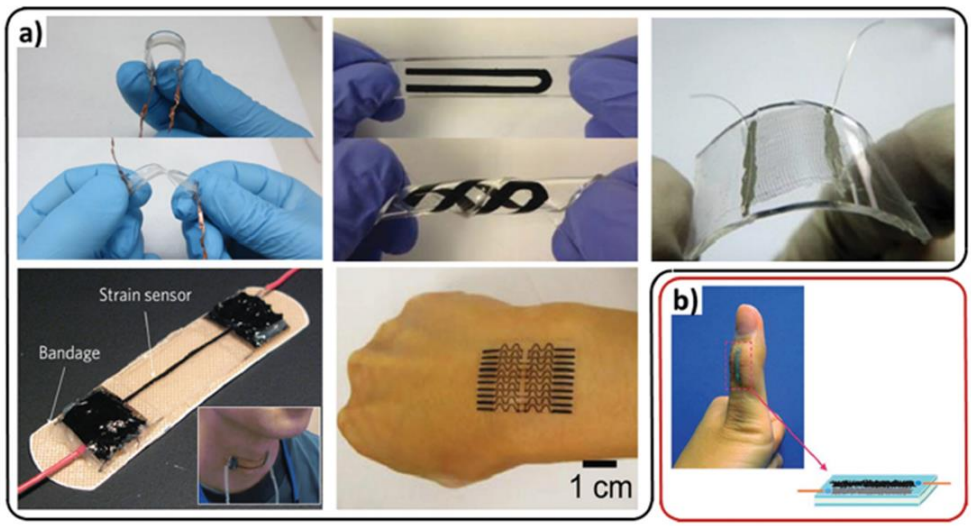

Figure 1.5. Various flexible, skin-mountable, and wearable (a) resistive and (b) capacitive strain sensors made of functional nanomaterials-polymer composites.

Type of sensor	Materials	Stretchability (%)	Gauge factor	Linearity
Resistive	AgNWs–PDMS	70	2–14	Linear up to 40%
Resistive	CNTs–Ecoflex	500	1–2.5	Linear
Resistive	CBs–PDMS	30	29.1	Linear
Resistive	Aligned CNTs–PDMS	280	0.82	Two linear regions
Resistive	ZnONWs–PDMS	50	114	Linear
Capacitive	CNTs–Dragon-skin elastomer	300	0.97	Linear
Resistive	Graphene foam–PDMS	70	15–29	Linear
Resistive	CBs–TPE	80	20	Nonlinear
Resistive	CBs–PDMS	10	1.8–5.5	Two linear regions
Capacitive	CNTs–Ecoflex	150	1	Linear
Resistive	CBs–Ecoflex	400	3.8	Nonlinear
Capacitive	CNTs–silicone elastomer	100	0.99	Linear
Resistive	Graphene–rubber	800	10–35	Nonlinear
Capacitive	AgNWs–Ecoflex	50	0.7	Linear
Resistive	Platinum (Pt)–PDMS	2	2,000	Nonlinear
Resistive	AuNWs–PANI–rubber	149.6	20.4–61.4	Linear
Resistive	AgNWs–PEDOT:PSS/PU[a)]	100	1.07–12.4	Nonlinear
Resistive	AuNWs–latex rubber	350	6.9-9.9	Linear
Resistive	CNTs–PEDOT:PSS/PU	100	8.7–62.3	Nonlinear

Figure 1.6. Summary of performance results of recently reported stretchable strain sensors

From the fabricated composite, the strain-sensing mechanisms the way strain sensors respond to the applied strain are dependent on the types of materials, micro/nano morphological structures, and fabrication process. Strain-response of most conventional strain sensors originates from geometrical effects and intrinsic piezo-resistivity of materials themselves. Unlike traditional strain gauges, mechanisms such as disconnection between sensing elements, crack propagation in thin films, and tunneling effect have been utilized to develop stretchable strain sensors. The resulted properties of strain sensors can be characterized by different performance parameters such as stretchability, sensitivity or gauge factor (GF), linearity, hysteresis, response, and recovery time, overshoot behavior, and stability. (Figure 1.6) These factors are crucial for stretchable and wearable strain sensor characteristics since large, repeated, and frequent strains may be applied to the strain sensors. The optimized strain sensors can be applicable to the specific area in numerous potential applications according to the purpose. For example, low-strain gauges can be implemented for the structural health-monitoring [42, 43], mass measurement [44], pressure sensing [18, 45], etc. On the other hand, highly stretchable and sensitive strain sensors are able to be utilized as body-integrated electronic devices. They can be attached onto the clothing or directly on the human skin for the measurement of strain on the body, ranging from minute skin motions including respiration, heartbeat, and arterial pulse to joint flexions. Although achieving strain sensors with high sensitivity, stability, and stretchability for uni-directional strain sensing applications is still a great challenge, only a few strain sensors that are capable of selectively detecting multi-dimensional strain on 2-dimensional stretchable substrate have been reported. Therefore, other strategies by new material approaches and structural designs are required to enable decoupled

strain sensing for complete stretchable applications.

1.3. Silver nanoparticle based (ANP) strain sensor

1.3.1. Inkjet-printed silver nano-particle (ANP) based films

Inkjet-printing process is one of fabricating methods for depositing various organic/inorganic materials such as electrodes [46-48], dielectrics [49, 50], semiconductors [51, 52], and sensors. Unlike other solution processes, the desired patterning of materials is allowed without additional mask, which enables low-cost and time-effective fabricating procedures by inputting pre-designed pattern to the inkjet-printer machine. Furthermore, wide range of materials can be chosen according to the solvent versatility and manipulating printing conditions such as substrate temperature, wetting properties, annealing conditions, and jetting waveform. Such merits accordingly enable the deposited films to be utilized as large-area scale applications, which is a crucial factor in industrialization.

In this Ph. D. dissertation, I basically fabricated all the main devices by inkjet-printing silver nanoparticle (ANP) based inks on the elastomeric PDMS. (Figure 1.7) I used silver ink, which has a concentration of 32 wt% of silver nanoparticles dispersed in a polar solvent (triethylene glycol monoethyl ether), and the silver particle size was smaller than 50 nm. Although direct printing of ink containing ANP on diverse polymeric substrates using a drop-on-demand (DOD) inkjet-printing is challenging due to its elastomeric and hydrophobic nature, the substrate was treated with UV ozone to increase the surface energy, which increases the wettability between silver film and PDMS. The fabricated ANP based thin film has widely been utilized as interconnects on the device due to its high conductivity (~ 12 $\mu\Omega$*cm).

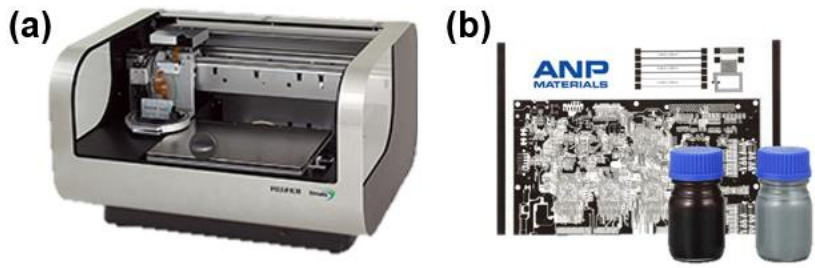

Figure 1.7. (a) A piezoelectric drop-on-demand inkjet printer (DMP-2831, Dimatix Corp.) and (b) Silver nanoparticle (ANP) based ink

However, for the film to be utilized in stretchable applications, it is well-known that inkjet-printed metal thin films on bare elastomer substrate are easily fractured even at small tensile strain, finally resulting in a rupture over the whole region. (Figure 1.8) In general, there are two reasons for poor mechanical behavior of the inkjet-printed metal thin film. First, hydrophobic surface properties of the elastomeric substrate including PDMS cause poor surface profile of the printed film and lead to randomly formed holes in the film. When the tensile strain is applied, the hold edges can initiate crack formation. Compared to conventional metal thin film, cracks rapidly initiate and propagate at relatively low strain range. Second, the inkjet-printed ANP thin film has extremely low ductility. Other nanomaterials such as nanotubes and nanowires that are endowed with stretchability by mesh deformation while maintaining good percolating pathways for electrical conduction. On the contrary, metal nanoparticle-based film has no obstacle to suppress the crack propagation and thus the cracking occurs at high speed even in low-level deformation conditions. While the hydrophobic surface of the elastomeric substrate can be optimized via roughening PDMS surface and UV ozone treatment conditions,

the improvement of crack propagation suppression properties requires further studies for the printed thin films. Therefore, there are two primary strategies to make stretchable properties out of the brittle materials [53]. The first approach is to disperse the particles in an elastomeric matrix [54, 55]. Such composites are simultaneously conductive and stretchable when the nanofillers form percolating pathways. The other strategy is to exploit new strain absorbing structures, such as wavy, serpentine, and wrinkle structures where the external strain is dissipated by unfolding and releasing the winding structures (Figure 1.9). [56, 57] As the brittle materials in this dissertation are deposited as films, wrinkle structure was engineered to obtain high stability of the film under tensile strain. The wrinkle structure was formed by inkjet-printing Ag ink onto the pre-stretched PDMS and releasing the composite. From the fabricated structure, the wrinkled film enables the film to maintain constant electrical resistance up to the strain where the composite was pre-stretched (Figure 1.10).

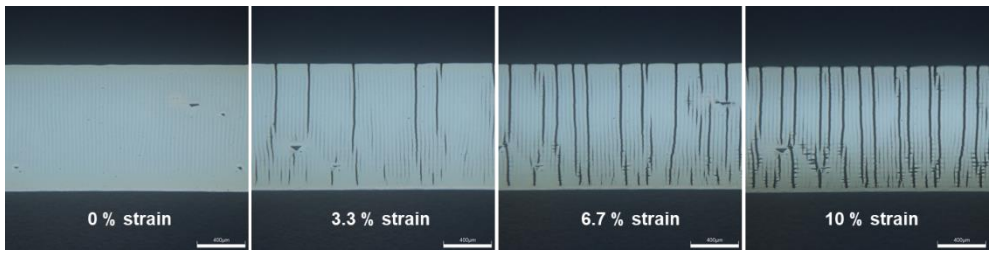

Figure 1.8. Inkjet-printed ANP thin film and its crack generating phenomenon under tensile strain (<10%)

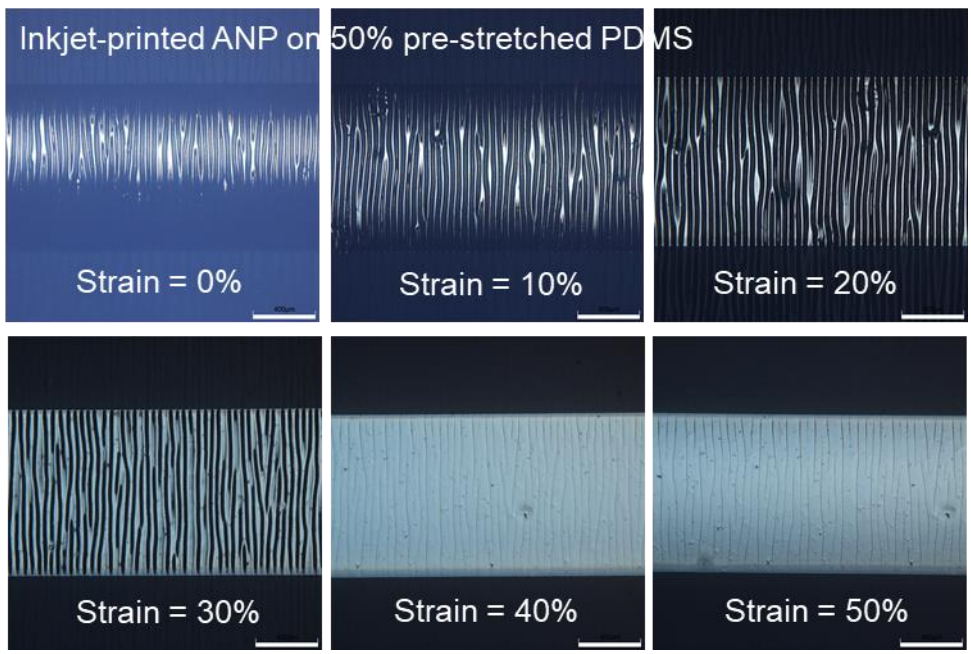

Figure 1.9. Optical images of wrinkle structure on inkjet-printed ANP film that was pre-stretched to 50% strain under external tensile strain (<50%)

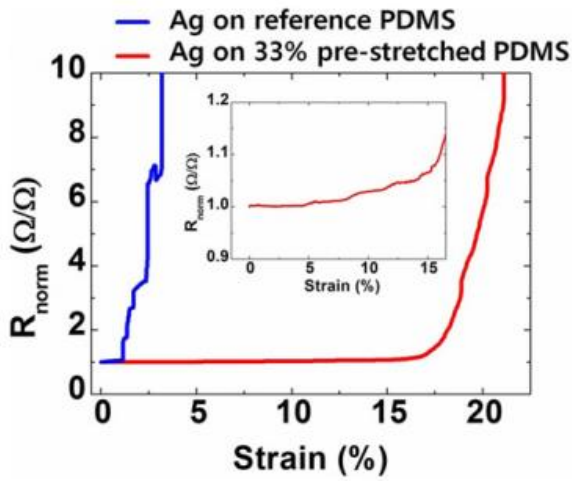

Figure 1.10. Resistance variations of inkjet-printed silver film on bare PDMS and pre-stretched PDMS substrate. [6]

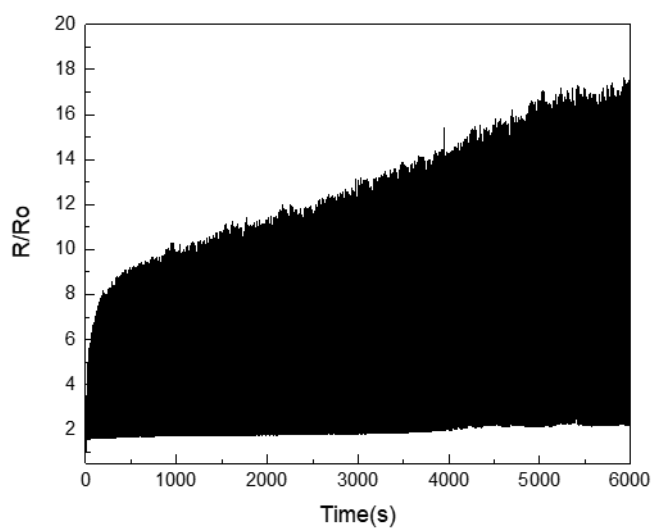

Figure 1.11. Repeated resistance variations of inkjet-printed silver from on bare PDMS under 1,000 cycles of tensile strain.

1.3.2. Crack-generated silver film for strain sensor

Cracks originate and propagate in brittle thin films coated on the top of soft polymer layers upon stretching. Indeed, cracks intend to initiate at the stress concentrated areas to release the accommodated stress. Microcracks were generated in CNT, ANP, nanowire materials, and graphene thin films coated on flexible substrates under stretching. [34, 36, 58-61] Stretching led to opening and enlargement of microcracks in thin films, critically limiting the electrical conduction through thin films due to the separation of several microcrack edges. Moreover, the electrical resistance of thin films drastically increased by the applied strain. This mechanism was employed to obtain highly sensitive strain sensors. In case of ANP films, although the brittle nature renders the film to be highly sensitive to external strain, the concentrated stress on the film by tensile strain provokes huge cracks that causes exponential increase in resistance and entire ruptures of the conductive channel at low-level strain (< 10%). Moreover, when the repeated strain is applied to the composite, cracks gradually increases at each cycle. (Figure 1.11) Thus, considering the poor stability of ANP film under tensile strain, more strategies to enhance stretchable properties are needed to be utilized as reliable strain sensor.

In this dissertation, based on intrinsic properties of the materials and crack-generating mechanism on the inkjet-printed ANP films, proper strategies were considered according to the purpose of the applications. A series of studies were conducted to solve the following issues in the ANP based film for strain sensor : (1) instability of the ANP film under tensile strain (2) coupled resistance of bi-axial strain sensing affected by high Poisson's ratio of elastomeric substrate (3) limitations

in fabrication of large area 2 dimensional strain sensing matrix. By solving those representative issues, I optimized the stretchable characteristics of the Ag strain sensor combined with high strain-sensitivity. Thus, in each chapter, I will propose various structural strategies with low-cost fabrication process to pursue versatile utility of the Ag strain sensor by exhibiting various demonstration applicable to numerous areas such as wearable device and user interface technologies in stretchable electronics.

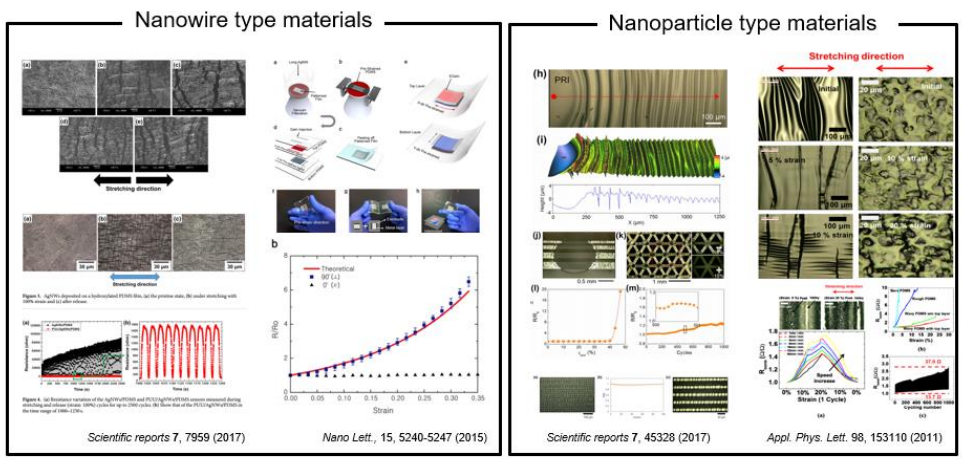

Figure 1.12. Previous works reported about crack-generating strain sensors.

1.4. Organization of this dissertation

Each following chapter will introduce the unique strategy of structural modulation on the ANP based film to be utilized as strain sensor according to the desired applications that require the fabricated sensor. And procedures of fabricating sample were identically conducted by inkjet-printing ANP based ink onto the PDMS substrate. Each chapter will contain an introduction to the research, fabrication process, a series of experiment to certify electrical and mechanical properties, then demonstration from the fabricated strain sensor will be presented. This dissertation consists of 5 chapters including Introduction and Conclusion. Details of each chapter are as follows:

Chapter 1 briefly covers the recent progress of stretchable electronics, and resulted applications of wearable device and advanced user interface technique, that require flexible strain sensor. Then, inkjet-printed ANP based film to be applicable to strain sensor is introduced with explaining crack-generating mechanism of the film under tensile strain to emphasize the core theme of this dissertation.

Chapter 2 introduces a simple and facile approach to effectively turn strain-tolerant conductive metal thin film with wrinkle structure into crack-rich thin film to obtain strain sensor with high sensitivity and stability. The intended phenomenon was controlled by additionally inkjet-printing Ag thin film onto the wrinkle structure, and the structure and performance will be also systemically optimized to enhance sensitivity and stability of the sensor. Then, integrated strain sensor system will be presented by combining interconnects and strain sensors to demonstrate dimensionally customizable wearable device that can be tailored to the subject's

hand size.

Chapter 3 reports highly sensitive micro-crack based strain sensors of Ag inkjet-printed on an asymmetrically pre-strained roughened PDMS substrate which remarkably reduces the influence by perpendicular strain. Furthermore, 2-dimensional stretchable LED array which makes up for reduced resolution as the platform is bi-axially stretched was fabricated using the strain sensors.

Chapter 4 presents crack-induced metal thin film based strain sensor that is inkjet-printed on PDMS, engineering concentrated micro-cracks around vertical patterns to extremely enhance sensitivity of the sensor. Then, the composite can be integrated with various force-receiving layers of different rigidity, to demonstrate various user-interface applications such as wearable device and large are force touch applications.

Chapter 5 finally summarizes the concept, methodology, and meaningful demonstrations of ANP based strain sensor, and also suggests the future perspective.

Chapter 2

Selective Crack Formation on Stretchable Silver Nano-particle based Thin Films for Customized and Integrated Strain-sensing System

2.1. Introduction

Recently, stretchable electronics [62-64] has attracted great interest for the next generation electronic devices owing to their high feasibility with surrounding environment. Integrated systems composed of various device components exhibit excellent performances for interesting bio-inspired areas such as health-monitoring [62, 65] and human motion detecting [18, 65, 66] applications. To practically realize the use of stretchable electronic devices, it is important that the integration of each component should be durable and reliable under harsh conditions.

Strain sensor is one of the most popular components in the stretchable electronic devices. Previous role of strain sensor has been confined to detecting vibration or small-level expansion and typically used in the macro-scale civil engineering. [67]

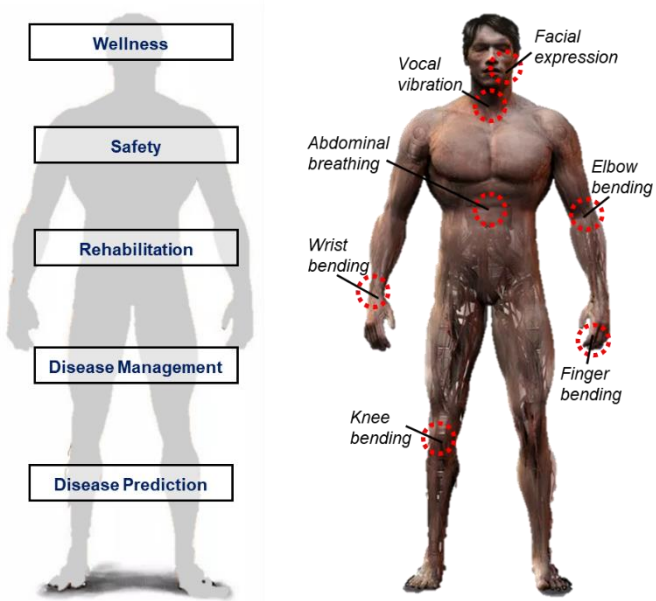

Figure 2.1. Purpose of wearable device and various human motions that are needed to be detected for health monitoring.

However, over the past decades, the facile use of strain sensor has been continuously involved in the stretchable electronics, as the strain sensor with high flexibility can be attached on human body and detect various human motions with wide range of strain signals such as jumping, finger-bending and grasping. (Figure 2.1) Consequently, a number of research groups have reported interesting flexible strain sensors with high strain-sensitivity. [17, 19, 22, 68, 69] However, as the systematic integration of interconnecting line and strain sensor at high-level strain loading is still a huge challenge, the stretchable sensors should be reliable under high-level deformation. Furthermore, although all component parts are fabricated to be stable against the external deformation, it is still difficult to develop strain-tolerant interface between interconnection line and strain sensor. The poor interface causes not only a severe error but also low reliability of the entire sensor system. To

overcome this issue, the eutectic liquid metal has been used for the conducting interface between device and interconnection, but limited to confined materials due to its intrinsic phase transition effect. In addition, although composite-based integration using carbon nanomaterials has high reliability, it is hard to design a complex configuration that consists of narrow and long interconnector for its high resistance level. [70] Therefore, a facile strategy to use highly conductive materials should be addressed for various and complex configurations.

Silver nanoparticles (Ag NPs) is one of the most useful materials for various stretchable applications for its good conductivity and solution-process availability. [2, 5, 62, 71, 72] However, the Ag NPs based thin film is intrinsically brittle and heavily vulnerable to the external strain. Therefore, the easy use of silver (Ag) material for stretchable applications has been mainly resulted from some extrinsic stress-releasing wrinkle structures. [1, 2] While, if the vulnerable nature can be selectively evoked in the intended area on the wrinkle structure, mechanically different structures of wrinkle and crack-rich regions can coexist. Accordingly, based on the different strain-responses of each structure, they can be utilized as stretchable electrode or strain sensor, respectively.

In this study, I implemented an integrated strain sensor system which consists of strain sensor and stretchable line on a stretchable PDMS substrate by inkjet-printing Ag ink. The stretchable Ag line has the wrinkled structure which enables the brittle Ag line to be durable and reliable up to specific strain through fold-unfolding behavior. Furthermore, by inkjet-printing additional Ag layer onto the specific area of the wrinkle structure, the easily patternable crack-based Ag strain sensor was fabricated. The strain-responses of each structure were analyzed by measuring the resistance variation and morphological changes under tensile strain, and the sensor

performance was optimized to certify high sensitivity and stability. Finally, as the inkjet printing method enabled the customizable configuration of stretchable interconnects and strain sensor, the integrated system was utilized for selectively detecting different joint motion in a hand without interferences.

2.2. Experimental methods

To fabricate PDMS substrate (thickness: 300 μm), 10:1 weight ratio mixture of PDMS (Sylgard 184 from Dow Corning) and curing agent was spin-coated onto glass substrate, followed by annealing at 120 ℃ for 30 minutes. After detaching the cured PDMS substrate from the glass, I fixed it onto the stretching equipment, and stretched the elastomer to 100 % strain as shown in Figure 2.2. To make the surface of PDMS hydrophilic, the surface was treated with UV ozone. Then, Ag NP ink (DGP-40 from ANP Corp.) was inkjet-printed onto the PDMS substrate which was located on a heated plate (60 ℃), by using a piezo electric inkjet printer (DMP-2831 from Dimatix Corp.) with 21 μm diameter nozzles. The nozzle squirted ~10 pL droplets of the Ag NP ink and the droplet formed a circle with a diameter of ~40 μm on the UV ozone treated PDMS substrate. And the distance between the centers of adjacent droplets was 35 μm. After annealing the sample at 120 ℃ for 30 minutes, the elongated elastomer was released to flattened state, and wrinkled Ag base layer was formed. Then, double layers of Ag NP ink were additionally inkjet-printed onto the Ag wrinkled film on the heated plate (60 ℃) to form crack-inducing Ag layer. The distance between the centers of adjacent droplets of Ag ink was 40 μm. After annealing process (120 ℃ for 30 minutes), the hybrid structured Ag strain sensor was fabricated. Optical measurement for the sensor was performed with scanning electron microscopes (SEM) (S-4800 from HITACHI) to obtain structural data such as surface morphology and crack generation. Moreover, to measure the electrical characteristic of the strain sensor under tensile strain, I fixed the sample to the customized stretching device to apply strain to the sensor. Then, electrical

measurement for the sensor was performed with a source meter (Keithley 2400 from Tektronix). The resistivity of the strain sensor was measured by applying voltage of 0.1V throughout the sample.

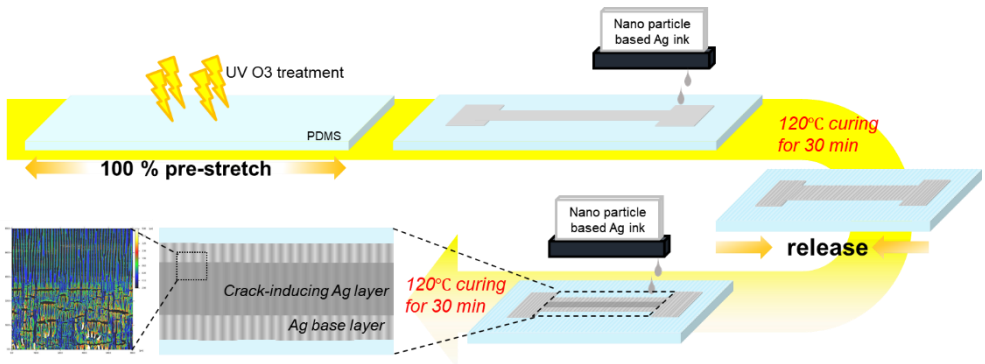

Figure 2.2. Schematic illustration of the whole process flow of fabricating Ag strain sensor by inkjet-printing process.

2.3. Results and discussion

2.3.1. Crack-induced phenomenon on Ag strain sensor

There are various interesting phenomena about strain-response resulted from structural or morphological change of the materials. In stretchable electronics, capacitive and piezo-resistive types have widely been utilized for stretchable strain sensor. The former has high accuracy, but it is difficult to design their structures on the wearable system because of the metal-insulator-metal structure. The latter has some advantages in easy fabrication and the choice of material, but it is hard to simultaneously obtain two sensing performances of strain-sensitivity and reliability. Among the piezo-resistive strain sensors, cracking is one of the most popular phenomena in stretchable electronics. [16, 17, 19, 21, 22, 73-77] In general, the factors that determine crack formation are the mechanical properties of the materials and induced strain on the material. So, if stress-releasing structures including wrinkles are well-constructed on the metal materials, crack formation even at high tensile strain can be avoided in spite of their extremely poor mechanical properties. In contrast, highly tough materials with stress-focusing notch structures can be easily fractured even at small strain loading. In previous study, by using selective toughening methodology, different crack formations in same material were obtained, and the two regions (fracture-designed and fiber-reinforced regions) showed different roles on the stretchable strain sensor. It means that selective crack controlling method enables the piezo-resistive strain sensor to have both the strain-sensitivity and reliability by separating the roles.

Ag NPs based thin films on bare elastomer substrate are well known to be fragile even at small external tensile strain, leading to entire channel rupture due to their intrinsically poor ductility under tensile strain. To complement the poor electrical stability, in this study, wrinkle structure of the metal thin film formed by inkjet printing Ag NPs based ink onto the pre-stretched platform was utilized to dissipate the strain energy from elongated platform and lessen the abrupt channel fractures, which allowed the film to be durable at strain loading as shown in Figure 2.3. Afterwards, by additionally inkjet-printing Ag ink onto the specific area of the wrinkled metal thin film, Ag ink flew down to the valley of the corrugated Ag film. As a result, thickness-gradient Ag film was deposited onto the wrinkled film as shown in Figure 2.3. As cracks are more likely to be generated on the thicker metal film, [78] I were able to generate controlled cracks on the film, which gradually increased electrical resistance under tensile strain. As a result, the whole film is systematically divided into two parts. One is Ag base layer that maintains stable electrical property, and the other is hybrid structured Ag film with additionally printed crack-inducing layer, which leads to a highly sensitive strain-sensing device.

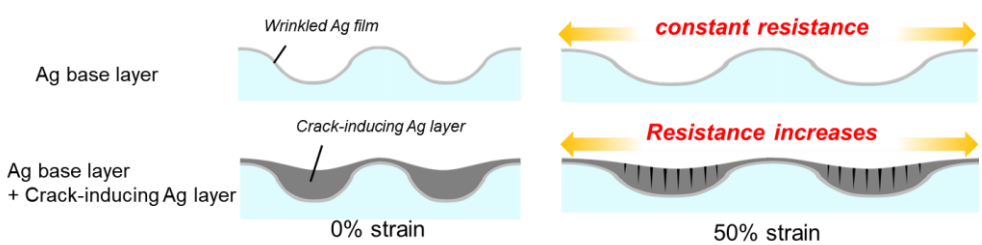

Figure 2.3. Schematic illustration of working principles of the Ag base layer without or with the crack-inducing Ag layer under tensile strain.

2.3.2 Morphological analysis on the crack generation of Ag strain sensor under tensile strain

In order to verify the strain-response of the Ag strain sensor, microstructural changes on the metal thin film are optically explained in Figure 2.4. The optical images of samples were exhibited at its initial state and 50% strain, respectively. Figure 2.4 shows the crack-inducing layer which is deposited onto the wrinkled Ag film at 0% strain. It is noted that unintended lateral cracks are generated on the film owing to Poisson's effect of the elastomeric substrate. However, vertically generated cracks that cause change in resistance are not noticed, even on the film where the crack-inducing layer and the base layer meets as shown in Figure 2.4. On the contrary, as comparably thicker film is supposed to be more easily cracking, complete large cracks are vertically generated on the crack-inducing layer at 50% strain loading, which makes the film be electrically isolated. (Figure 2.4 (d)) The large cracks gradually decrease in size as the thickness of the Ag sensing film decreases, then accordingly disappear on the wrinkled film as depicted in Figure 2.4 (e). In addition, as shown in Figure 2.4 (c) and (f), only micro-scale cracks are seen on the Ag base film under 50% strain, but don't have a significant effect on the noticeable change in electrical resistance.

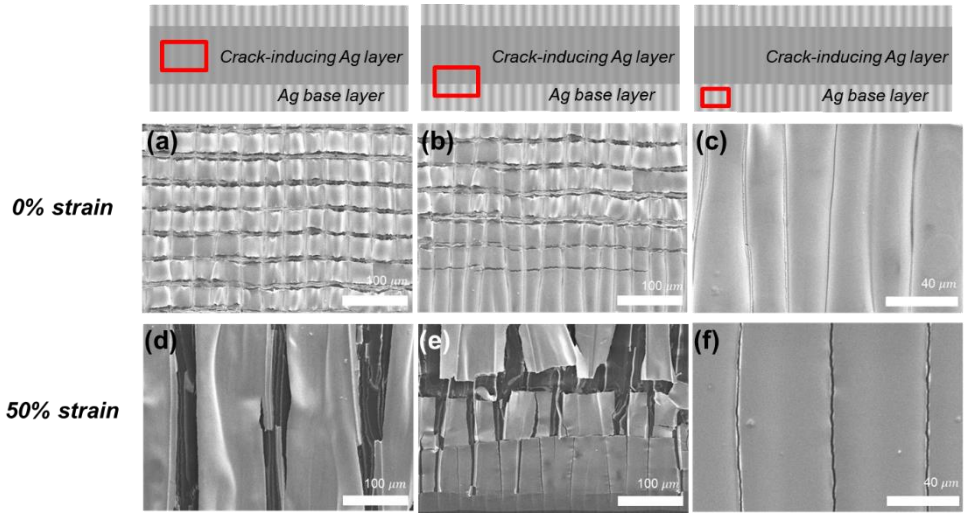

Figure 2.4. Optical images of crack generation on the Ag strain sensor scanning from the crack-induced layer to base layer, at (a-c) 0% strain and (d-f) 50% strain.

2.3.3 Electrical characteristics of Ag strain sensor under tensile strain

Based on the morphological analysis, I analyzed the resistance variation of the metal thin film under tensile strain. The stretchable properties of Ag wrinkled base layer that were formed on the pre-stretched elastomer are featured in Figure 2.5 (a) and (b), and the hybrid structured Ag thin films that includes crack-inducing layer, are shown in Fig. 2.6 and 2.7, respectively. The extent of the strain which wrinkled base layer can stand without changing electrical resistance is determined by how the elastomer was pre-stretched. Therefore, as shown in Figure 2.5 (a), Ag base layer that had been implemented on 100% pre-stretched platform maintained constant resistance up to higher strain than that with 50% pre-strain. In addition, as the thickness of metal film increases, the resistance starts to increase slightly earlier and more sharply. As a result, it was certified that single layered Ag film with 100% pre-strain was preferred for the base layer, which assured wide strain range. Furthermore, to certify the mechanical stability of the base layer of 100% pre-strain, cyclic test for 1,000 times was also performed as shown in Figure 2.5 (b). While the sample showed poor resistance repeatability under 70% strain, the sample showed reliable and durable property when it was repeatedly stretched to 50% strain. Thus, the working range of the strain sensor was determined as 50% strain to meet the mechanical stability.

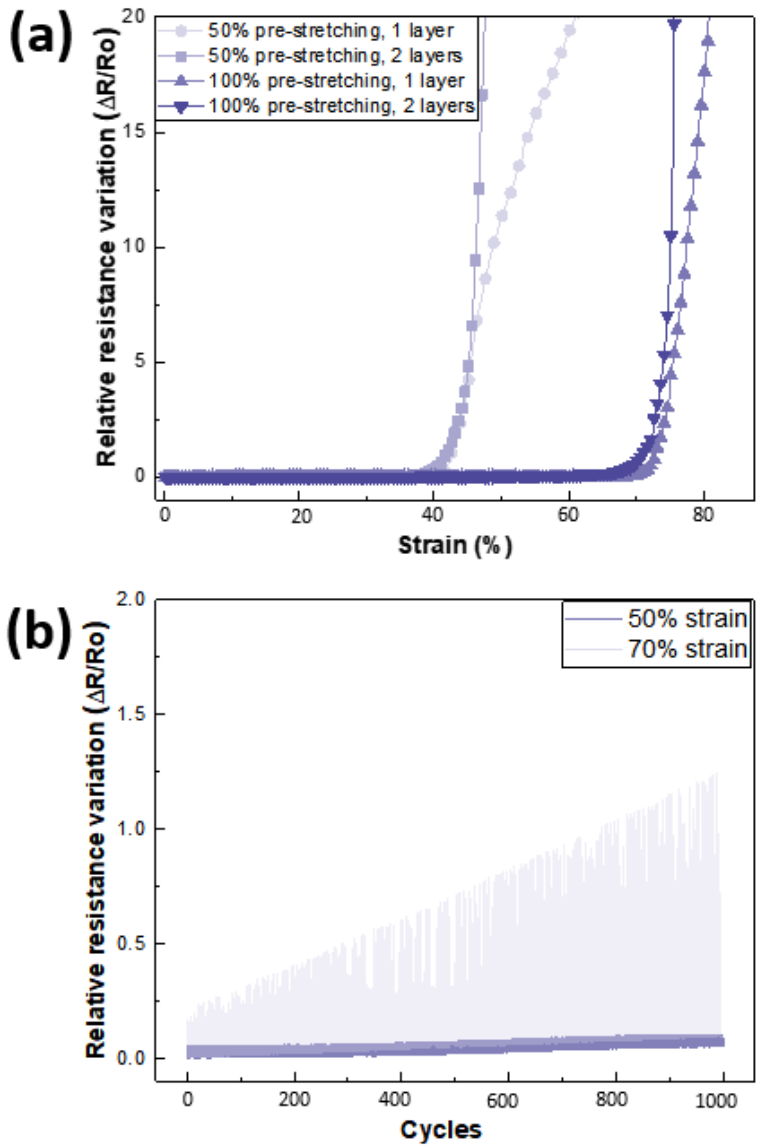

Figure 2.5. Electrical resistance variations of (a) base layer according to the extent of pre-strain (50%, 100%) and the number of layers (1, 2) and (b) the repeated cyclic tests (1000 times) of the Ag base layer (pre-strain : 100%) as the function of strain loadings (50%, 70%).

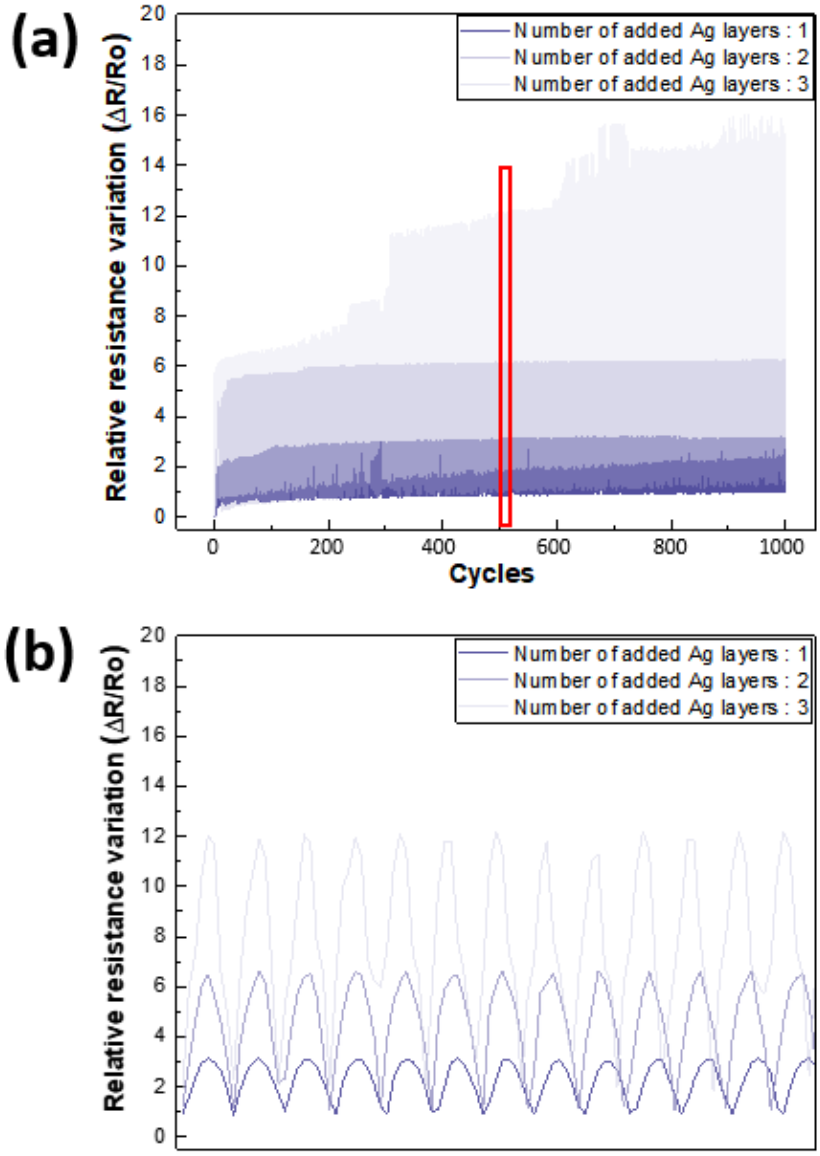

Figure 2.6. (a, b) Electrical resistance variations in repeated cyclic tests of strain sensor with various number (1, 2, 3)

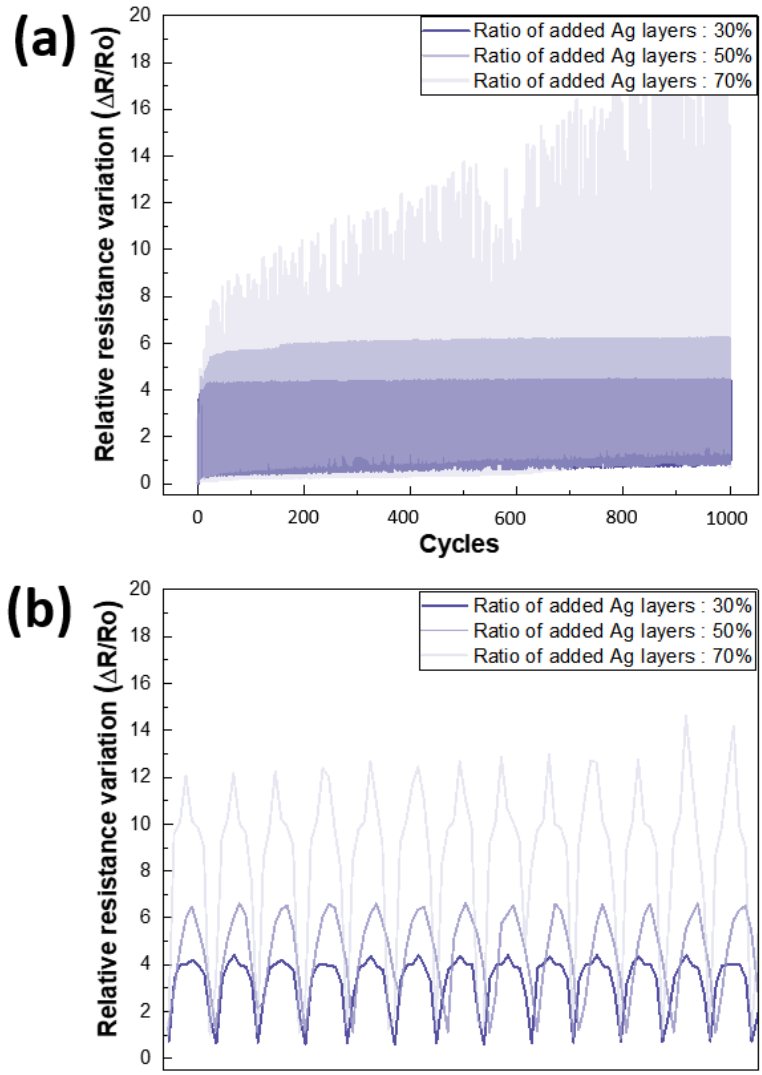

Figure 2.7. (a, b) Electrical resistance variations in repeated cyclic tests of strain sensor with various ratio (30%, 50%, 70%) of added Ag layers.

In Figure 2.6 and 2.7, when it comes to investigate the resistance variation of hybrid structured Ag strain sensor, cyclic tests were performed in harsh conditions (cycling number : 1,000 times, strain range : 50%). As shown in Figure 2.6, the sensor showed higher sensitivity as the number of crack-inducing layers increases from 1 to 3. However, the cyclic repeatability of the sensor was guaranteed up to double layers, as too bulky additional film induced unintended cracks propagated to the base layer. In addition, the sensitivity of the sensor could be enhanced by optimizing the patterned ratio of crack-inducing layer to base layer as shown in Figure 2.7. By increasing the ratio up to 50%, the sensor showed higher sensitivity with fairly excellent stability. Here, to quantitatively state the sensitivity of the strain sensor, gauge factor can be analyzed [79, 80], which can be calculated as

$$\text{Gauge factor} = \frac{\Delta R/R_o}{\Delta L/L_o}$$

where R and L denotes the resistance value and the length of the strain sensor, respectively. Thus, the strain sensor with higher sensitivity shows bigger gauge factor as the resistance increases higher when the same strain loading is applied. In conclusion, as single-layered Ag wrinkle film which had been formed at 100% pre-stretched PDMS and double-layered films that were coated on the 50% of the base layer were combined, the strain sensor with high sensitivity (gauge factor ~10) and stability was obtained.

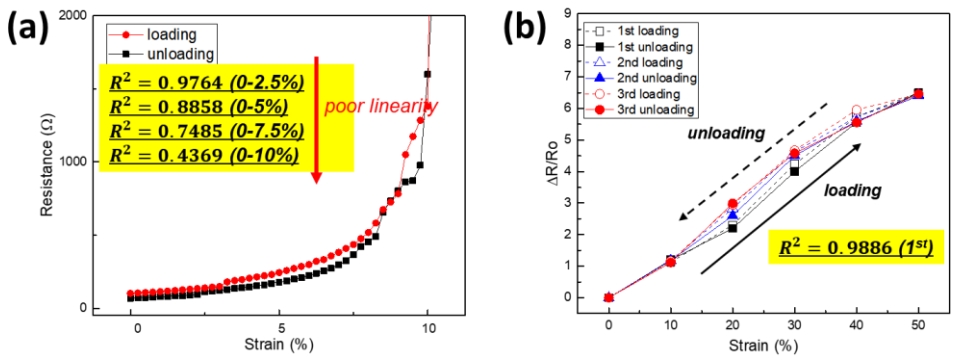

Figure 2.8. Electrical hysteresis and linearity in (a) Ag film on bare PDMS and (b) crack-induced Ag strain sensor under tensile strain.

Electrical resistance variations of the strain sensor under tensile strain loaded and un-loaded (Fig. 2.8 (b)) are also exhibited to certify the electrical hysteresis and linearity of the sensor. The electrical hysteresis in metal thin film on PDMS inevitably appears due to the viscoelasticity of elastomeric substrate, and inconsistency in electrical change is shown on both Ag film and crack-induced Ag strain sensor (Fig. 2.8 (a) and (b)). However, as the wrinkled structure prevented the brittle Ag film from abrupt increase in crack generation, linearity in resistance change is much more enhanced on crack-induced Ag strain sensor as shown in Fig. 2(b).

2.3.4. Dimensionally customizable wearable device

As the wrinkled Ag film has widely been utilized as stretchable interconnects, the strategy of additionally inkjet-printing crack-inducing layer onto the wrinkled Ag film enabled the large-area integrated strain-sensing system. Therefore, in order to show the practical usage of Ag strain sensor, I demonstrated a human motion detecting device which could help measure the joints flexion of finger in Figure 2.9. The device is dimensionally customizable to the users of different finger size with the merit of easily patterning additional layer onto the desired region by inkjet-printing process. As depicted in Figure 2.9, the device, that was conformally attached onto the index finger, consisted of 4 Ag wrinkled lines (**1**~**4**). The common line **1** was electrically connected to the other lines (**2**~**4**) that were parallelly connected one another, and, as a result, 3 Ag stretchable electrodes (**1**-**2**, **1**-**3**, **1**-**4**) were implemented. Then, additional Ag film was patterned on the specific area of wrinkled electrode, to exactly align with the joints of index finger for the accurate measurement. Each Ag strain sensor which were located on each line **2** and **3**, was supposed to detect the flexion of PIP (Proximal Inter-Phalangeal) joint and MP (Metacarpo-Phalangeal) joint of index finger, respectively, and, '**d**' denotes the distance between the middle points of two strain sensors. The line **4** was for the reference result of Ag wrinkled electrode.

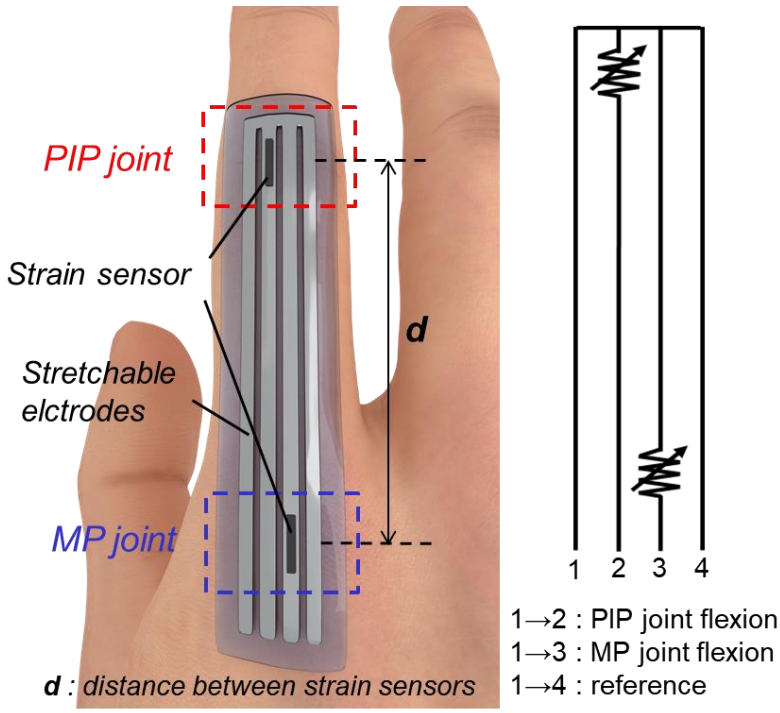

Figure 2.9. Schematic depiction of the joint-flexion detecting device (d: distance between strain sensors).

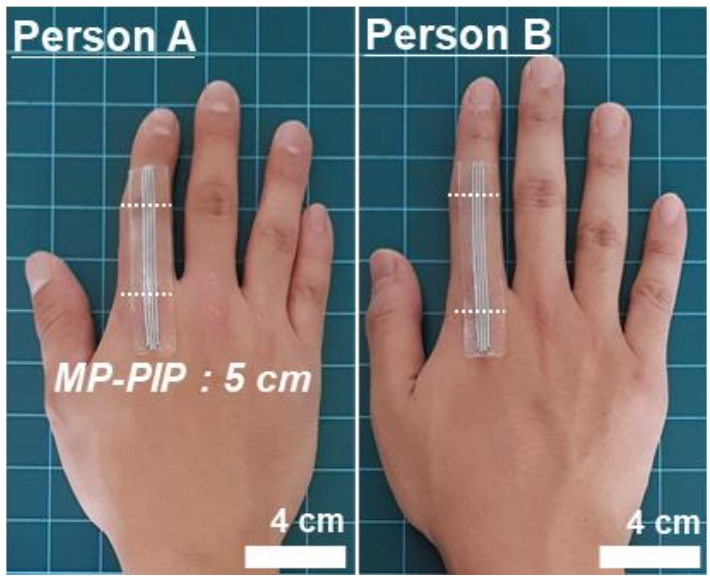

Figure 2.10. Optical images for dimensional customization of the device for the users (person A, person B) with different hand size.

In Figure 2.10, from the distance between PIP and MP joints of users, the device could be dimensionally tailored regardless of the size of their fingers (length between PIP and MP joints of person 'A' and person 'B' are 5 cm and 6.4 cm, respectively).

In Figure. 2.11, to analyze the tailoring effect of the device, the device (**d** : 5 cm) showed remarkable change in resistance from the PIP joint flexion (90° degree) of a person whose PIP-MP joint distance was correspondingly 5 cm. On the other hand, the misalignment of the sensors with joints (**d** was either 4 cm or 6 cm) caused the device to malfunction. Moreover, with the high sensitivity and wide working range of strain sensor, excellent performance of the device was observed from the result that the change in resistance linearly increased according to the degree of PIP joint flexion (30°, 60°, 90°) (Figure 2.12).

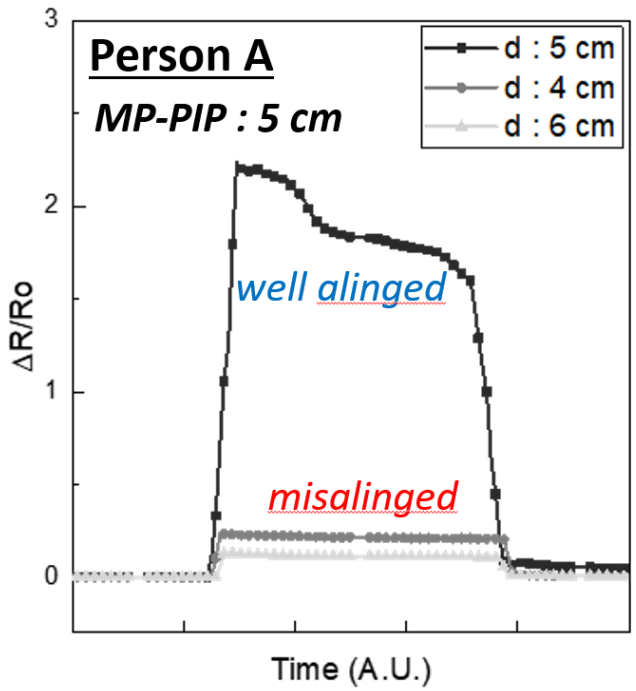

Figure 2.11. Resistance variation of the devices of various size (d: 4 cm, 5 cm, 6 cm) by the PIP joint-flexion of Person A (MP-PIP length : 5cm).

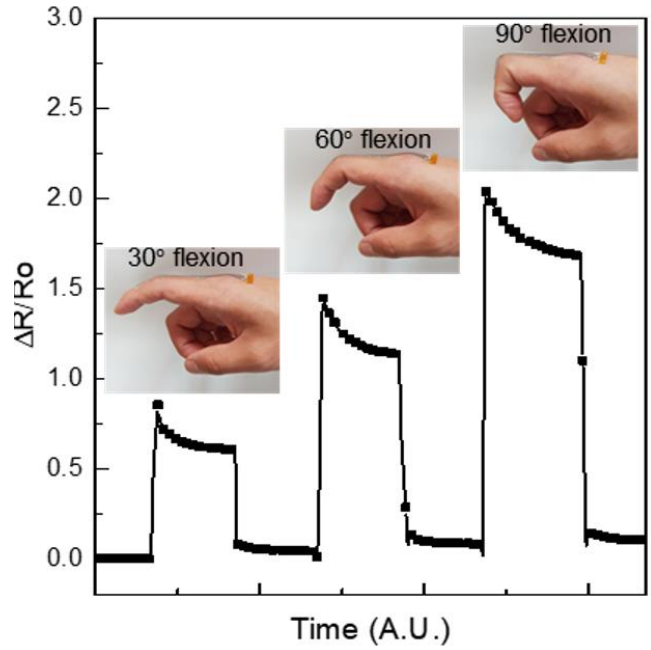

Figure 2.12. Resistance variation of the device according to the degree of PIP joint flexion (30°, 60°, 90°).

Finally, as shown in Figure 2.13, for the integrated strain-sensing device to selectively detect PIP and MP joints of finger, I performed an experiment that verified the ability to distinguish signals from the various flexions of index finger. Through the various movements of index finger (stretching, PIP bending, MP bending and PIP & MP bending) at regular intervals of 5 seconds, it was observed that the resistance variation from each joint flexion was independent without any interference. In addition, compared to the reference line that showed no resistance change under joint flexion, the resistance change of well-aligned Ag strain sensor was further notable.

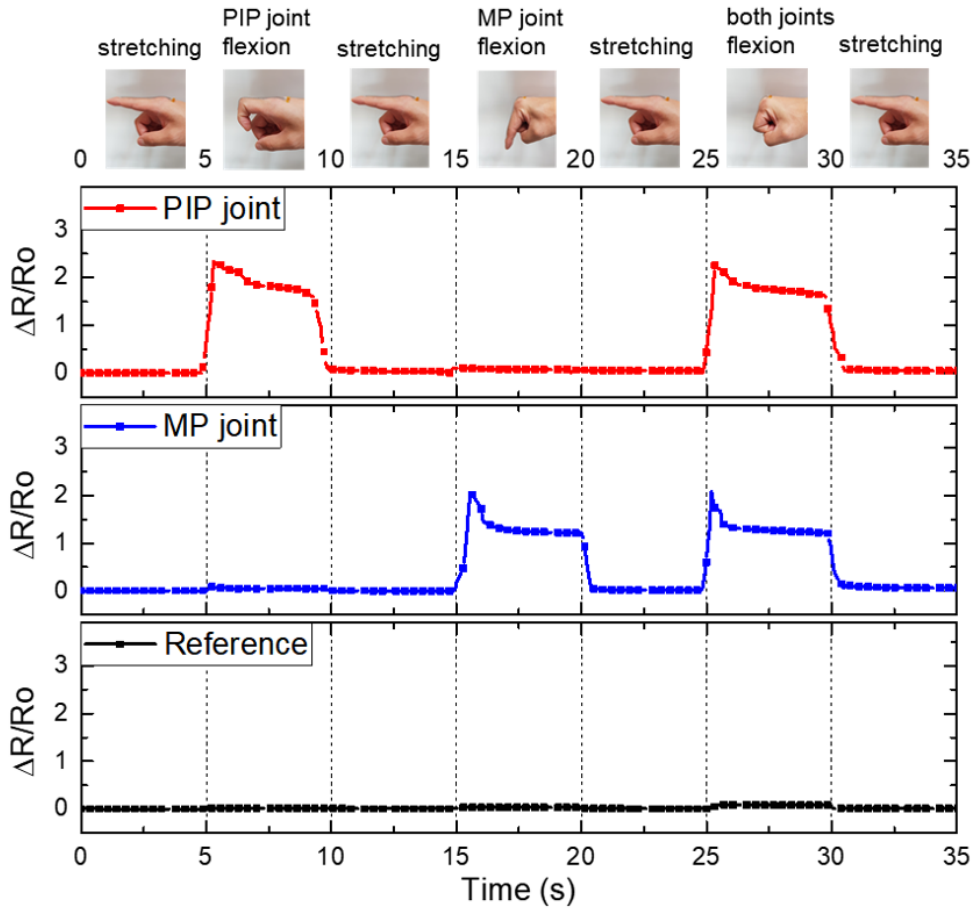

Figure 2.13. Resistance variation of the device by various movements of index finger in regular sequences.

2.3.5. Selective monitoring of the wearable device for common actions of finger

In order to emphasize the feasibility of the wearable device applicable to real life, I demonstrated the device to accurately detect several common actions with finger movement, which were clicking mouse (Figure 2.14 and Figure 2.15) and grabbing bar (Figure 2.16). Detecting mouse clicking motion was conducted in two ways: the resistance variations that were caused by clicking frequently using only the PIP joint, and clicking slowly using only the MP joint are exhibited in Figure 2.14 and Figure 2.15, respectively. By selectively monitoring the movement of each finger joint, it was noteworthy that more precise motion detecting of the device was available by subdividing the clicking action that could be regarded as the same motion. Meanwhile, as shown in Figure 2.16, the resistance variation by repeatedly grasping and releasing bar shows the ability of the device to detect the finger movement with both joints at the same time. Our results well demonstrated the characteristics of Ag strain sensor and the use of integrated strain sensing system as customizable human motion monitoring device application.

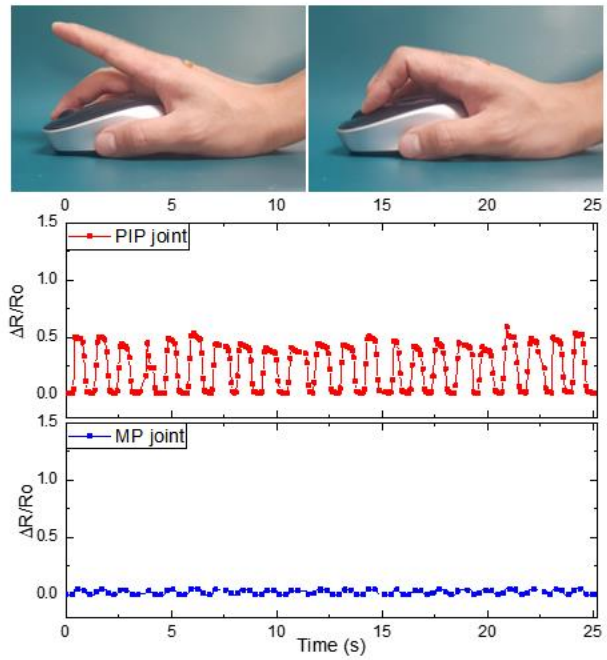

Figure 2.14. Resistance variation of the device by frequent mouse-clicking with PIP joint flexion.

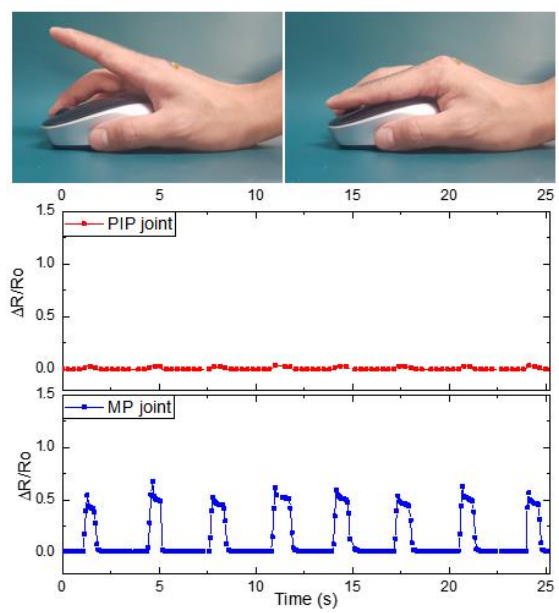

Figure 2.15. Resistance variation of the device by slow mouse-clicking with MP joint flexion.

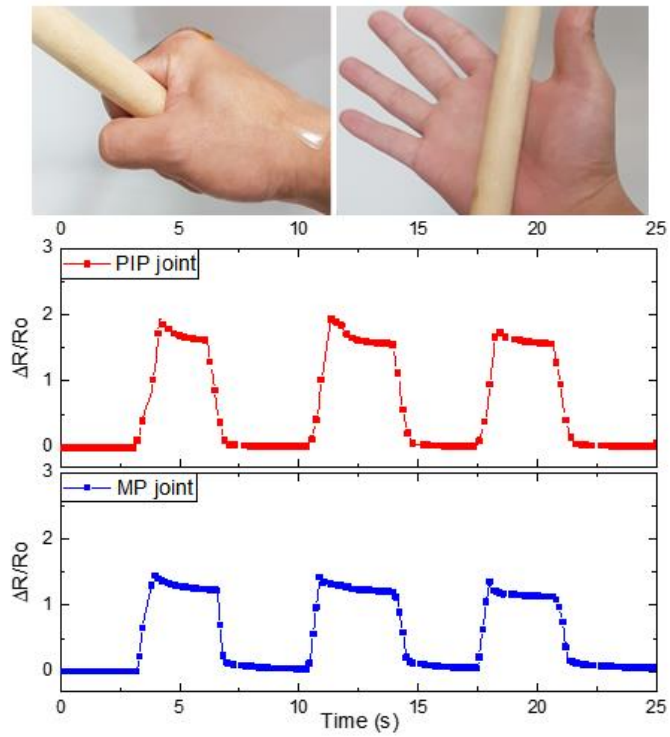

Figure 2.16. Resistance variation of the device by grasping and releasing bar.

2.4. Summary

To summarize, I have presented a Ag NPs based strain sensor by patterning additional layers onto the desired area of the wrinkled Ag film to induce intended crack formation with a facile and low-cost inkjet-printing fabrication process. Thus, the hybrid structured Ag film was systematically divided into two parts to accomplish both sensitivity and reliability of the brittle material based strain sensor. In addition, by optimizing fabrication conditions and structures of the strain sensor, I obtained a stable resistance variation with high gauge factor of ~10 up to 50% tensile strain. Based on the combination of fabricated strain sensor and wrinkle film that can be utilized as Ag stretchable electrode, I demonstrated an integrated strain-sensing system applicable to the human-motion detecting device. The integrated device is able to detect flexion of multiple joints, and it can be dimensionally tailored regardless of users' hand size. It is noted that the selectively crack-inducing strain sensor is applicable to various wearable devices which require accurate measurement of common actions in human life.

Chapter 3

2-D Strain Sensors Implemented on Asymmetrically Bi-axially Pre-strained PDMS for Selectively Switching Stretchable Light Emitting Device Arrays

3.1. Introduction

Stretchable strain sensors have received great attention as one of the most useful measurement tools in the stretchable electronics area because of their facile interaction with subject and high utility of perceived information. Various interesting phenomena have been widely studied in order to meet the demand of recent stretchable electronics that are wide strain range [34, 81], high strain-sensitivity [68, 69], and multi-directional deformation [73, 82-84]. Among the phenomena for detecting strain, piezoresistive phenomenon including cracking has been further reported in the stretchable strain sensor due to the merit of easy fabrication and high sensitivity [16, 17, 19, 22, 68, 76, 77]. In addition, a variety of conductive nanomaterials such as carbon nanotubes (CNTs) [21, 85], poly(3,4-ethylenedioxythiopene):poly(styrenesulfonate) (PEDOT:PSS) [86], metal nanoparticles (NPs) [17, 18, 22], metal nanowires [73, 74] and fancy structures such

as corrugated [17, 21, 73] or micro-woven platform [87, 88] have been also studied to improve working strain range. Combination of those two strategies on the stretchable substrates provide reliable conductive networks that can be repeatedly connected and disconnected under deformation, and thus, show excellent strain-sensing performance in wider strain range.

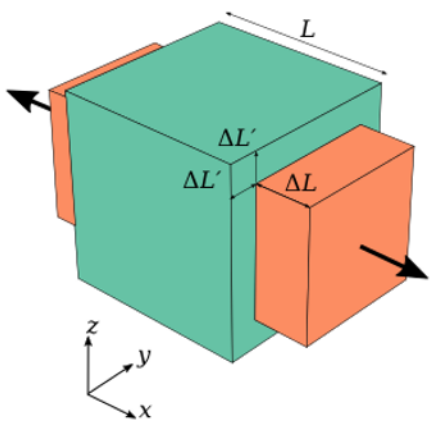

$$\nu = -\frac{d\varepsilon_{\text{trans}}}{d\varepsilon_{\text{axial}}} = -\frac{d\varepsilon_{\text{y}}}{d\varepsilon_{\text{x}}} = -\frac{d\varepsilon_{\text{z}}}{d\varepsilon_{\text{x}}}$$

$\boldsymbol{\nu}$: *Poisson's ratio,*

$\boldsymbol{\varepsilon_{trans}}$: *transverse strain*

$\boldsymbol{\varepsilon_{axial}}$: *axial strain*

Figure 3.1. Definition of Poisson's ratio ($\boldsymbol{\nu}$) of an elastic material subject to tensile strain

Most of the strain sensor research has mainly reported uni-axial detection and thus its applications have been limited to one-dimensional bending applications. In order to expand the application areas of strain sensors considering actual deformation in practical use, a multi-axial sensing capability of the strain sensors is required. However, there is a technical challenge in developing multi-dimensional strain sensors on elastomeric substrates with high Poisson's ratio (~0.5) (Figure 3.1.) [89], which can separately detect strain signals in each direction. Due to the high Poisson's ratio, a large compressive strain is simultaneously applied in a direction

perpendicular to the one of the intentionally applied tensile strains. The unintentional compressive strain produces additional deformation and then fractures in the sensor. Thus, most of the crack-based sensors have an intrinsic limitation in independent detecting multi-axis stimuli sensing. To avoid this directional strain-coupling effect, several works have been reported [73, 82-84]. For instance, interlocked pre-strained strain sensing system composed of two layers for respective detection of x- and y-axis strain signals, and an elastomeric platform of various moduli for strain concentration have been proposed [82]. However, there are still several disadvantages of complex fabrication processes and crosstalk in multidimensional sensing.

Therefore, in this study, I propose a strategy for both directional strain-decoupling engineering and facile printing process by using conductive thin films made of silver nanoparticles (Ag NPs). Although metal NP materials have been widely used for printed and stretchable electrode applications [1, 3-5, 72], only a few papers have been reported regarding metal NP-based strain sensors [17, 18, 22], due to its intrinsic poor mechanical properties that can cause crack propagation even at low tensile strain ranges. I introduced asymmetric wrinkle structure for two-dimensional (2-D) strain sensors made of Ag NPs by using similar pre-stretching method that I used for our previous stretchable electrode papers [1, 3, 72]. One important change is that I applied, asymmetrical pre-strain to a poly(dimethylsiloxane) (PDMS) substrate during inkjet-printing process of the Ag thin films, resulting in a selective design of the direction-dependent strain sensing and stable interconnection between each component in the system. The Ag thin films on the asymmetrically pre-strained PDMS substrate showed anisotropic crack formation under various tensile strains and significant resistance change only to the

intentionally designed direction. As previously reported[1, 90], the one on a symmetrically pre-strained PDMS substrate showed a strain-releasing herringbone structure and a stable conductivity under bi-axial stretching. The microstructural changes of each engineered thin film were studied and the effects of pre-strained PDMS on the electrical performances of the strain sensor and interconnection were also investigated. Finally, I also demonstrated a conceptual strategy for resolution-sustainable stretchable display by using lighting device array, where hidden pixels located between normally-on-pixels are selectively operated by the engineered strain sensors that detect strain signals only from the intended axis. (Figure 3.2.) The hidden pixels can compensate the resolution degradation from the increased distance between neighboring pixels in the stretchable platform [4].

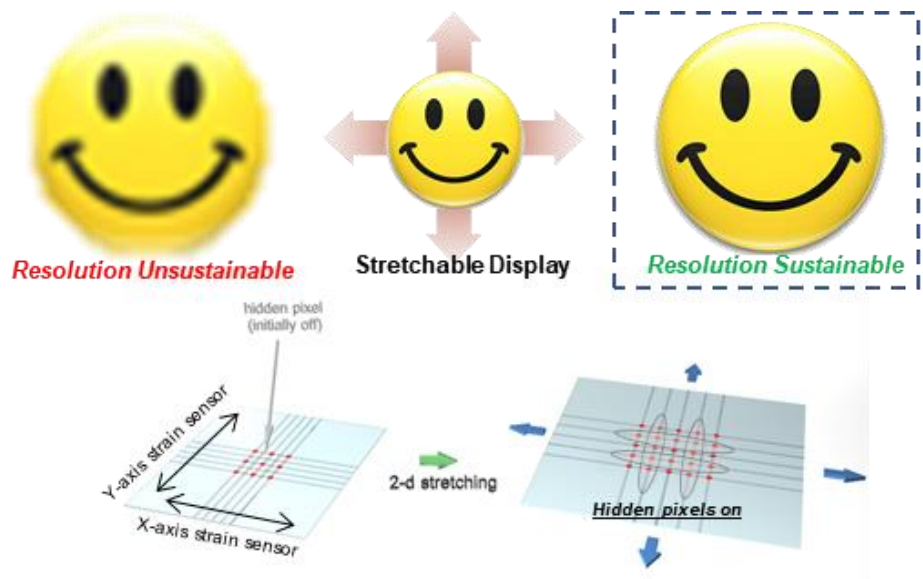

Figure 3.2. Feedback functionality between 2-D strain sensors and 2-D LED stretchable array to complement the reduced resolution of stretchable display.

3.2. Experimental methods

3.2.1. Fabrication of strain sensors

To fabricate a PDMS substrate (thickness: 300 μm), the 20:1 weight ratio mixture of PDMS (Sylgard 184 from Dow Corning) and curing agent was spin-coated onto an aluminum mold with roughened surface, followed by annealing at 120 ℃ for 30 minutes. After detaching the cured PDMS substrate from the mold, I fixed it onto the 2-dimensional stretching equipment with the roughened side of PDMS upside, and asymmetrically stretched the elastomer in 2-directions (x : 20%, y : 40%) as shown in figure 3.3. Then, Ag NP ink (DGP-40 from ANP Corp.) was inkjet-printed onto the PDMS substrate which was located on a heated plate (60 ℃) by using a piezo electric inkjet printer (DMP-2831 from Dimatix Corp.) with 21 μm diameter nozzles to fabricate strain sensor (thickness ~ 1μm) detecting x-axis strain signal. Before the printing process, in order to increase the surface energy, i.e. to make the surface more hydrophilic, the specific area where the Ag thin film is formed was treated with UV ozone while other areas were covered by aluminum mask. The nozzle extruded 10 pL silver ink for each droplet and the drop space was 35 μm. The same procedure was repeated with the reversely stretched configuration (x : 40%, y : 20%) for the substrate with the x-axis strain sensor in order to fabricate the strain sensor detecting y-axis strain signal.

3.2.2. Fabrication of stretchable lighting device

Silver electrodes and pads (thickness ~ 1 μm, 1 μm) were inkjet-printed onto 2-directionally (x : 40%, y : 40%) pre-stretched PDMS substrate on which the x-axis and y-axis strain sensors were already formed (Figure 3.3). I set the dynamic range of strain sensor according to the maximum bi-axial stretchability of 2-dimensional stretchable LED array. To form the crossover dielectric for electrical insulation between crossing electrodes, thin PDMS layer (thickness ~ 1 nm) was located at the crossing points as reported in the previous results [1, 2]. To place and solder the LED chips, silver epoxy (ABLEBOND 84-1LMISR4; Henkel) as soldering material was dispensed onto the inkjet-printed Ag pads. (Figure 3.4) Each LED chip was then placed by pick-and-place machine (TM200A; Hangzhou NeoDen Technology Co., Ltd) at accurate positions followed by silver epoxy curing at 170 ℃ for 30 minutes. Finally, pre-stretched substrate was released to form wrinkles in herringbone shaped patterns on the printed silver interconnects and 2-dimensionally stretchable lighting device was fabricated. (Figure 3.5)

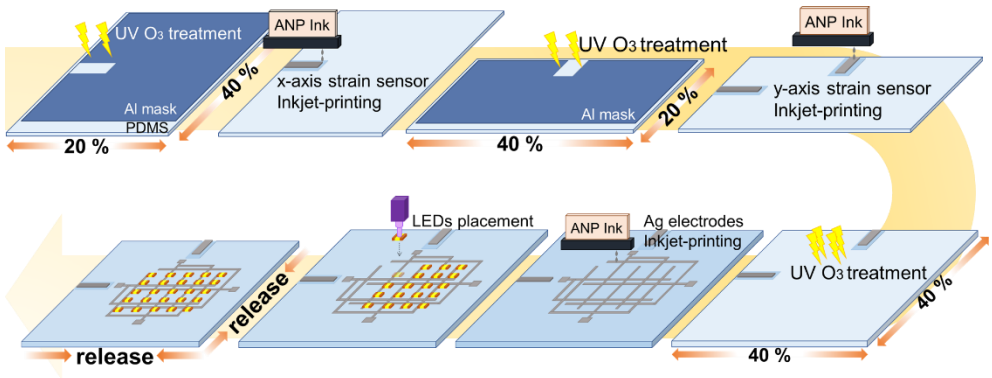

Figure 3.3. Schematic illustration of the whole process flow of fabricating asymmetrically pre-stretched x-axis and y-axis strain sensors and two-dimensional stretchable LED array on a common PDMS substrate by inkjet-printing process.

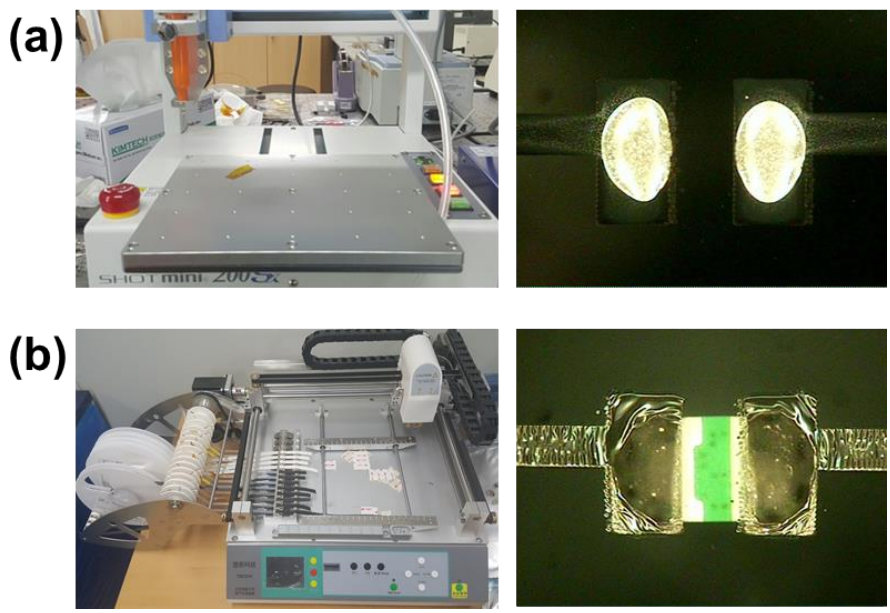

Figure 3.4. Optical images of (a) dispensing machine (ABLEBOND 84-1LMISR4; Henkel) to pattern soldering material Ag pads and (b) pick-and-place machine (TM200A; Hangzhou NeoDen Technology Co., Ltd) to place LEDs.

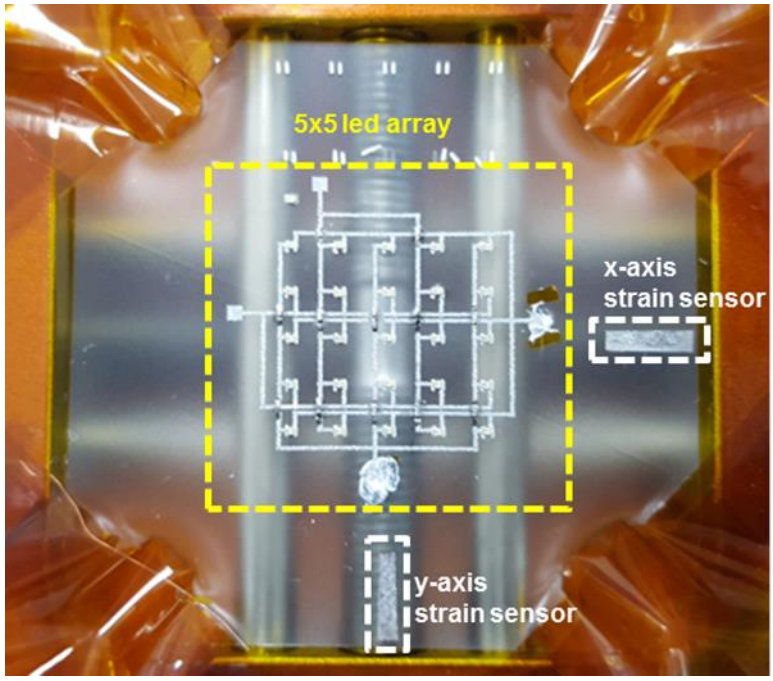

Figure 3.5. Optical image of integrated configuration of bi-axial strain sensors and light emitting device to demonstrate hidden pixels.

3.3. Results and discussions

3.3.1. Characteristics of wrinkled Ag thin film

It is well-known that inkjet-printed metal thin films on bare elastomer substrate start to be fractured even at small tensile strain, finally resulting in a rupture over whole region. In general, there are two reasons about poor mechanical behavior of the inkjet-printed metal thin film. First, hydrophobic surface properties of the elastomeric substrate including PDMS cause poor surface profile of the printed thin film and lead to randomly formed holes in the film. When tensile strain is applied, the hole edges can initiate crack formation. Compared to conventional metal thin film, cracks rapidly initiate and propagate at relatively low strain range. Second, the inkjet-printed metal thin film has extremely low ductility that is resistant to the crack propagation. Unlike other nanomaterial-based thin films, metal NPs-based thin film has no obstacle to suppress the crack propagation and thus the crack propagation occurs at high speed even in low-level deformation conditions. While the former can be optimized via roughened PDMS and the UVO_3 condition [91], the latter requires further continuous study in order to overcome the intrinsically low mechanical properties of the printed thin films.

Wrinkle structure is one of the most popular and effective methods for dissipating external deformation energy applied on the brittle material [3, 17, 72]. A thin film formed on the pre-stretched elastomer has wrinkle structure when the strain is released, and its durability is improved up to the level of pre-strain. However, high Poisson's ratio of the PDMS substrate can cause more complex deformation based

on stress tensor. In addition, low ductility of metals always renders its thin film to be easily fractured. Thus, it should be noted that, in the stretchable electronics, the use of metal thin film is very challenging. Especially, because the unintended crack propagation in the metal thin film causes an abrupt increase in resistance at a certain level of tensile strain, the strain sensors based on metal thin film require a careful optimization process for minimizing the external effect.

3.3.2. Morphological analysis on the asymmetrically pre-strained Ag thin films

In order to emphasize the effect of stress-dissipating structure on the metal thin film, microstructural changes of the thin film were systematically investigated. The samples were uni- or bi-axially stretched as shown in Figure 3.6 and Figure 3.7. In general, the stress-dissipating wrinkle structure allows a conductive thin film to be durable up to the applied pre-strain levels. If the pre-strain is appropriately engineered, the conductive thin film can be used as a strain sensor. while the pre-strain was used for the stretchable electrode application in our previous studies. (Figure 3.8) As mentioned before, it is noted that a metal thin film has unintended cracks parallel to the external force direction due to Poisson effect. If additional external force is applied in the parallel direction, the cracks become larger. Figure 3.6 shows that when only one-directionally (x-axis) pre-strained, the cracks initiated at 20% x-axis tensile strain become larger as y-axis tensile strain increases to 40%. Although the thin film can be used as an x-axis strain sensor over 20% x-axis tensile strain range, unintended large cracks at large y-axis tensile strain deteriorate its strain-sensing performance. On the other hand, when two-directional (both x- and y-axis but with different pre-strain levels) pre-strain is applied, the unintended parallel crack formation is significantly suppressed under bi-axial deformation as shown in Figure 3.7. The thin film has cracks propagated only to the perpendicular direction with respect to the external force even under high y-axis strain ranges. It is also noted that the uni-axially applied pre-strain causes sinusoidal wrinkles, while the thin film that was bi-axially pre-stretched has herringbone pattern. The y-axis strain makes the

herringbone pattern become sinusoidal wrinkle structure by dissipating the y-axis directional strain energy without unintended crack formation.

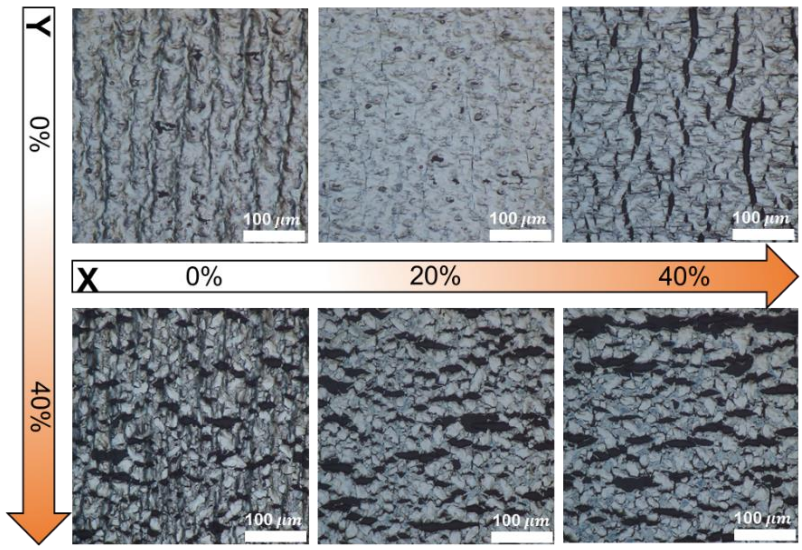

Figure 3.6. Optical images of crack generation on the horizontally pre-stretched (x : 20%, y : 0%) under bi-axial tensile strain. (x : 0%, 20%, 40%, y: 0%, 40%)

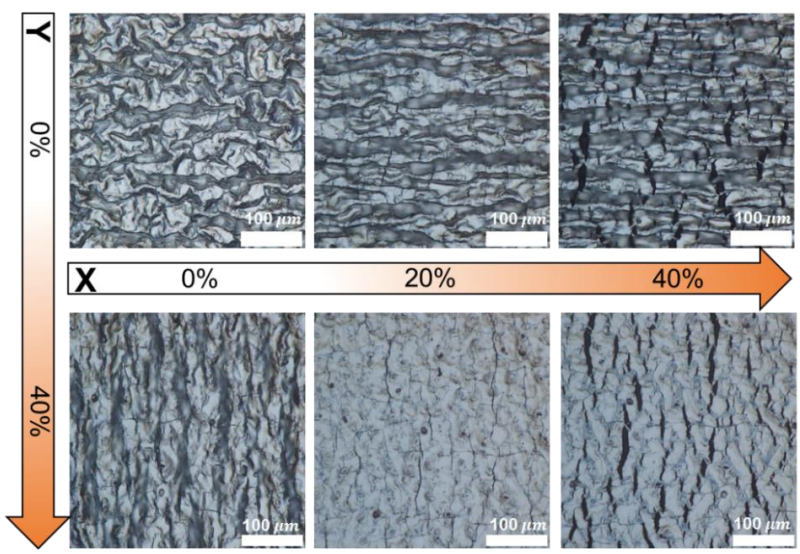

Figure 3.7. Optical images of crack generation on the horizontally pre-stretched (x : 20%, y : 40%) under bi-axial tensile strain. (x : 0%, 20%, 40%, y: 0%, 40%)

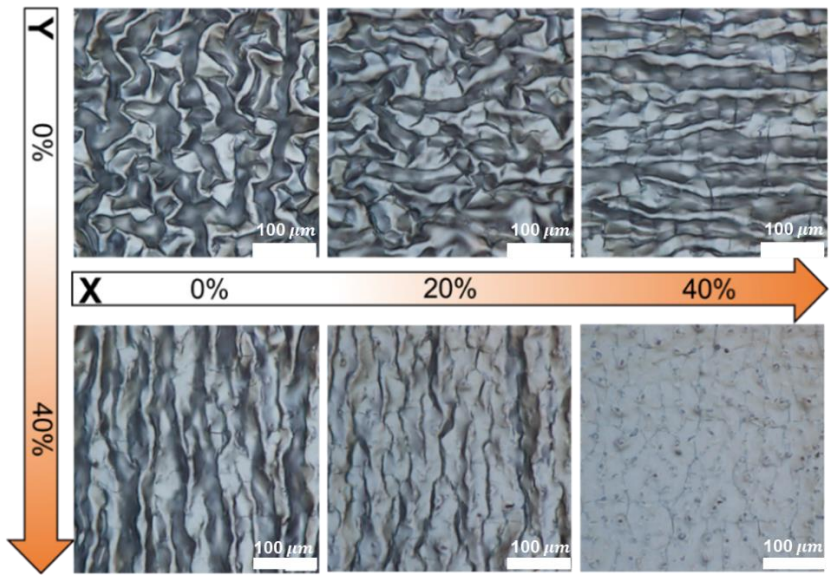

Figure 3.8. Optical images of crack generation on the symmetrically pre-stretched (x : 40%, y : 40%) Ag electrode under bi-axial tensile strain. (x : 0%, 20%, 40%, y: 0%, 40%)

3.3.3. Electrical characteristics of asymmetrically pre-strained Ag film for 2-D strain sensors

Based on the morphological analysis, I analyzed resistance variation for both uni-axially and bi-axially pre-strained thin films. In Figure 3.9, the metal thin film formed on uni-axially pre-strained PDMS substrate (x : 20%, y : 0%) shows no change in resistance at strain range lower than 20% x-axis tensile strain but linearly increasing resistance change is observed at strain ranges between 20 and 40% x-axis tensile strain ranges when there is no external force in y-axis direction. When additional y-axis strain is applied (10, 20, 30, 40%), the resistance variations start to be significantly degraded when compared to the uni-axially pre-strained films. Exponential increase in resistance is observed at strain range greater than 20% x-axis strain, which is closely affected by the unintended crack formation as shown in Figure 3.9. In contrast, when the pre-strain is applied in both x- and y- axis directions (x : 20%, y : 40%), resistance consistently, repeatedly varied resulting in a stably operating x-axis strain sensor as shown in Figure 3.10. This shows that the appropriately engineered metal thin films can act as a strain sensor that responds only to the intended uni-axial direction.

To effectively use the anisotropic strain sensor in bi-axially stretchable electronics, detecting accurate strain signal as well as responding to the intended directional deformation is important. When I use the strain sensor as a trigger device that controls other components in a stretchable system, separate and accurate detection ability becomes more essential. For example, as shown in Figure 3.9, let's assume that I set an input value as 200 ohms at which the trigger device operates. Ag

thin films under x-axis tensile strain (x : 0 ~ 40%) at different y-axis strain loadings (y : 0%, 40%).

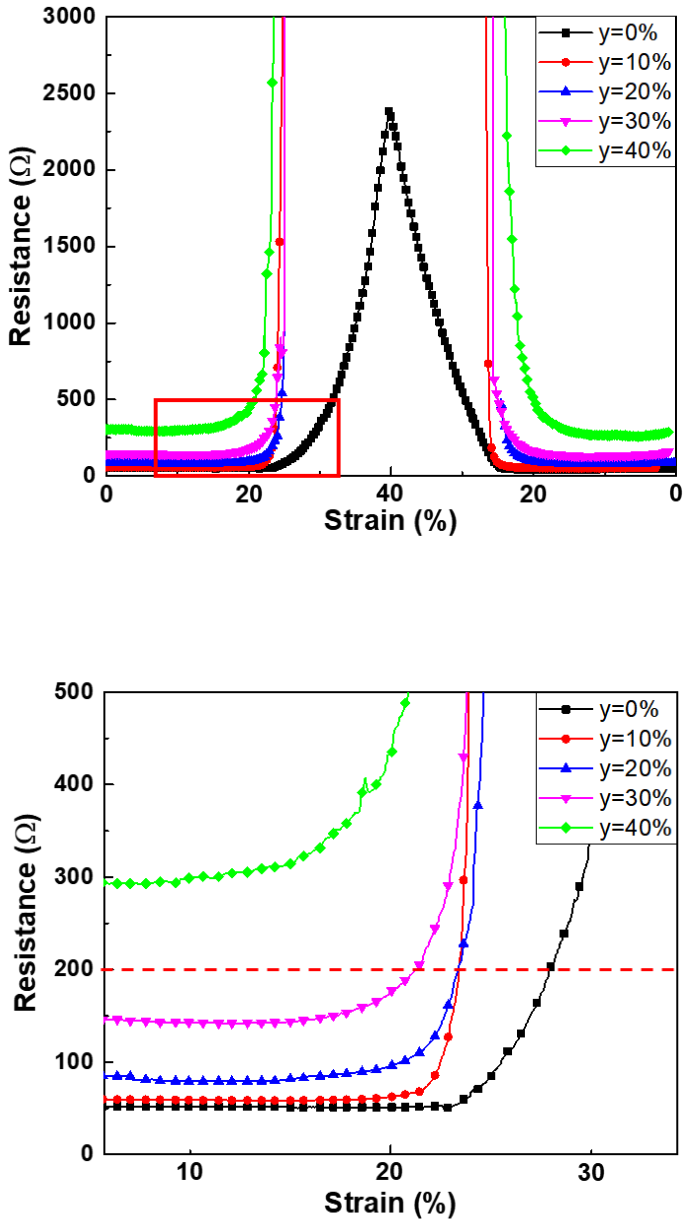

Figure 3.9. Electrical resistance variations of uni-axially pre-strained (x : 20%, y : 0%) x-axis strain sensor under 1 cycle of x-axis tensile strain (x : 0 ~ 40%) at various y-axis strain loadings (y : 0%, 10%, 20%, 30%, 40%).

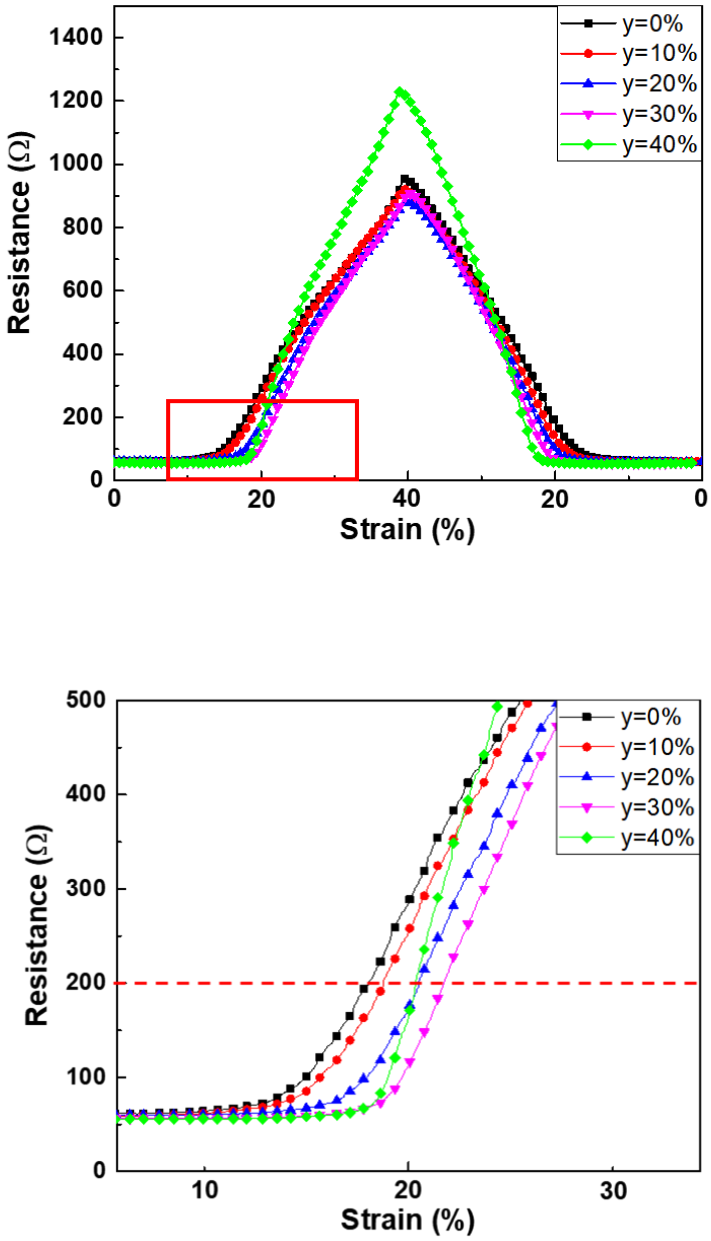

Figure 3.10. Electrical resistance variations of bi-axially pre-strained (x : 20%, y : 40%) x-axis strain sensor under 1 cycle of x-axis tensile strain (x : 0 ~ 40%) at various y-axis strain loadings (y : 0%, 10%, 20%, 30%, 40%).

The uni-axially pre-strained strain sensor shows operating range of 22~28% strain for y-axis strain (0 ~ 30%) range. At high strain (y-axis : 40%) level, the operating trigger loses its function. In contrast, the bi-axially pre-strained strain sensor has operating range of 18~22% with relatively constant steps in the applied strain range. In addition, high sensitivity (gauge factor ~ 20) and linear resistance change allows relatively easy control for adjusting the input triggering value. In addition, to certify the electrical hysteresis and linearity of the strain sensor, electrical resistance variation of the bi-axially pre-strained x-axis strain sensor (x : 20%, y : 40%) under 1 cycle of x-axis strain shows subtle hysteresis due to the visco-elasticity of the elastomeric substrate and excellent linearity (R^2 ~ 0.992) as shown in Fig. 3.11. To investigate reliability of the strain sensor, cyclic tests were performed as shown in Figure 3.12. In spite of harsh conditions (cycling number: 1,000 times, x-axis strain range: 40%), the sample showed reliable and repeatable resistance variation under the bi-axial deformation.

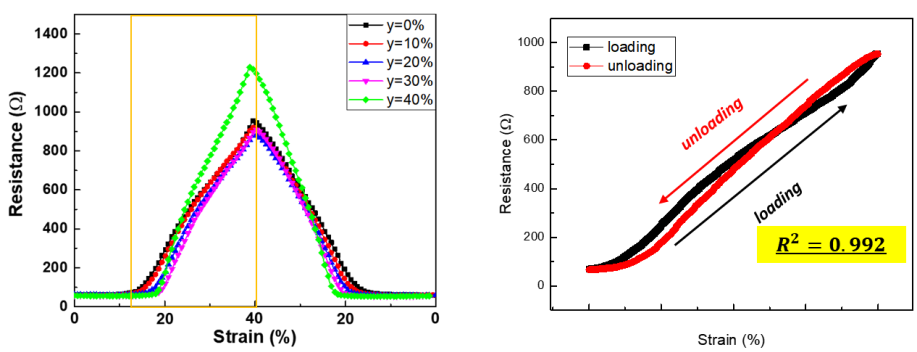

Figure 3. 11. Electrical hysteresis and linearity in bi-axially pre-strained (x : 20%, y : 40%) x-axis strain sensor under 1 cycle of x-axis tensile strain (x : 0 ~ 40%).

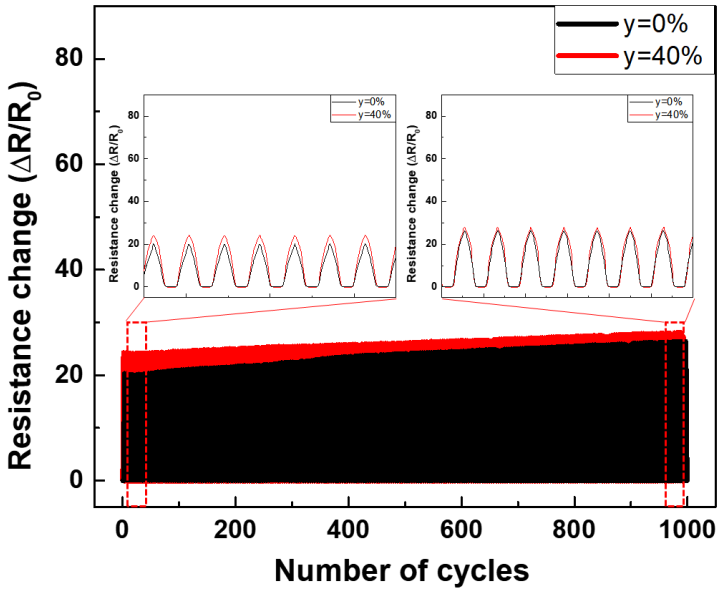

Figure 3.12. Resistance variations of the asymmetrically bi-axially pre-strained x-axis strain sensor (x : 20%, y : 40) in repeated cyclic tests (1000 times) with the strain up to 40% as the function of number of cycles and y-axial tensile strain (y : 0%, 40%).

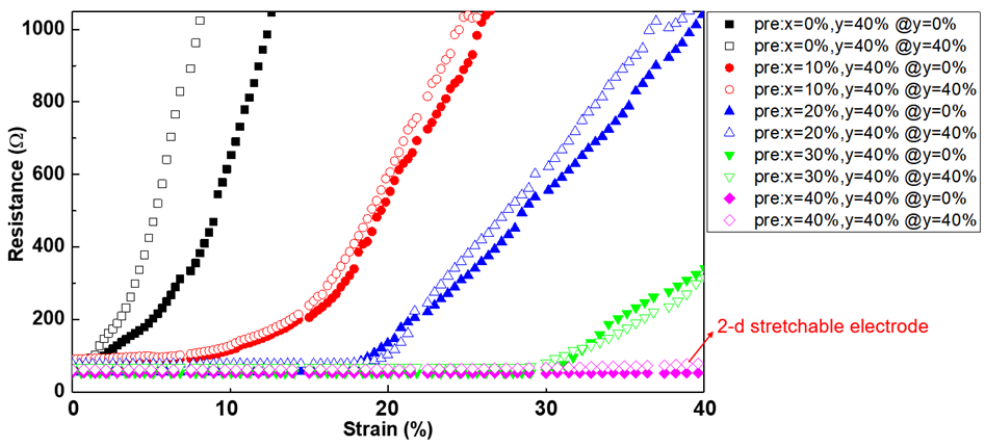

Figure 3.13. Electrical resistance variations of asymmetrically pre-stretched (x : 0%, 10%, 20%, 30%, 40%, y : 40%) and symmetrically pre-stretched (x : 40%, y : 40%)

3.3.4. Hidden pixel demonstration using 2-D strain sensors

3.3.4.1. Principles of selective operation of hidden pixels

In order to show practical usage of the two-directional sensor, I demonstrated a concept of hidden pixel and resolution-sustainable stretchable lighting devices, by utilizing an abrupt resistance increase at a pre-designed strain level as a trigger signal. Figure 3.14 and Figure 3.15 explain how the strain sensors can selectively operate the hidden pixels of the 2-dimensional stretchable array via a trigger device consisting of a voltage divider and a micro controller unit (MCU). As depicted in Figure 3.14, The changes of electrical voltage responding to the resistance variations of strain sensors in each direction (x- and y-axis) are delivered to the programmed MCU, and then, the output voltages of the MCU are individually connected to each contact pad of $\boldsymbol{V_A}$ and $\boldsymbol{V_K}$ on the 2-dimensional LED array in order to change the logic value of the x-axis and y-axis hidden pixels. $\boldsymbol{V_A}$ is connected to every anode of x-axis hidden pixels; $\boldsymbol{V_K}$ is connected to every cathode of y-axis hidden pixels. As shown in Figure 3.15, if we denote the state of voltage HIGH as '1' and voltage LOW as '0', VCC and VK are set to 1, and VA and GND are set to 0 at initial state. All LEDs are designed to turn on only when the cathode value is 0 and the anode value is 1. Whatever the magnitude of applied tensile strain is, the LEDs connected to GND and VCC always turn on (normally ON LEDs) because GND and VCC are always 0 and 1, respectively. When x-axis tensile strain load is more than 20%, MCU converts VK from 1 to 0 switching on the x-axis hidden pixels ((2), (4), (12), (14), (22), (24)). When y-axis strain is loaded more than 20%, MCU converts VA from 0

to 1 switching on the y-axis hidden pixels ((6), (8), (10), (16), (18), (20)). In the same way, when the bi-axial strains over 20% are loaded, VK is converted from 1 to 0 and VA is converted from 0 to 1, switching on all hidden pixels.

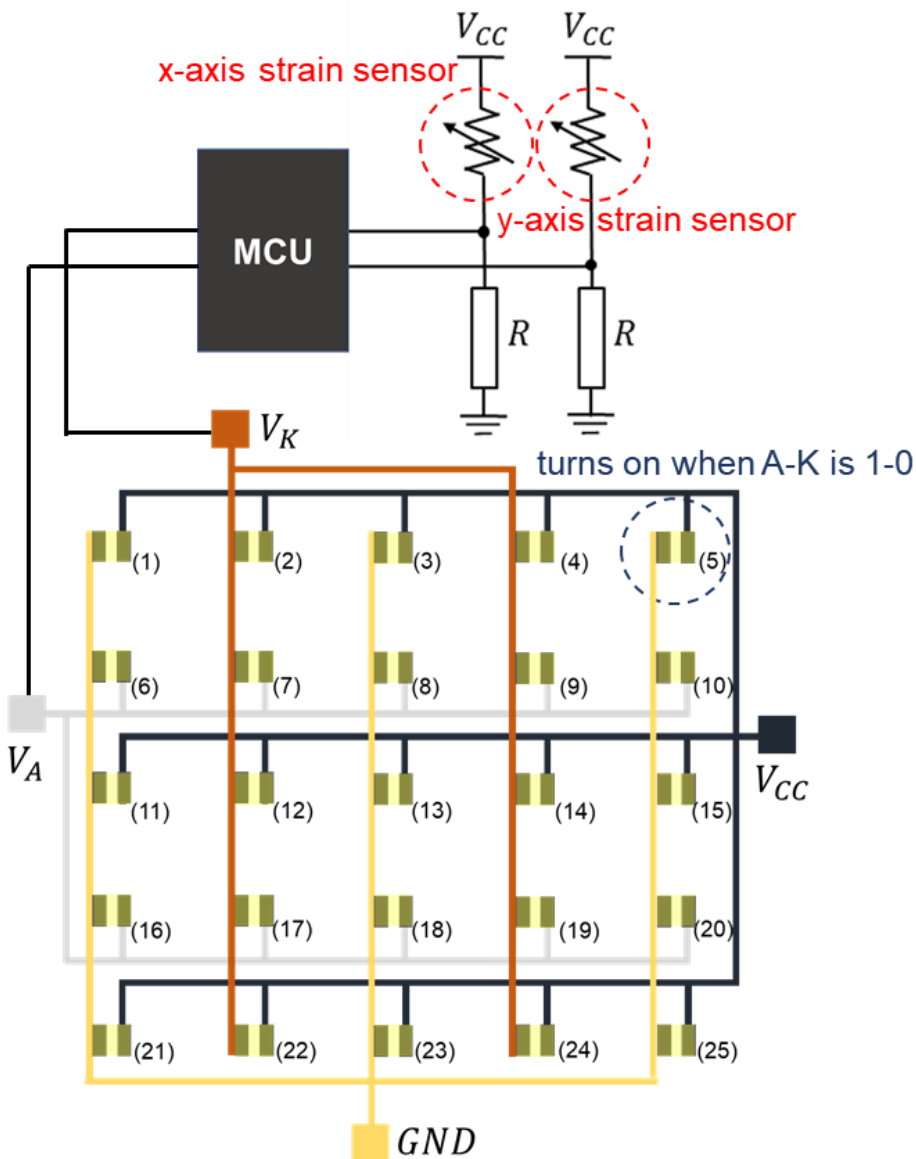

Figure 3.14. Schematic depiction of electrodes array and electrical signal transmission for hidden pixel operation by processing x-axis and y-axis strain information.

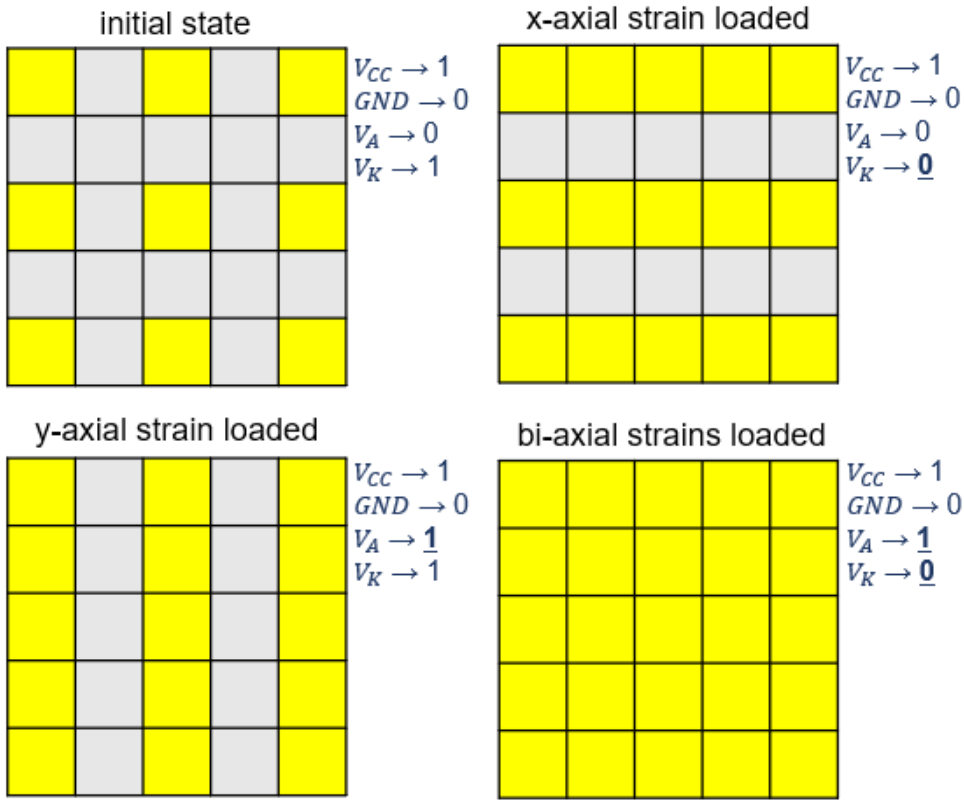

Figure 3.15. Schematic depiction of switching on hidden pixels according to the computed electrical signals under bi-axial tensile strain.

3.3.4.2. Hidden pixel demonstration on 2-D lighting device

Figure 3.16 - 3.19 show optical images of actual operation of 2-dimensional lighting device array through selective hidden pixel switching process under bi-axial strains. The stretchable Ag electrodes connected with 5×5 LEDs and the bi-axial Ag strain sensors are all integrated on a single PDMS layer, and the inevitably following overlapped areas of Ag electrodes were insulated by coating a thin PDMS layer between the crossed electrodes. The strain sensors and the electrode pads were electrically connected to the external MCU by thin copper wires contacted with liquid metal. The elastomeric platform is firmly bi-axially fixed to the commercially customized bi-axial stretching equipment, and it can be easily stretched and released by simple manipulation. According to the logic flow described above, the pixels other than the LEDs which are switched on at the initial state are respectively switched on and off according to the tensile strains of the x-axis and/or the y-axis. The Ag strain sensors provide independent switching operation of the hidden pixels by responding to the directional deformation, and it also works well when releasing the strain. The hidden pixels and the selective operation serve sustainable resolution to the stretchable lighting devices. It is also noted that the application fully utilizes its stretchability under bi-axial deformation when considering Poisson's ratio of the PDMS substrate. Our results well demonstrated the characteristics of the anisotropic crack-based strain sensor and the use of direction-designed switches on the bi-axially stretchable application.

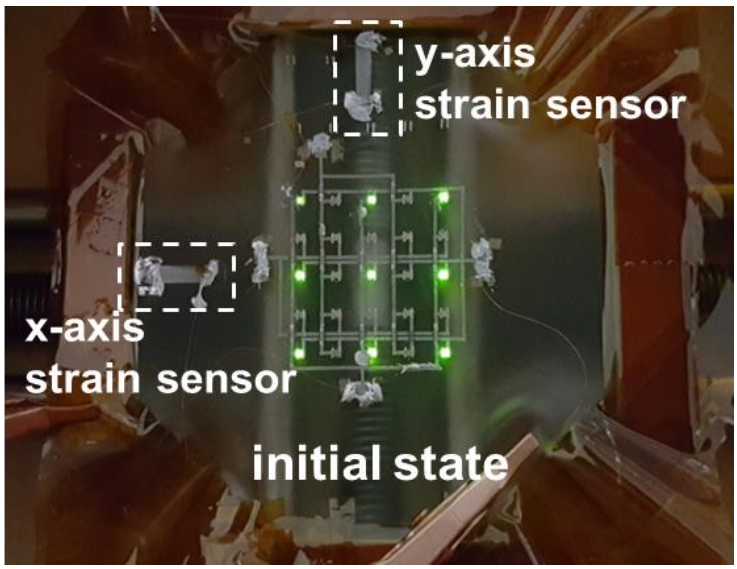

Figure 3.16. Optical image of selective pixel operation of stretchable lighting device from electrically decoupled x-axis and y-axis Ag strain sensors at initial state.

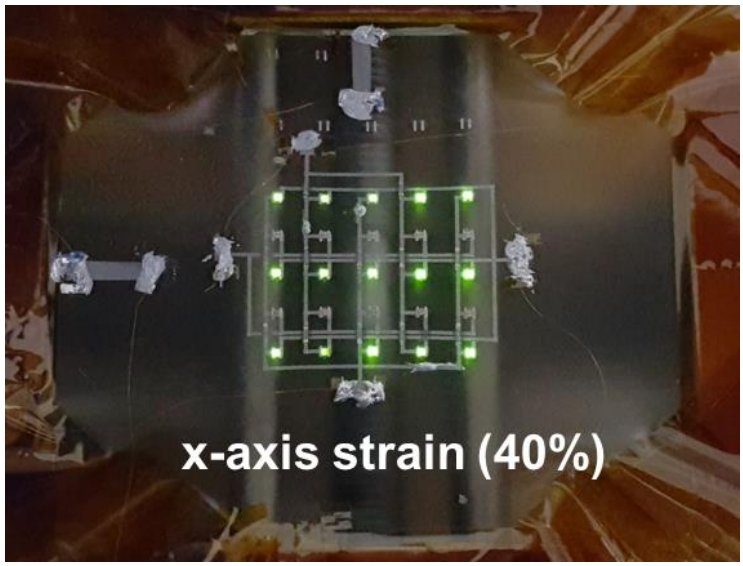

Figure 3.17. Optical image of selective pixel operation of stretchable lighting device from electrically decoupled x-axis and y-axis Ag strain sensors under x-axis strain (40%).

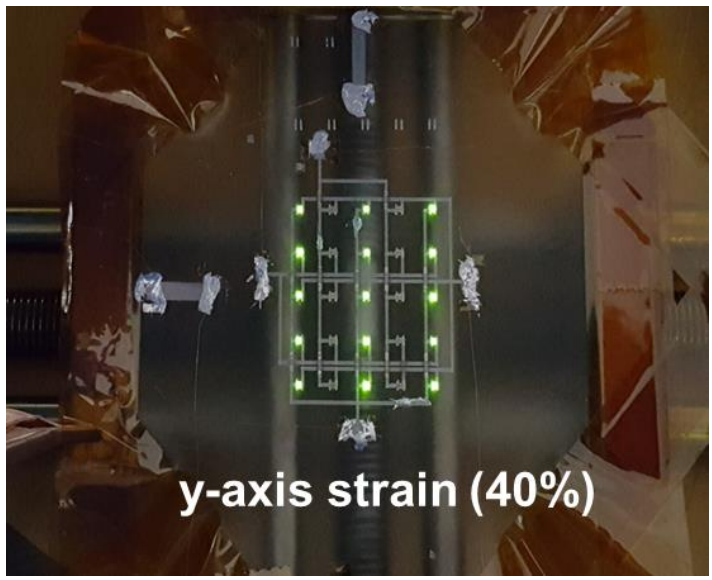

Figure 3.18. Optical image of selective pixel operation of stretchable lighting device from electrically decoupled x-axis and y-axis Ag strain sensors under y-axis strain (40%).

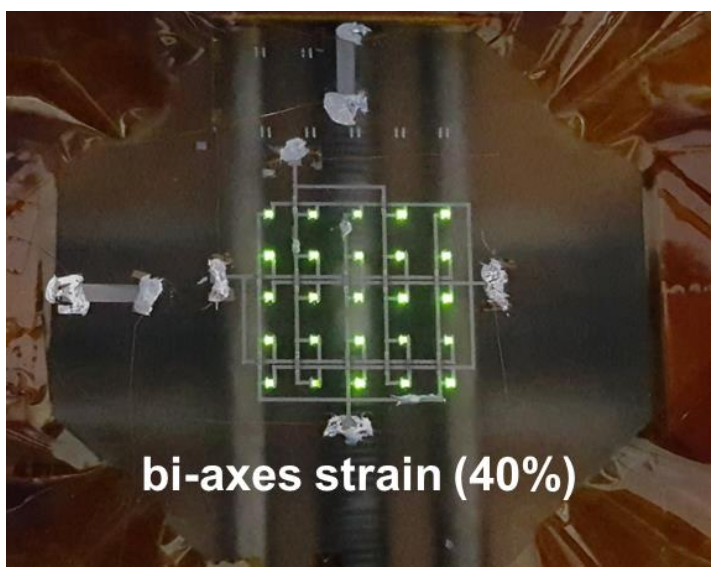

Figure 3.19. Optical image of selective pixel operation of stretchable lighting device from electrically decoupled x-axis and y-axis Ag strain sensors under bi-axial strain (x : 40%, y : 40%).

3.4. Summary

To summarize, I have presented Ag NPs based multidimensional strain sensors, which can separately detect strain signal in each orthogonal direction, by utilizing asymmetric pre-stretching technique through facile and low-cost inkjet-printing fabrication process. From the fabricated strain sensor, I obtained a linear and stable resistance variation with high gauge factor of ~20 from 20% to 40% tensile strain. Besides, our approach based on the anisotropic cracking mechanism can not only reduce the effect of high Poisson's ratio of PDMS on the strain-sensing performance but also provide a convenience of single-layered platform for two-directional strain sensing. According to this method, I demonstrate a conceptual lighting device which sustains constant image resolution utilizing hidden pixels that turn on to compensate the reduced resolution from the increased distance between adjacent pixels when the platform is stretched. As these multi-dimensions detectable strain sensors are also applicable to wearable electronics, it is expected that it may have an impact on future devices which are capable of monitoring and controlling of complex surface conditions.

Chapter 4

Crack-focused Phenomenon on Inkjet-printed Silver Strain Sensor with High Sensitivity for Applications in Human-machine Interactions

4.1. Introduction

With the progress of robotic systems and wearable devices [14-22], many efforts have been devoted to user-interface technology between human and electronic devices to more efficiently operate device in the way which produces desired result. Among them, force touch system [20, 23-25], which is capable of sensing how deeply users press the solid screen as well as the location of the touch, has been one of the most representative strategies. (Figure 4.1) It enables users to more intuitively manipulate their devices by offering versatile input methods. For the sensor that is placed at the backside of the display screen to detect the slight bending of it, to accurately distinguish between the levels of the force applied to the rigid surface, it is imperative to implement sensor with great sensitivity. To obtain commercially available sensing device, there have been various pressure sensing mechanisms such as capacitive [20, 24], resistive [14, 23, 68] and piezo-electric [92] sensors.

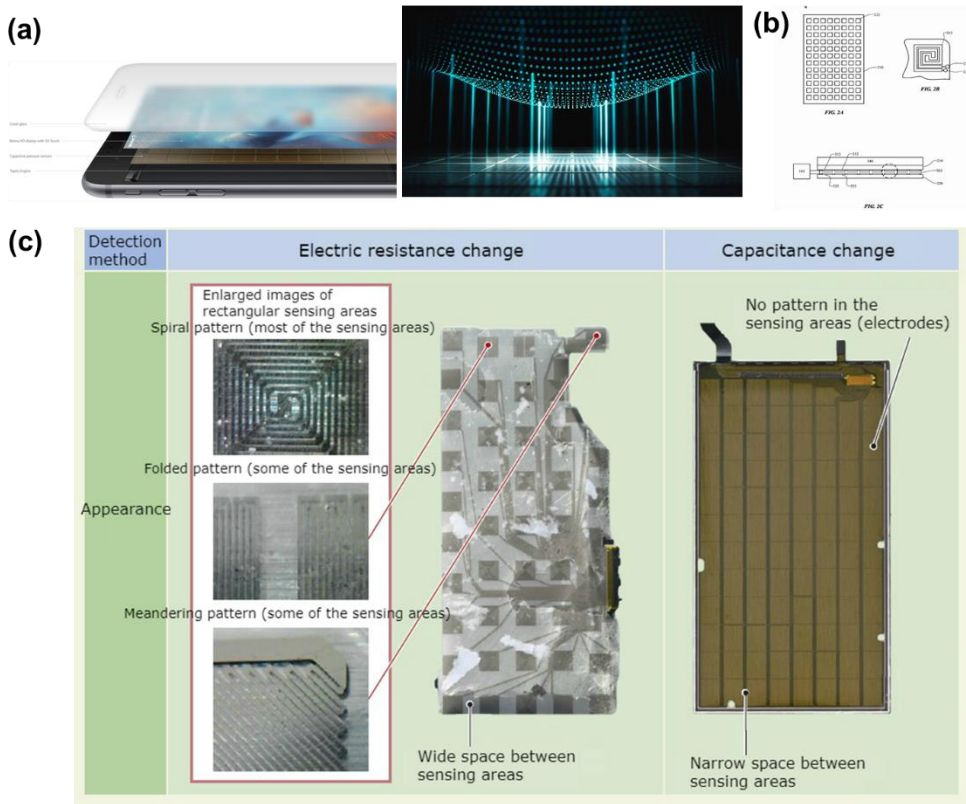

Figure 4.1. (a, b) Commercialized force touch sensing modules embedded in smartphone and (c) resistive and capacitive strain-gauge matrix to precisely detect both the locations and extent of force applied to the surface.

Among them, capacitive type sensor that detects the distance of electrodes has been preferred for its high sensitivity and low power consumption, which, however, gets bulky as it necessarily contains dual electrode layers. On the other hand, resistive sensing could be mostly realized by the resulted resistance variation due to the change in conduction paths that are connections of conductive materials, which results from the deformation of the elastomeric medium by external force. However, highly sensitive resistive sensor has been obtained with morphological modification such as interlocked or pyramidal structures which demand complex fabrication

process.

Unlike conventional resistive pressure sensor, exerted force could be also transduced to the change in electrical resistance according to the geometrical or morphological deformation of the strain sensor [23]. Moreover, each strain sensor could be configured in the form of single-layered matrix in a large-area scale, which helps to elaborately specify the amount and the position of applied force. Among the various phenomena for detecting strain, piezoresistive phenomenon including crack generation [16, 17, 19, 21, 22, 41, 69, 73-77] has widely been utilized in many strain sensing fields for its high sensitivity [17, 19, 22, 68, 69]. A variety of conductive materials such as carbon nanotubes (CNTs) [21, 75, 85], poly (3,4-ethylenedioxythiopene) :poly (styrenesulfonate) (PEDOT:PSS) [75, 86], metal nanoparticles (NPs) [17, 18, 21, 22, 41], metal nanowires [73, 74, 82], and graphene [93] have been proposed for use in crack-based strain sensor, forming complex percolated conductive networks which are connected and disconnected by external strain to determine electrical conductance change. Although the brittle nature of metal NPs enables the film to be highly strain-sensitive, few papers regarding metal NPs-based strain sensor have been reported owing to its intrinsically poor mechanical stability which causes entire rupture of channel even under low strain range. However, for the strain sensor to be utilized as force touch application, it ought to detect the minute flexure of rigid force receiving layer (FRL) on top of it. Thus, cracking phenomenon at slight bending is suitable for the sensor that requires extreme sensitivity.

Here, I propose a strategy by using strain sensor with Ag nanoparticles (Ag NPs) based thin film that is inkjet-printed onto a poly(dimethylsiloxane) (PDMS) substrate. In addition, to enhance sensitivity of the sensor, vertical silver (Ag) patterns were

inkjet-printed prior to the Ag film, which aimed to generate increased cracks around them. Also, the serpentine geometry of Ag film enabled the sensor to contain multiplied number of vertical patterns, which accordingly multiplied the sensitivity. In addition, the sensitivity of the sensor was not only determined by the structures of sensor, but by the rigidity of the FRL that was positioned on top of the sensor as well. Accordingly, the sensor integrated with thin plastic FRL was applicable to the health monitoring device that is capable of measuring arterial pulse which requires great sensitivity. Besides, since the impact of the force applied on the device was supposed to be transmitted via elastic FRL, the pulse detecting device was not necessarily put on the skin above artery, which allowed users to casually wear the monitoring device on their wrists. On the contrary, the sensor attached to rigid FRL was able to detect the small flexure of solid substrate with lower crosstalk effect, which enabled the sensor to be implemented as force touch sensor. Thus, I fabricated integrated system with single-layered 5 × 5 strain sensor matrix to demonstrate the force touch application. The performance of the fabricated device was verified by showing the output signals of each sensing pixel in response to external force applied on a pixel in 3-level pressures, and it was noticeable that the sensitivity of sensor surpassed that of commercialized sensor.

4.2. Experimental methods

4.2.1. Fabrication of strain sensor

As shown in Figure 4.2, to fabricate a PDMS substrate (thickness : 300 μm), the 10:1 weight ratio mixture of PDMS (Sylgard 184 from Dow Corning) and curing agent was spin-coated onto an aluminum mold, followed by annealing at 120 ℃ for 30 minutes. After detaching the cured PDMS substrate from the mold, 6 Ag vertical patterns were formed by inkjet-printing 10 layers of non-particle based Ag ink (Jet-600C from KS Hisense) onto the hydrophobic PDMS substrate which was located on a heated plate (60 ℃) by using a piezo-electric inkjet printer (DMP-2831 from Dimatix Corp.) with with 21 μm diameter nozzles. The nozzle extruded 10 pL Ag ink for each droplet and the drop space was 40 μm. Afterwards, to increase the surface energy, the composite was treated with UV ozone and a layer of NP based Ag ink (DGP-40 from ANP Corp.) was additionally inkjet-printed onto the vertical patterns at 60 ℃ to fabricate strain sensor. The nozzle extruded 10 pL Ag ink for each droplet and the drop space was 35 μm.

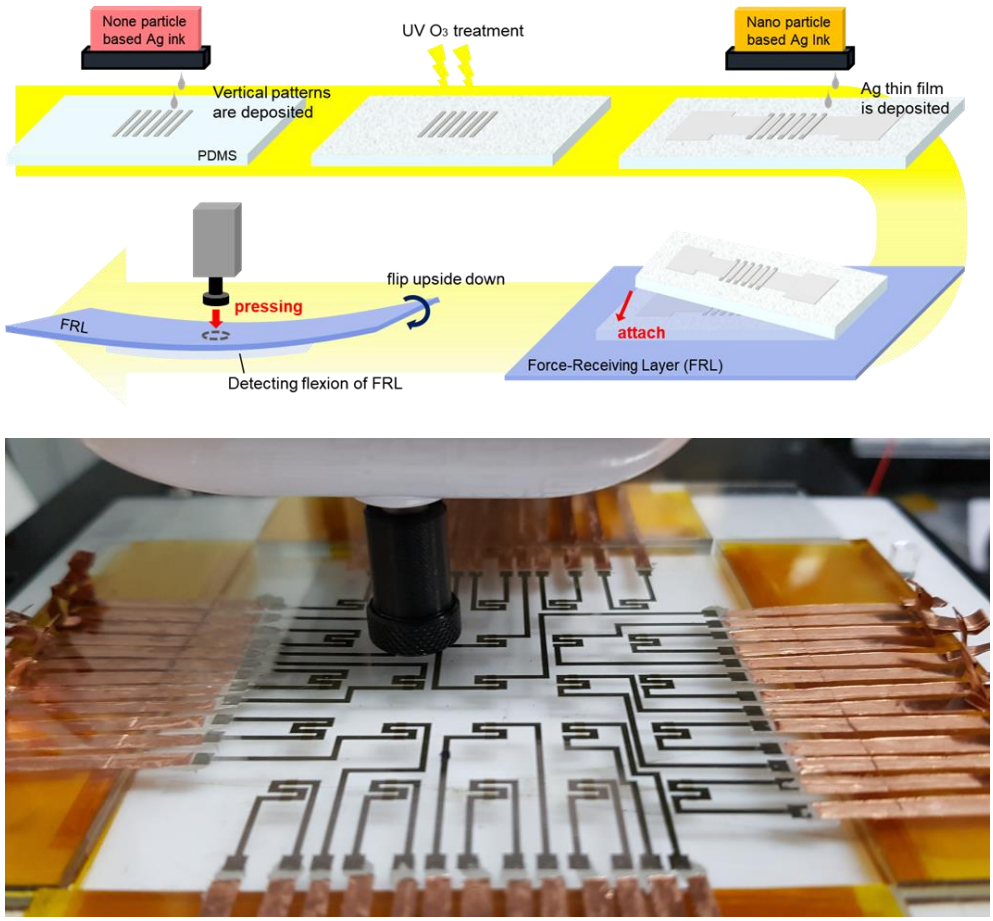

Figure 4.2. Schematic illustration of the whole process flow of fabricating vertically patterned strain sensor by inkjet-printing process and measuring flexion of FRL that was caused by pressure loading.

4.2.2. Measurement

As the main purpose of the strain sensor is to measure the flexure of the FRL, I turned the composite upside down and attached it to the bottom of FRL as depicted in Figure 4.2. Several types of FRLs (100 μm thick PET (polyethylene terephthalate), 1200 μm thick PET, 400 μm thick glass) were used according to the purpose of the measurement in this work. Then, I applied external pressure onto the top of FRL using push-pull gauge (DTG-1 from Digitech Corp.) with 7mm width load cell to obtain output signals of the strain sensor under pressure loading. Measuring the electrical characteristics of the resistive strain sensor was performed with a source meter (Keithley 2400 from Tektronix). The resistivity of the strain sensor was measured by applying voltage of 0.1 V throughout the sample.

4.3. Results and discussions

4.3.1. Crack-focused phenomenon on Ag strain sensor for high sensitivity

For the stretchable strain sensor development, conductive films made up of 2D nanomaterials such as nanotube and nanowire have been widely utilized owing to their excellent mechanical stability, which is maintaining good electrical conduction paths under external strain. On the other hand, researches on metal NPs based films have rarely been reported owing to their poor durability, as the cracks on the film start to easily propagate at the edges of randomly formed voids according to the poor surface property between deposited film and PDMS substrate. Besides, metal NPs thin film itself is intrinsically vulnerable to external strain, which brings about rapid crack initiation and generation even under in low-level deformation conditions, which accordingly leads to entire channel rupture. Hence, metal NPs based films have rarely been utilized as strain sensors with wide working range, unless further strategies to dissipate the strain energy from the elongated platform have not been taken. Nevertheless, crack based Ag NPs strain sensor can be utilized in detecting very small applied pressure such as human monitoring device measuring pulse [16, 17, 19, 21] or force touch sensor for user-interface technology that demands extreme sensitivity at a very low stimuli level in order to measure the amount of small bending of the FRL by the applied pressure on it.

In order to increase the sensitivity of the inkjet-printed Ag NPs strain sensor, in this work, Ag vertical patterns were inkjet-printed layer by layer onto the

hydrophobic surface of PDMS previous to the deposition of the Ag NPs based film as shown in Figure 4.3 (a). Then, as the cracks are well known to be easily generated at the region on the film with high difference in height, where the stress by external strain is most focused, I aimed to control and augment the cracks generated around the patterns. (Figure 4.3 (b))

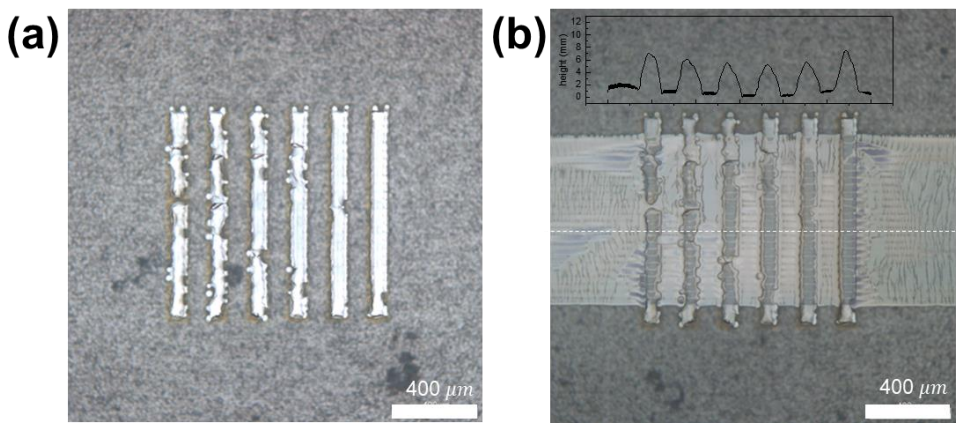

Figure 4.3. Optical images of (a) inkjet-printed Ag vertical patterns and (b) fabricated Ag strain sensor.

4.3.2. Morphological analysis on the effect of vertical patterns to crack generations on Ag strain sensor

To certify the effect of the vertical patterns to the crack phenomenon on the strain sensor, microstructural changes were optically analyzed in Figure 4.4. The samples were prepared as bending state to exert very small strain on them. Compared to the Ag film without vertical patterns (Figure 4.4 (a) and (b)), it was observed that the ridge-like structure caused micro-cracks at the edges of patterns, where the stress by external stimuli was mostly concentrated, as shown in Figure 4.4 (c-f). In addition, compared to the film (10 layers of vertical patterns) that generated regular width of vertical micro-cracks along the patterns as shown in Figure 4.4 (c) and (d), it is noted that much larger cracks were generated around patterns on the film (30 layers of vertical patterns) leading to complete isolation of the conduction paths in Figure 4.4 (e) and (f).

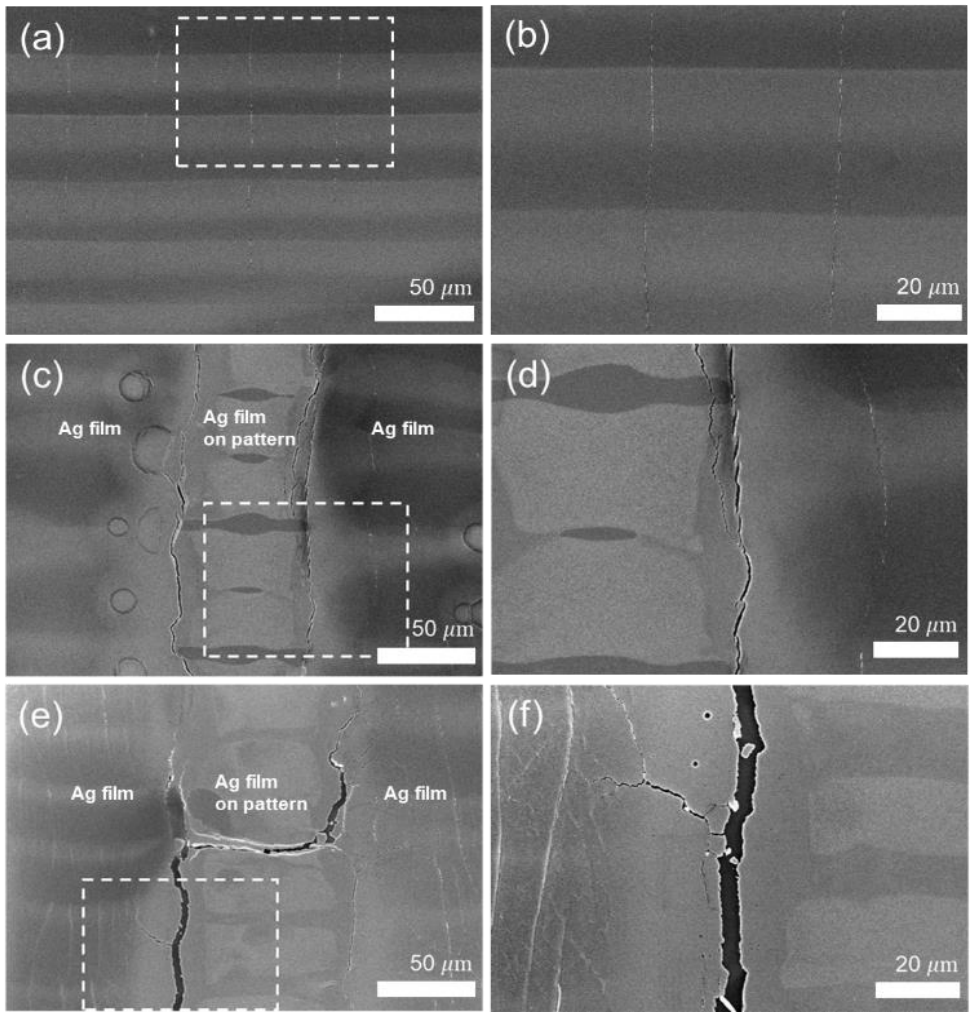

Figure 4.4. Optical images of crack generation on the (a, b) Ag film without vertical patterns, and (c-f) Ag film with vertical patterns ((c, d) 10 layers and (e, f) 30 layers) under very small strain.

4.3.3. Gauge factor for sensitivity of Ag strain sensor

Based on the morphological analysis, electrical resistance variations of the sensor were analyzed. First, to evaluate the sensitivity of a resistive strain sensor, the rate of relative change in electrical resistance to mechanical strain, termed as gauge factor (GF), is usually denoted as equation (1) :

$$\text{Gauge factor} = \frac{\Delta R/R_o}{\Delta L/L_o} \tag{1}$$

where R and L denotes the resistance and the length of the strain sensor, respectively. Therefore, the calculated high gauge factor value represents high strain-sensitivity of the sensor. However, in this work, as the extent of elongation of the sensor by applied touch is too small to be measured in degree of strain, the induced strain on the sensor can be theoretically derived from the equation (2) [94, 95] :

$$\varepsilon = \left(\frac{1}{r} - \frac{1}{r_o}\right)\left(\frac{t_f + t_s}{2}\right)\frac{1+2\eta+\chi\eta^2}{(1+\eta)(1+\chi\eta)} \tag{2}$$

where r is the bending radius ($r_o = 19.5\,mm$), and t_f and t_s are film (PDMS (thickness ~ 300 μm) and substrate (PET (thickness ~ 100 μm) thickness, respectively. χ and η are defined as $\chi = {Y_f}/{Y_s}$ and $\eta = {d_s}/{d_f}$, where Y_f and Y_s are Young's moduli of film and substrate. As χ is negligible in our experiment, equation (2) can be simplified as

$$\varepsilon \approx \left(\frac{1}{r} - \frac{1}{r_o}\right)\left(\frac{2t_f + t_s}{2}\right) \quad (3)$$

As a result, GF of ~70 of the strain sensor was obtained by from the induced strain and the changes in resistance of the sensor at the bending state that are shown in Figure 4.5.

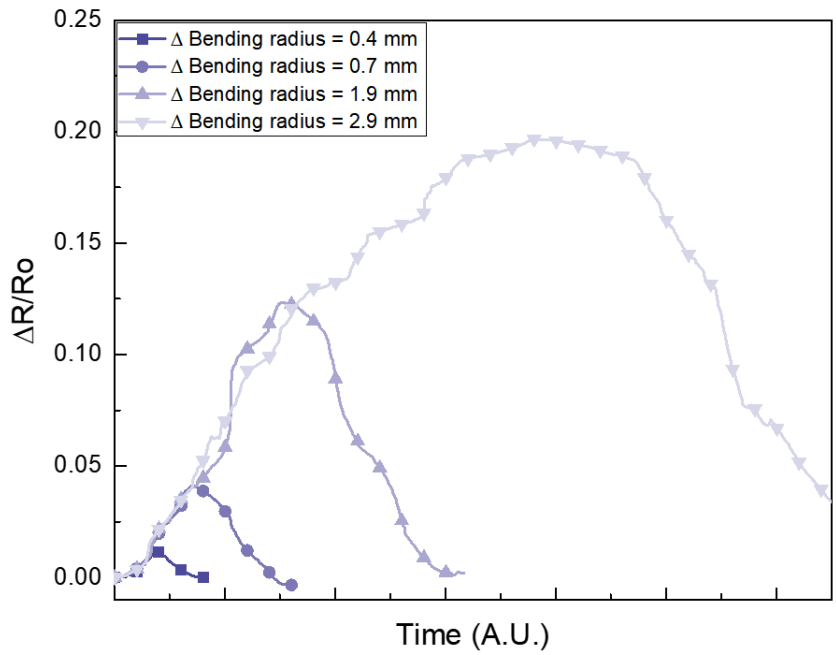

Figure 4.5. Electrical resistance variations of strain sensor under bending state at various changes in bending radii (Δr = 0.4, 0.7, 1.9, 2.9).

4.3.4. Electrical characteristics of Ag strain sensor

Thus, to investigate the strain-response of the sensor that was integrated with FRL to measure the flexure of it, the experiments for the resistance variations of the strain sensor exhibited in Figure 4.5 - 4.10 were conducted by assembling the sensor with 1200 μm thick PET layer as FRL. Figure 4.6 and Figure 4.7 show the effect of the thickness of vertical Ag patterns to the resistance variation of the sensor when external force (800 gf) was applied on it. As the Ag vertical patterns, denoted as the number of printed pattern layers, got thicker, cracks were more easily generated along the vertical patterns due to the higher difference in height, which caused the steeper change in resistance as depicted in Figure 4.6. Yet, the linearity of resistance variation got poorer with the printed layers of the patterns over 10, which was caused by abrupt and huge crack generation. Besides, through the repeated cyclic test (cycling number : 1,000 times, applied force : 800 gf), the mechanical stability of the sensor was not guaranteed on the sensor with more than 10 pattern layers, as shown in Figure 4.7. In addition, to certify the electrical hysteresis and linearity of the strain sensor, electrical resistance variation of the strain sensor under 1 cycle of pressure loading shows inevitable hysteresis due to the visco-elasticity of the elastomeric substrate and decent linearity (R^2 ~ 0.992) as shown in Fig. 4.8. Similarly, in Figure 4.9, increase of the number of patterns (n = 0, 1, 2, 3, 6) caused the increase of resistance variation of the strain sensor, as the overall cracks that were generated on the film accordingly increased under external force (800 gf). The maximum number of patterns of the sensor in transverse direction was determined to the area where the external force was applied. Furthermore, as shown in Figure 4.10, for the sensor to

contain more patterns, serpentine design that was also included in longitudinal range of the pressed area was utilized to enhance the sensitivity of the sensor. Therefore, the resistance variation was followingly multiplied in proportion to the number of the patterns (n = 6, 12, 18) under the same applied force (800 gf). (Figure 4.11) Then, to insist the ability to distinguish the exerted force within wide working range up to 1,000 gf, the fluctuations of resistance variation at various applied forces from 100gf to 1000 gf were also exhibited. (Figure 4.12)

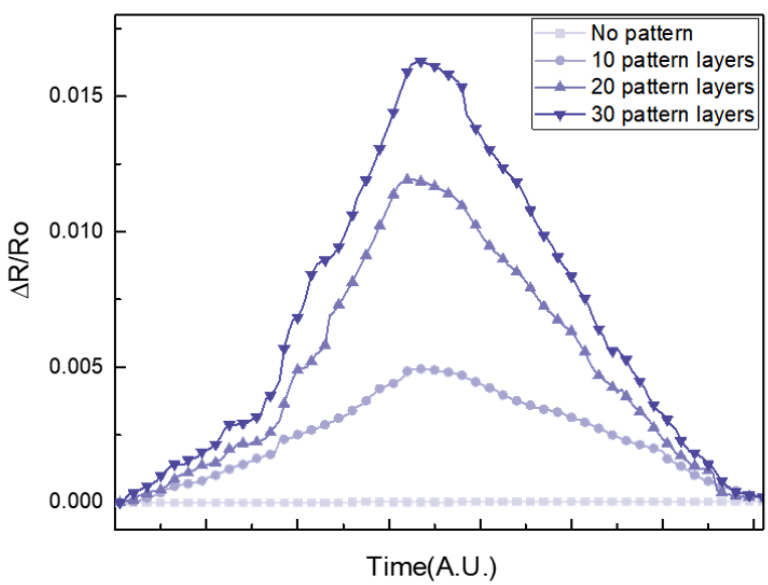

Figure 4.6. Electrical resistance variations of strain sensor under pressure loading (800 gf) at various number of vertical patterned layers (n = 10, 20, 30)

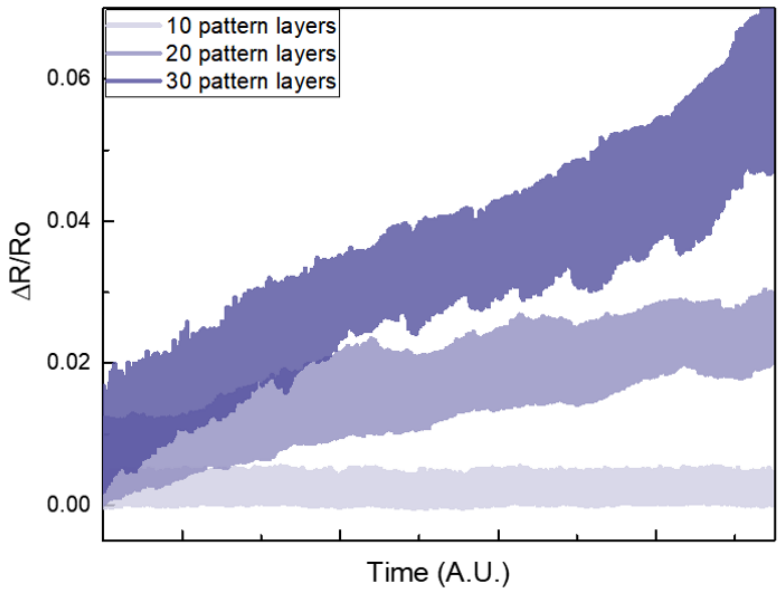

Figure 4.7. Repeated resistance variations of strain sensor under 1k cylces of pressure loading (800 gf) at various number of vertical patterned layers (n = 10, 20, 30)

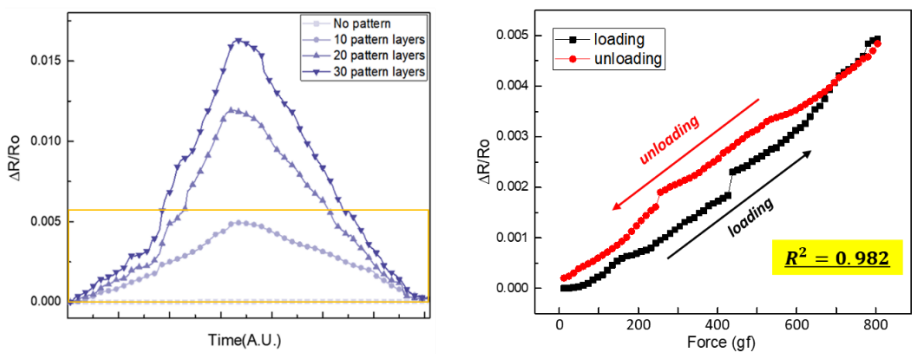

Figure 4.8. Electrical hysteresis and linearity of strain sensor under pressure loading (800 gf) at 10 layers of vertical patterns.

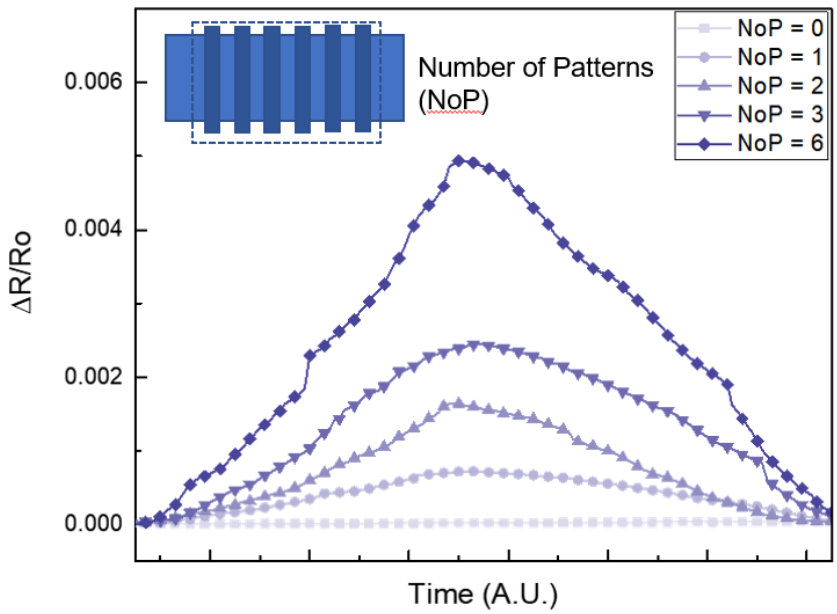

Figure 4.9. Resistance variations of strain sensor according to the number of vertical patterns. (n = 0, 1, 2, 3, 6)

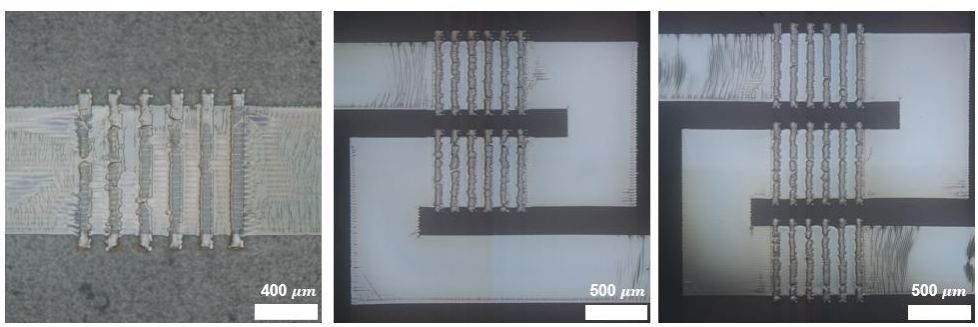

Figure 4.10. Serpentine design of Ag strain sensor to contain increased number of vertical patterns. (n = 6, 12, 18)

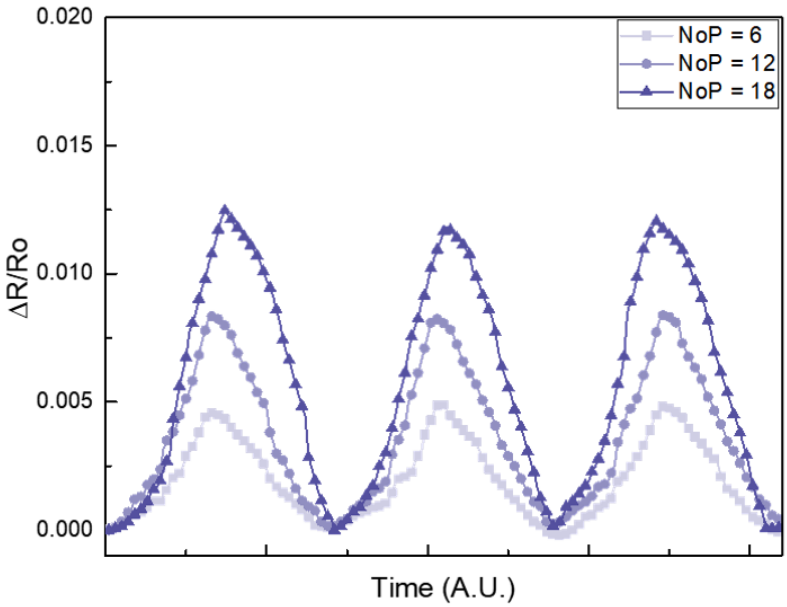

Figure 4.11. Resistance variations of strain sensor according to increased number of vertical patterns by serpentine design. (n = 6, 12, 18)

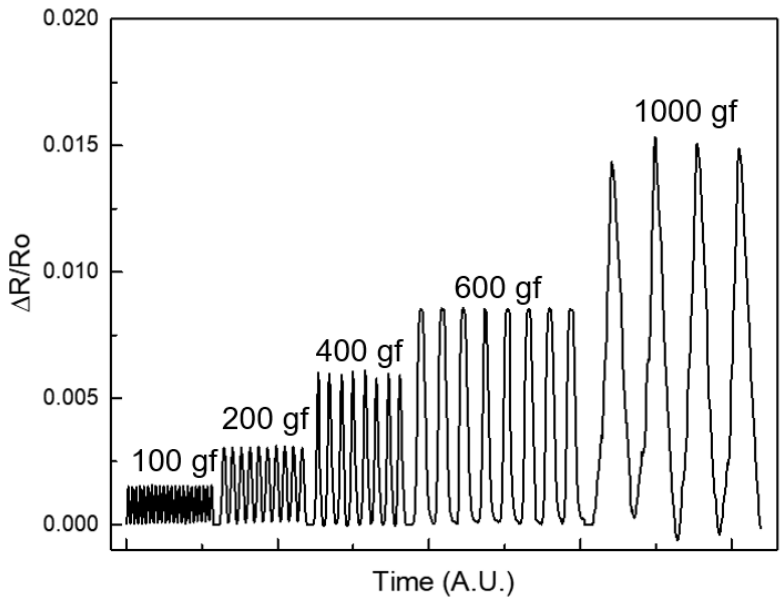

Figure 4.12. Fluctuations of resistance in strain sensor as a function of various range of pressure loadings (100 gf, 200 gf, 400 gf, 600 gf, 1000 gf).

4.3.5. The effect of FRL to the sensitivity and crosstalk-effect of Ag strain sensor

As the strain sensor was structurally designed to measure how the FRL deflected by external force, the physical properties of FRL such as rigidity and thickness played a crucial role in performances of the sensor. If the thin PET (thickness : 100 μm) was chosen as FRL instead of solid FRL such as thick PET (thickness : 1,200 μm) and solid glass (thickness : 400 μm), the sensor responded much more sensitively to the applied force (10 gf) as exhibited in Figure 4.13. However, as shown in Figure 4.14, the excessive flexure of the elastic FRL by external force over 10 gf caused the channel on metal film to be electrically isolated, thus the strain sensor integrated with thin PET (thickness : 100 μm) was suitable for measuring very small force. On the other hand, similar resistance variations of sensors were obtained by the integration with solid FRL (PET (thickness : 1200 μm), glass (thickness : 400 μm) under external force of 200 gf. Furthermore, as the force applied on the FRL caused adjacent area of the layer to be deformed as well, the crosstalk effect of the sensor array was analyzed as shown in Figure 4.15. When I applied external force to a sensing pixel (P_O), the relative sensitivities of each pixel (P_1, P_2, P_3, P_4) to that of P_O were verified according to various FRLs. It is noted that the crosstalk effect of the sensor combined with thin PET was remarkable due to its high elasticity compared to other FRLs.

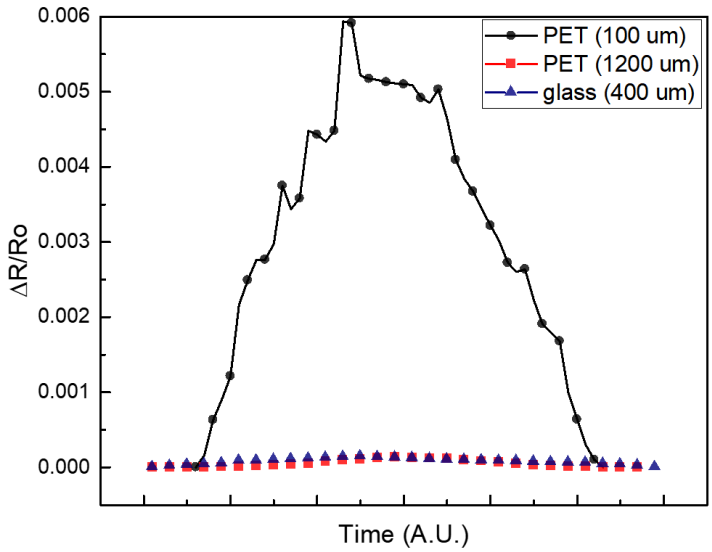

Figure 4.13. Resistance variations of strain sensor attached to the various FRL (100 μm and 1200 μm thick PET, 400 μm thick glass) under external pressure loading (10 gf).

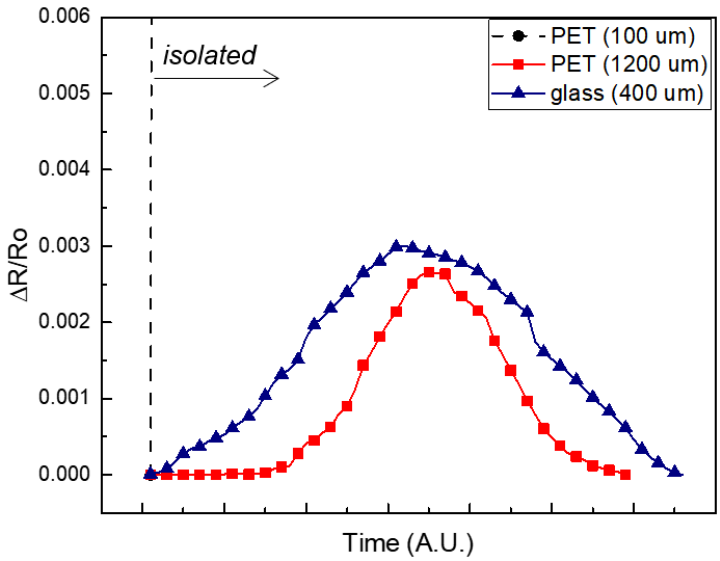

Figure 4.14. Resistance variations of strain sensor attached to the various FRL (100 μm and 1200 μm thick PET, 400 μm thick glass) under external pressure loading (200 gf).

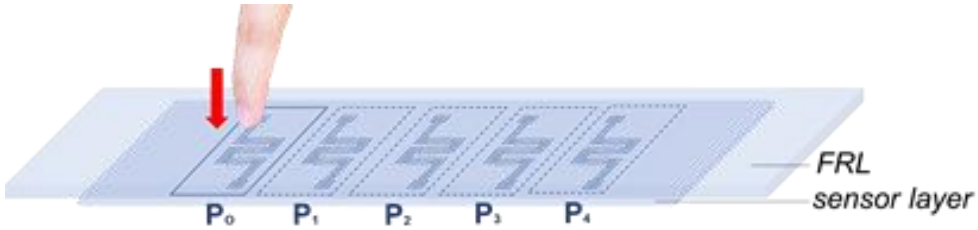

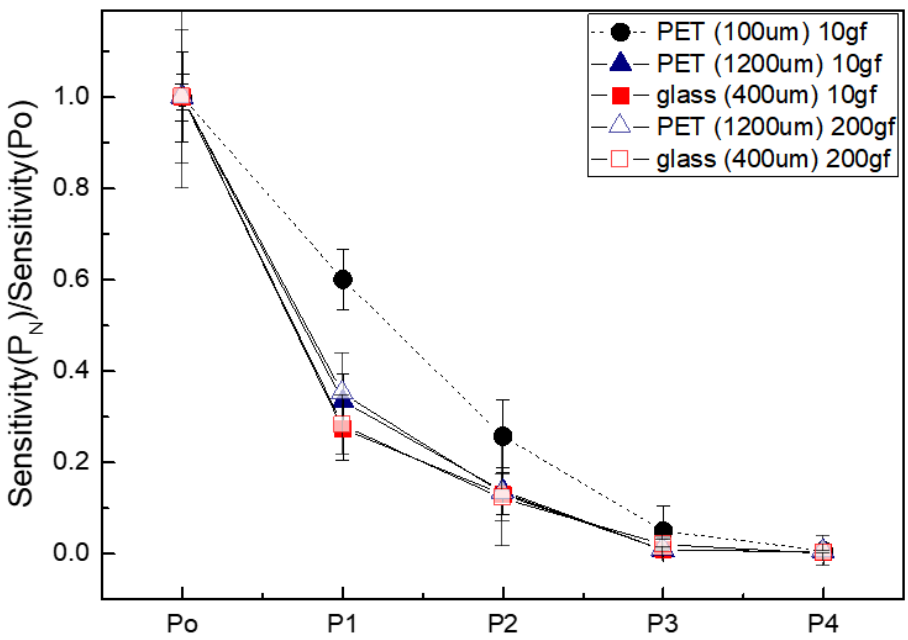

Figure 4.15. The effect of the pressure onto a sensor (P_O) to the sensitivity of neighboring sensors (P_1, P_2, P_3, P_4) at various FRL and pressing conditions. (FRL - PET (thickness : 100 μm, 1200 μm), glass (thickness : 400 μm), pressing condition - 10gf , 200 gf).

4.3.6. Demonstration of casually mountable pulse-detecting device

Regarding the results about the effect of FRL to the sensor, the strain sensor combined with thin PET can be utilized in the applications that require high sensitivity at very small force and high crosstalk effect. Thus, I demonstrated a wearable device that is casually mountable on the user's wrist to detect arterial pulse. As depicted in Figure 4.16, the descriptive concept of the device is that Ag strain sensor which is combined with thin PET is not necessarily put on the exact point along the artery and can be attached onto the surrounding area of the arterial points of wrist. As the tiny shock on the skin from arterial pulse are transmitted via FRL, the extremely sensitive strain sensor is able to sense the dampened signal. Thus, in this work, the device was not necessarily located on specific spots (a_0, b_0, c_0) that were aligned with artery, but also on the spots ($a_{-9\sim9}, b_{-9\sim9}, c_{-9\sim9}$) that were away from the strongest points to certain distance (3 mm, 6mm, 9mm). As shown in Figure 4.17, the resistance variations of the pulse-detecting device that was put on each point was exhibited. Even though the amplitude of the detected pulse descended according to the distance from artery, the frequency of pulse was well measurable up to the distance of 6 mm, which enabled casual wearing of the device.

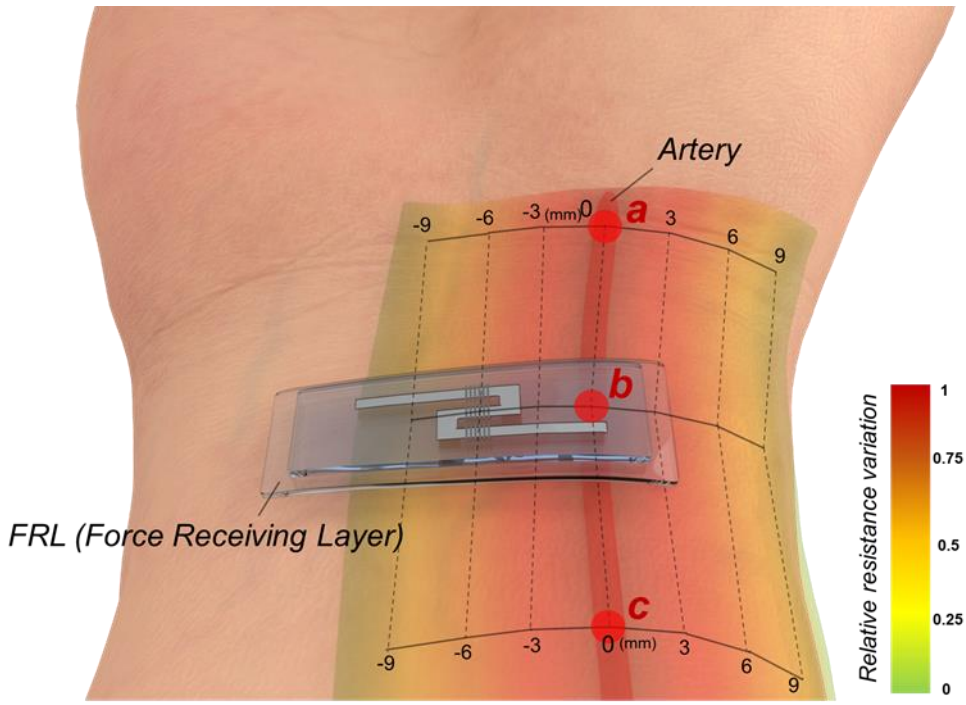

Figure 4.16. Schematic illustration of casually wearable pulse-detecting device attached to various spots on user's wrist.

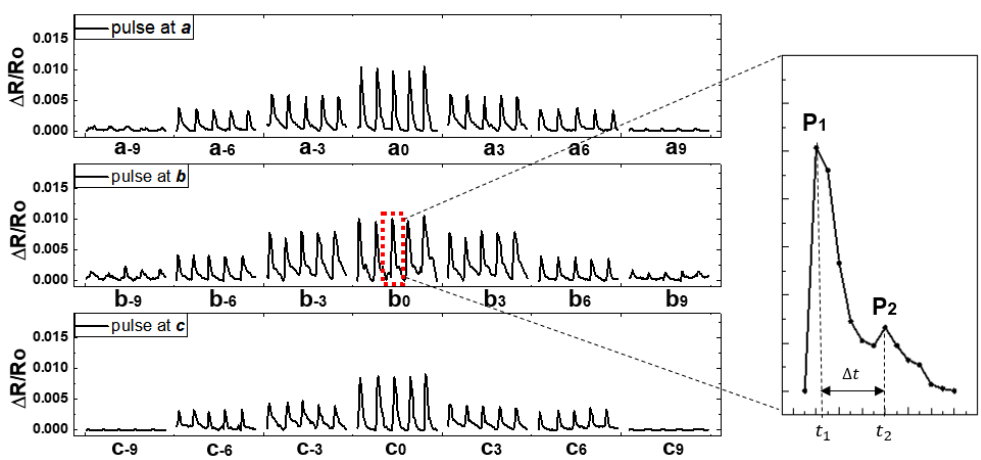

Figure 4.17. Electrical resistance variations of the arterial pulse detected by the device attached at various points as a function of the distance (3mm, 6mm, 9mm) from the points (a_0, b_0, c_0) on artery.

4.3.7. Demonstration of integrated strain-sensing system for force touch application

In addition, I demonstrated integrated system with 5 × 5 strain sensor matrix to realize multi-level force touch sensor. Figure 4.18 shows the optical image of 5 × 5 Ag strain sensor array which was implemented to recognize the location as well as pressure of touch on it. Each strain sensor was designed to be 3 mm in width and height with a spacing of 6mm, and all of the strain sensors and electrodes were inkjet-printed with Ag ink and integrated onto a single PDMS layer. To demonstrate the comparable configuration of the force touch sensor embodied in commercial smartphone, solid glass (thickness : 400 μm) layer was attached on top of the Ag strain sensor matrix layer. The resistance variation of single sensing pixel (2, 2) that was pressed with finger-touch like force (maximum 200 gf) is exhibited as shown in Figure 4.19. Thus, in Figure 4.20, considering the crosstalk effect of the device, the location and the amount of the force were described at the same time by exhibiting entire resistance variations of each strain sensor on the matrix. The force applied to the (2, 2) pixel on the device was divided into 3 levels (50 gf, 100 gf, 200 gf) to realize the distinct force touch measurement. Although the changes in resistance of surrounding pixels inevitably occurred owing to the crosstalk effect, the distinguished response to various inputs were remarkably observed. Moreover, in Figure 4.21, to insist the capability of detecting multi-touch inputs, static forces using light weights (10 gf, 20 gf) were applied to (1, 4) and (4, 2) pixels, respectively. As a result, high sensitivity of the strain sensors enabled the device to apparently detect the locations and amounts of the small forces with high selectivity.

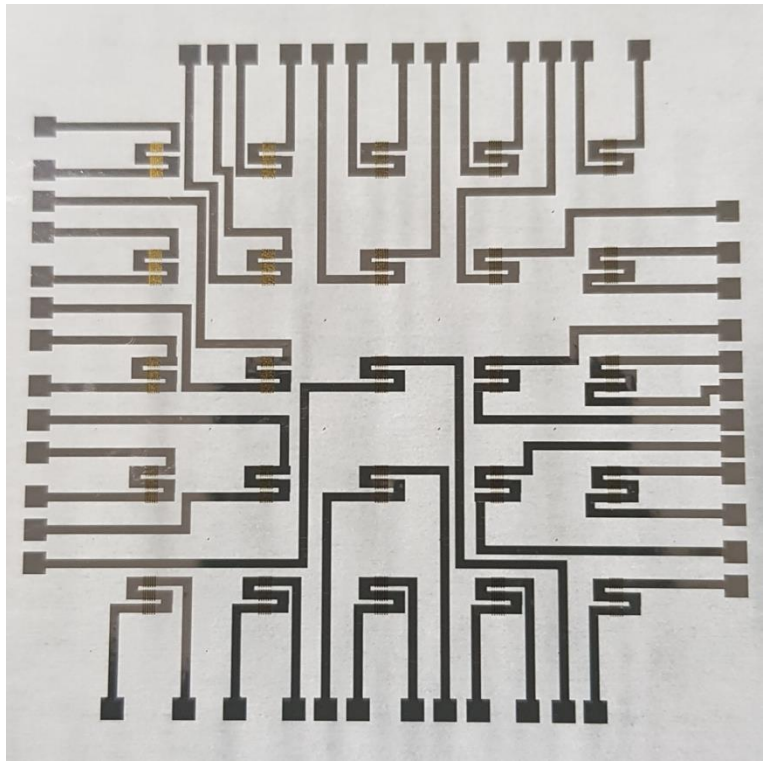

Figure 4.18. Optical image of integrated system of 5 × 5 strain sensor matrix.

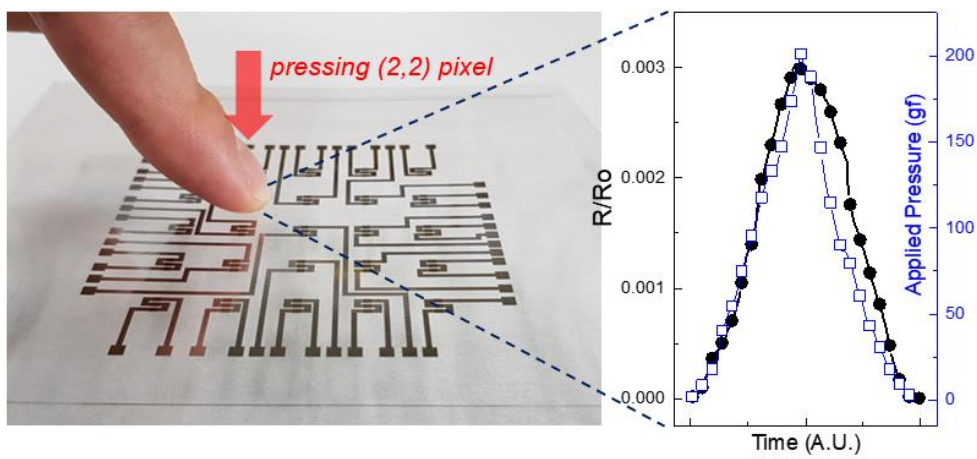

Figure 4.19. Optical image of 5 × 5 strain sensor matrix for force touch application, and electrical resistance variation of (2,2) pixel at 1 cycle pressure loading. (200 gf)

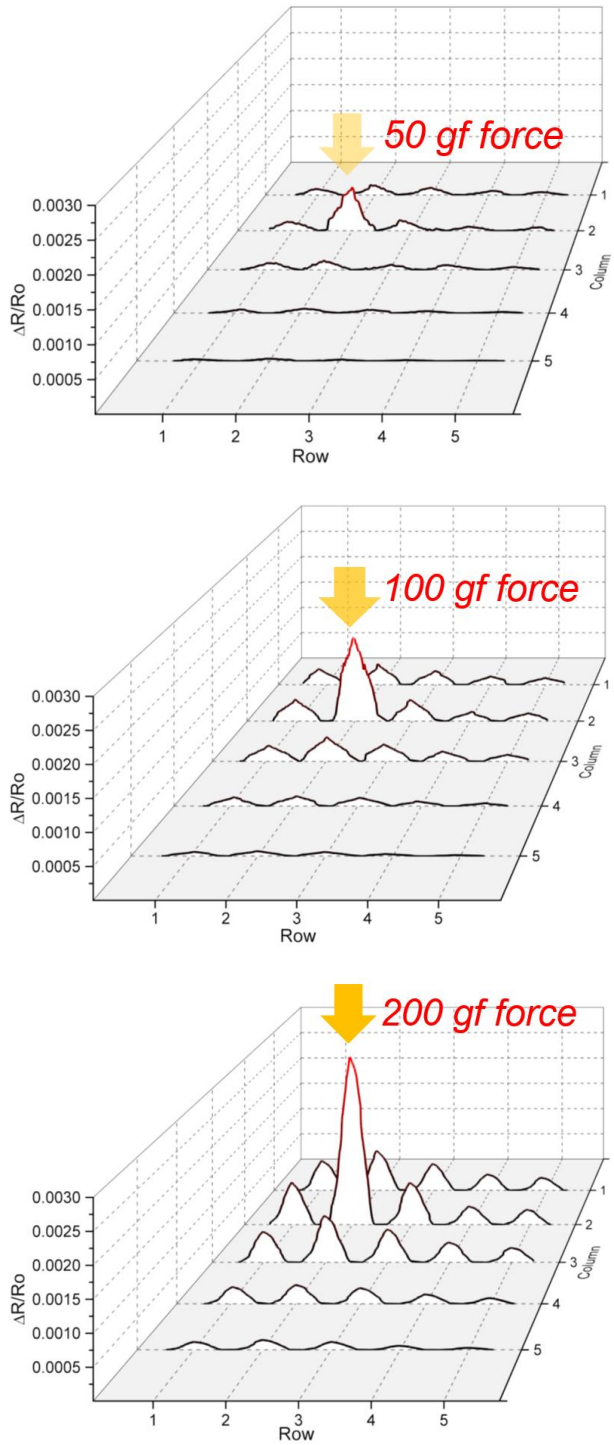

Figure 4.20. Resistance variations of every pixel of the device under 1 cycle of external forces (50 gf, 100 gf, 200 gf) applied on (2,2) pixel.

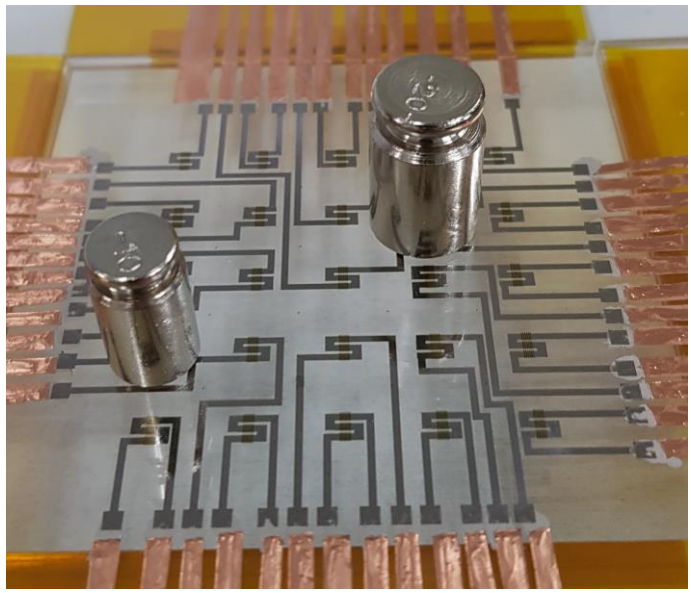

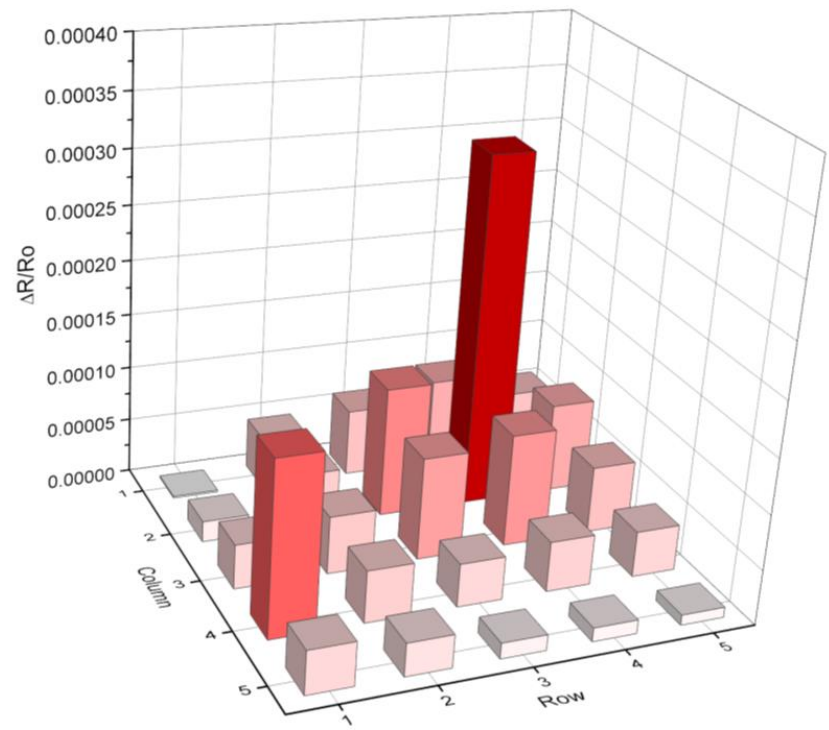

Figure 4.21. Resistance variation of the device under static forces with 10 gf and 20 gf weights put on (2,4) and (4,2) pixel, respectively.

The force touch sensors at industrial grade are mostly divided into capacitive and resistive types. In fact, capacitive force sensor had been chosen as commercial purpose owing to its high sensitivity. However, contrary to the bulky structure and the difficulty in elaborately measuring the varied distance between electrodes in capacitive force sensor, the resistive type force touch sensor has been recently utilized in commercialized smartphone for their high force-sensitivity and single-layered structure (Fig 4.22). The high sensitivity at pressure loading enables the device to have wide dynamic range which is necessary for various user interface applications. As the ultimate purpose of this force touch application is to be practically utilized in user-interface technology of commercial electronic device, it is necessary that the performance of device is verified by the comparison with the performance of the commercialized device. Therefore, the sensitivity of the commercialized resistive touch sensor was measured in the same way that I performed on our device by integrating it with 400 μm thick glass and exerting external force to a sensing pixel. In Figure 4.23, the resistance variations of the commercialized one and ours were obtained as a function of variously applied force. The result indicated that the sensitivity of our device surpassed the other one as much as 10 times or more all over the pressure range. Thus, our results well demonstrated the properties of the integrated system of crack-induced Ag strain sensor with FRL, and the use as casually mountable wearable device and integrated system for force touch applications.

	Capacitive type	Resistive type
2D touch (location)	In-cell capacitive type	Out-cell capacitive type
3D touch (pressure)	Out-cell capacitive type (beneath backlight) - change in distance between electrodes - bulky (dual layers) - complex algorithm is needed to measure the distance between electrodes	Resistive strain-gauge type (beneath display screen) - deformation of strain gauge - single layer - high sensitivity and selectivity

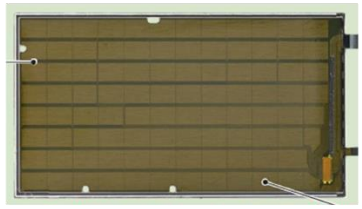

"New Method Employed for Pressure Sensor", XTECH, Jan 21 (2018)

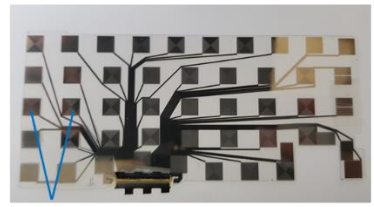

wider space between sensors

Figure 4.22. Specification of capacitive and resistive touch sensor in commercialized smartphone.

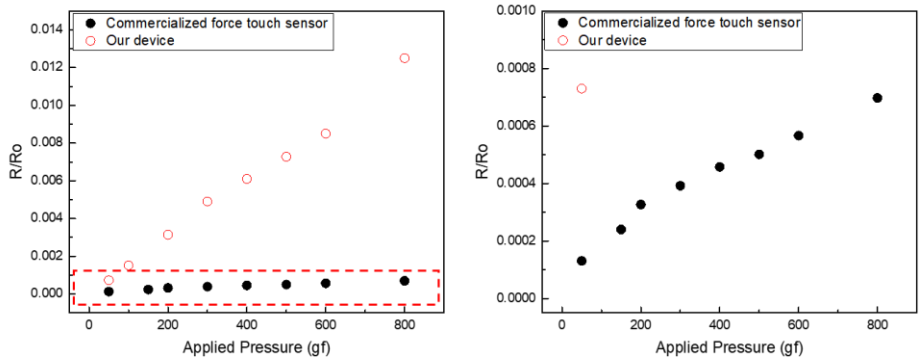

Figure 4.23. Comparison on the electrical resistance variations of unit sensing pixel of the fabricated device and commercialized force touch sensor at various pressure loadings.

4.4. Summary

To sum up, I have presented inkjet-printed crack-induced Ag NPs based strain sensor, which can detect the flexure of the FRL that was attached on the sensor. To enhance the sensitivity of the sensor, Ag vertical patterns were inkjet-printed prior to the Ag film made large difference in height of the film to induce concentrated and controlled cracks around them. To further enhance sensitivity of the sensor, I optimized structures of the vertical patterns and the design of the strain sensor. Moreover, as the performance of the sensor was determined according to the rigidity of FRL, the sensitivity and crosstalk effect of the sensor integrated with various FRL were also verified. As a result, the high elasticity of thin PET for FRL enabled the sensor to be applicable to pulse-detecting device that could be mounted adjacent area on user's wrist. On the other hand, the solid glass FRL was combined with single-layered integrated system of 5 × 5 strain sensor matrix to demonstrate force touch sensor. The fabricated device well distinguished the single or multi inputs in multi-level forces, and the performance exceeded the commercialized sensor. It is noted that the highly sensitive Ag strain sensor is applicable to various wearable devices, where efficient interactions between human and machine are needed.

Chapter 5

Summary, Limitations and Recommendations for Future Research

5.1. Summary

In this dissertation, the novel structural strategies on the inkjet-printed silver nano particle-based film on stretchable substrate were proposed to obtain durable and sensitive strain sensors from intrinsically brittle nature of the material. Moreover, to complement the existing issues and to explore decent applications in stretchable electronics, crack-generating phenomenon on the film was able to be controlled by adequate structural modulations. The low-cost and facile fabrication process by inkjet-printing silver ink was commonly used all through the chapters, thus, the strain sensing device was not only confined to develop unit sensor but to effectively implement integrated strain sensing system that was able to be applicable to large-area stretchable applications. The integrated system consisted of highly sensitive crack-generated strain sensor and stretchable electrode with wrinkle structures with

common silver nano particle-based material.

To obtain stability of stretchable strain sensor from brittle silver nano particle-based film, wrinkle structure by inkjet-printing silver ink on the pre-stretched substrate was utilized in Chapter 2 and Chapter 3. Thus, the printed film was able to maintain constant resistance up to the pre-strain. In Chapter 2, the strain sensitivity of the film was accomplished by additionally inkjet-printing silver ink onto the wrinkle structure, and the cracks were generated onto the thickness-gradient layer under tensile strain. From the combination of wrinkled base layer and crack-inducing layer made the whole film to be both highly sensitive (gauge factor ~ 10) and stable (1,000 cyclic test) up to 50% tensile strain. Moreover, by utilizing inkjet-printing process, the crack-inducing layer could be patterned on the desired area, and the fabricated integrated strain sensing system was applicable to the dimensionally customizable human-motion detecting device. Each Strain sensor were exactly located on the joints regardless of user's hand size and selectively detected the joint flexion precisely.

In Chapter 3, to solve the coupling effect of the strain sensor on 2-dimensional stretchable substrate from high Poisson's ratio of elastomeric platform, asymmetrically pre-strained silver nano particle-based films were utilized. The inevitable stress by perpendicular strain was dissipated by the vertical wrinkle structures, and the parallel pre-strain enabled the film to be sensitive under certain strain range. From the fabricated bi-axial strain sensors, Integrated system that consisted of 2-dimensionally stretchable light emitting device and strain sensors was accomplished to demonstrate conceptual hidden pixels that turn on to compensate the reduced resolution from the increased distance between adjacent pixels on the

stretchable display.

In Chapter 4, the high sensitivity of silver nanoparticle based film was further enhanced by engineering vertical patterns on the film to focus controlled cracks around them. The extremely high sensitivity of the strain sensor was fabricated to measure the subtle flexure of the rigid layer that could be applied in various applications. The number of patterns that a strain sensor could contain was adjustable utilizing serpentine design. Moreover, as the sensitivity and crosstalk effect of the sensor was greatly affected by the physical properties of force receiving layers, the strain sensor attached to elastic layer was utilized in wearable device that could be casually mounted on user's wrist and detect arterial pulse. On the other hand, if the integrated system of strain sensing matrix was integrated with solid force receiving layer, force touch sensing device that was able to measure the locations and extent of the force applied to the surface was demonstrated.

In conclusion, I have introduced some practical methodology to obtain mechanically reliable strain sensors for various applications in stretchable electronics. With low-cost and facile inkjet-printing process, common silver nanoparticle was used with some morphological strategies to realize strain sensing systems of which performance was comparable with other works that had been fabricated under complex and costly process. Moreover, the integrated strain sensing system made the demonstrated devices be more conformable to actual uses. Ultimately, I expect that presented technologies will be helpful for future studies for the development of futuristic applications such as wearable device, stretchable display and advance user interface that require wide utilization with high electrical and mechanical sensing performances.

5.2. Limitations and Recommendations

5.2.1. Strain Sensor Application for Extremely High Sensitivity

5.2.1.1. Strain-insensitive Pulse-detecting Device

In Chapter 4, I demonstrated pulse-detecting device by integrating Ag strain sensor with elastic FRL to casually mount the device on the targeted human body. Although the casual wearing of device is novelty of our application, it is necessary that the device is capable of detecting pulse signals regardless of user's movement in order to be practically utilized. There have been a lot of previous works on pressure sensors that demonstrated pulse-detecting wearable device to emphasize high sensitivity of their devices. However, they were also demonstrated without insensitivity to body movement. For the sensor to selectively detect pulse signal, it needs to be preferentially insensitive to external tensile strain. There have been some strain-insensitive pressure sensors reported, which utilized asymmetric structures such as pyramid and porous composites. Then, as each direction of external stimuli (pressure and strain) that is applied to the composite is perpendicular each other, asymmetrically deformed composite can selectively detect the targeted stimulus. However, the pressure applied to the Ag strain sensor with vertical patterns (chapter 4) is to be detected by slightly bending the composite, and the curvature of the composite can be calculated as strain applied to the composite. Therefore, the pressure and strain applied to the strain sensor are not selectively separated as the

previously reported asymmetric structures. The way I considered to solve the issue about selectively detecting coupled stimuli (arterial pulse and body movement) applied to Ag strain sensor is that the overall electrical signals from pulse and body movement can be distinguished by signal processing afterwards using adequate filtering.

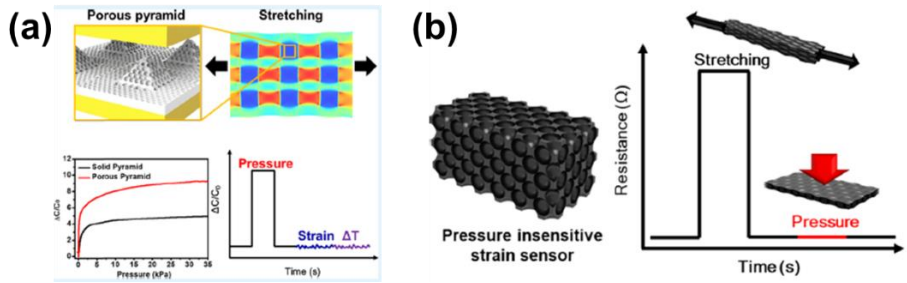

Figure 5.1. (a) Strain-insensitive pressure sensor and (b) pressure-insensitive strain sensor utilizing pyramid and porous structures. [96, 97]

5.2.1.2. Demonstration of Real-time Ant Tracing Device

To more highly emphasize the merit of extremely high sensitivity and inkjet-printability of the Ag strain sensor with vertical patterns, I demonstrated a real-time live ant tracing device using 5 × 5 strain sensor array that is integrated with elastic FRL. Moreover, using switching matrix machine (DAQ 6510, Tektronix) that is to acquire and log the multiple data almost simultaneously, the movement of a live ant can be traced in real time by measuring the change in resistance of each pixel of strain detecting device as shown in Fig 5.2. As the weight of an ant is 5-10 mg, the capability of detecting light weight supports the high sensitivity of the sensor. In addition, the measurement of the light subject in real time utilizing large-area strain sensor array is a distinctive demonstration compared to the previous works that had been almost confined to the single-pixel application. As a result, the complete experimental result of real-time tracing was not obtained yet, Fig 5.3 shows enough possibility with remarkable change in resistance of strain sensor at corresponding moments (t = 37s, 42s, 45s) that the live ant stepped on it.

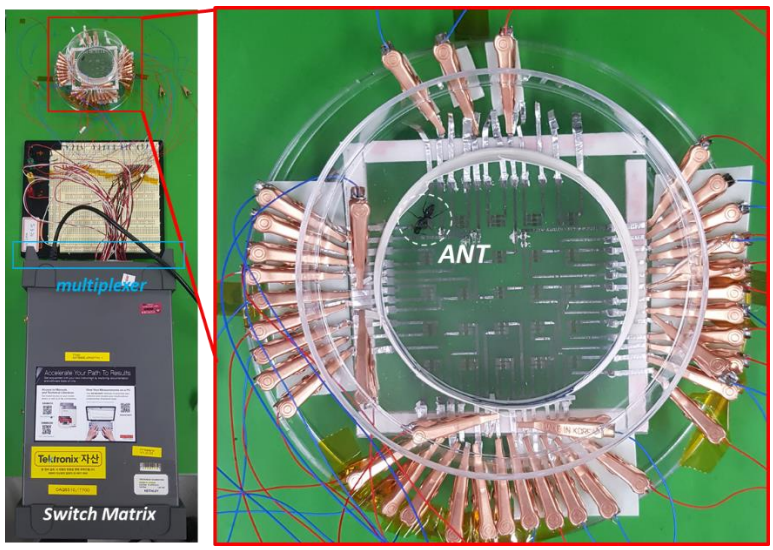

Figure 5.2. The image of tracing live ant using Ag strain sensor array integrated with elastic FRL and switch matrix multimeter.

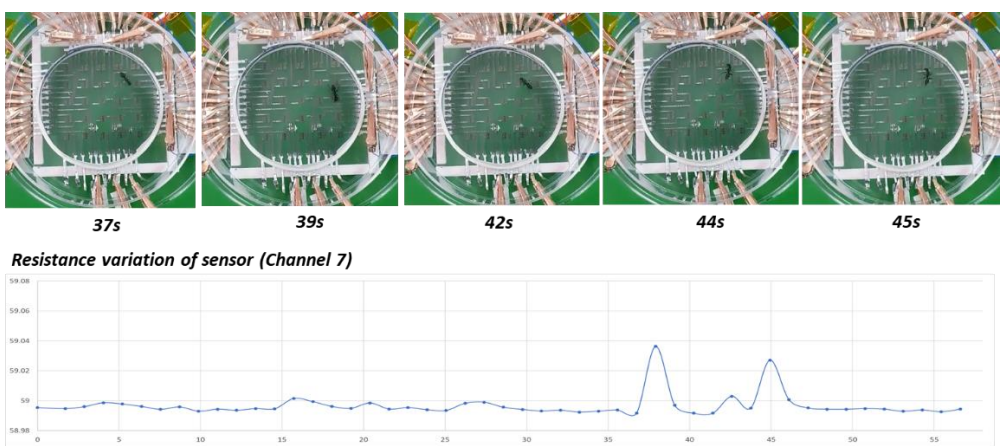

Figure 5.3. Resistance variation of a strain sensor (4, 2) applied from the applied pressure as the ant stepped on.

Bibliography

[1] J. Byun, B. Lee, E. Oh, H. Kim, S. Kim, S. Lee, Y. Hong, Fully printable, strain-engineered electronic wrap for customizable soft electronics, 7 (2017) 45328.

[2] J. Byun, E. Oh, B. Lee, S. Kim, S. Lee, Y. Hong, A Single Droplet-Printed Double-Side Universal Soft Electronic Platform for Highly Integrated Stretchable Hybrid Electronics, 27 (2017) 1701912.

[3] S. Chung, J. Lee, H. Song, S. Kim, J. Jeong, Y. Hong, Inkjet-printed stretchable silver electrode on wave structured elastomeric substrate, 98 (2011) 153110.

[4] S. Kim, J. Byun, S. Choi, D. Kim, T. Kim, S. Chung, Y. Hong, Negatively Strain-Dependent Electrical Resistance of Magnetically Arranged Nickel Composites: Application to Highly Stretchable Electrodes and Stretchable Lighting Devices, 26 (2014) 3094-3099.

[5] Y. Kim, X. Ren, J. Kim, H. Noh, Direct inkjet printing of micro-scale silver electrodes on polydimethylsiloxane (PDMS) microchip, 24 (2014) 115010.

[6] J. Lee, S. Chung, H. Song, S. Kim, Y. Hong, Lateral-crack-free, buckled, inkjet-printed silver electrodes on highly pre-stretched elastomeric substrates, 46 (2013) 105305.

[7] H.C. Ko, M.P. Stoykovich, J. Song, V. Malyarchuk, W.M. Choi, C.-J. Yu, J.B. Geddes Iii, J. Xiao, S. Wang, Y. Huang, A hemispherical electronic eye camera based on compressible silicon optoelectronics, 454 (2008) 748.

[8] J.A. Rogers, Electronics for the human body, 313 (2015) 561-562.

[9] J.A. Rogers, Y. Huang, A curvy, stretchy future for electronics, 106 (2009) 10875-10876.

[10] Y.M. Song, Y. Xie, V. Malyarchuk, J. Xiao, I. Jung, K.-J. Choi, Z. Liu, H. Park, C. Lu, R.-H. Kim, Digital cameras with designs inspired by the arthropod eye, 497 (2013) 95.

[11] Y. Cheng, R. Wang, J. Sun, L. Gao, Highly conductive and ultrastretchable electric circuits from covered yarns and silver nanowires, 9 (2015) 3887-3895.

[12] C. Larson, B. Peele, S. Li, S. Robinson, M. Totaro, L. Beccai, B. Mazzolai, R. Shepherd, Highly stretchable electroluminescent skin for optical signaling and tactile sensing, 351 (2016) 1071-1074.

[13] S. Xu, Y. Zhang, J. Cho, J. Lee, X. Huang, L. Jia, J.A. Fan, Y. Su, J. Su, H. Zhang, Stretchable batteries with self-similar serpentine interconnects and integrated wireless recharging systems, 4 (2013) 1543.

[14] J.K. Song, D. Son, J. Kim, Y.J. Yoo, G.J. Lee, L. Wang, M.K. Choi, J. Yang, M. Lee, K. Do, Wearable force touch sensor array using a flexible and transparent electrode, 27 (2017) 1605286.

[15] Y.-J. Liu, W.-T. Cao, M.-G. Ma, P. Wan, Ultrasensitive wearable soft strain sensors of conductive, self-healing, and elastic hydrogels with synergistic “soft and hard” hybrid networks, 9 (2017) 25559-25570.

[16] D. Kang, P.V. Pikhitsa, Y.W. Choi, C. Lee, S.S. Shin, L. Piao, B. Park, K.-Y. Suh, T.-i. Kim, M. Choi, Ultrasensitive mechanical crack-based sensor inspired by the spider sensory system, 516 (2014) 222.

[17] T. Yang, X. Li, X. Jiang, S. Lin, J. Lao, J. Shi, Z. Zhen, Z. Li, H. Zhu, Structural engineering of gold thin films with channel cracks for ultrasensitive strain sensing, 3 (2016) 248-255.

[18] J. Lee, S. Kim, J. Lee, D. Yang, B.C. Park, S. Ryu, I. Park, A stretchable strain sensor based on a metal nanoparticle thin film for human motion detection, 6 (2014) 11932-11939.

[19] M. Amjadi, M. Turan, C.P. Clementson, M. Sitti, Parallel microcracks-based ultrasensitive and highly stretchable strain sensors, 8 (2016) 5618-5626.

[20] J.Y. Yoo, M.H. Seo, J.S. Lee, K.W. Choi, M.S. Jo, J.B. Yoon, Industrial Grade, Bending-Insensitive, Transparent Nanoforce Touch Sensor via Enhanced Percolation Effect in a Hierarchical Nanocomposite Film, 28 (2018) 1804721.

[21] C. Luo, J. Jia, Y. Gong, Z. Wang, Q. Fu, C. Pan, Highly sensitive, durable, and multifunctional sensor inspired by a spider, 9 (2017) 19955-19962.

[22] S. Zhang, L. Cai, W. Li, J. Miao, T. Wang, J. Yeom, N. Sepúlveda, C. Wang, Fully Printed Silver-Nanoparticle-Based Strain Gauges with Record High Sensitivity, 3 (2017) 1700067.

[23] K.K. Kim, I. Ha, P. Won, D.-G. Seo, K.-J. Cho, S.H. Ko, Transparent wearable three-dimensional touch by self-generated multiscale structure, 10 (2019) 2582.

[24] K. Lee, J. Lee, G. Kim, Y. Kim, S. Kang, S. Cho, S. Kim, J.K. Kim, W. Lee, D.E. Kim, Rough-Surface-Enabled Capacitive Pressure Sensors with 3D Touch Capability, 13 (2017) 1700368.

[25] M. Kang, J. Kim, B. Jang, Y. Chae, J.-H. Kim, J.-H. Ahn, Graphene-based three-dimensional capacitive touch sensor for wearable electronics, 11 (2017) 7950-7957.

[26] A. Aliverti, Wearable technology: role in respiratory health and disease, 13 (2017) e27-e36.

[27] Y. Liu, M. Pharr, G.A. Salvatore, Lab-on-skin: a review of flexible and stretchable electronics for wearable health monitoring, 11 (2017) 9614-9635.

[28] T. Someya, T. Sekitani, S. Iba, Y. Kato, H. Kawaguchi, T. Sakurai, A large-area,

flexible pressure sensor matrix with organic field-effect transistors for artificial skin applications, 101 (2004) 9966-9970.

[29] L. Xu, S.R. Gutbrod, A.P. Bonifas, Y. Su, M.S. Sulkin, N. Lu, H.-J. Chung, K.-I. Jang, Z. Liu, M. Ying, 3D multifunctional integumentary membranes for spatiotemporal cardiac measurements and stimulation across the entire epicardium, 5 (2014) 3329.

[30] J.W. Ayres, F. Lalande, Z. Chaudhry, C.A. Rogers, Qualitative impedance-based health monitoring of civil infrastructures, 7 (1998) 599.

[31] S. Bhalla, C. Kiong Soh, Structural impedance based damage diagnosis by piezo-transducers, 32 (2003) 1897-1916.

[32] S. Bhalla, C.K. Soh, Structural health monitoring by piezo-impedance transducers. I: Modeling, 17 (2004) 154-165.

[33] S. Bhalla, Y. Yang, J. Zhao, C. Soh, Structural health monitoring of underground facilities–Technological issues and challenges, 20 (2005) 487-500.

[34] M. Amjadi, A. Pichitpajongkit, S. Lee, S. Ryu, I. Park, Highly stretchable and sensitive strain sensor based on silver nanowire–elastomer nanocomposite, 8 (2014) 5154-5163.

[35] J. Park, I. You, S. Shin, U. Jeong, Material approaches to stretchable strain sensors, 16 (2015) 1155-1163.

[36] T. Yamada, Y. Hayamizu, Y. Yamamoto, Y. Yomogida, A. Izadi-Najafabadi, D.N. Futaba, K. Hata, A stretchable carbon nanotube strain sensor for human-motion detection, 6 (2011) 296.

[37] L. Cai, L. Song, P. Luan, Q. Zhang, N. Zhang, Q. Gao, D. Zhao, X. Zhang, M. Tu, F. Yang, Super-stretchable, transparent carbon nanotube-based capacitive strain sensors for human motion detection, 3 (2013) 3048.

[38] N. Lu, C. Lu, S. Yang, J. Rogers, Highly sensitive skin-mountable strain gauges based entirely on elastomers, 22 (2012) 4044-4050.

[39] X. Xiao, L. Yuan, J. Zhong, T. Ding, Y. Liu, Z. Cai, Y. Rong, H. Han, J. Zhou, Z.L. Wang, High-strain sensors based on ZnO nanowire/polystyrene hybridized flexible films, 23 (2011) 5440-5444.

[40] M. Zheng, W. Li, M. Xu, N. Xu, P. Chen, M. Han, B. Xie, Strain sensors based on chromium nanoparticle arrays, 6 (2014) 3930-3933.

[41] J. Tolvanen, J. Hannu, H. Jantunen, Stretchable and washable strain sensor based on cracking structure for human motion monitoring, 8 (2018) 13241.

[42] I. Kang, M.J. Schulz, J.H. Kim, V. Shanov, D. Shi, A carbon nanotube strain sensor for structural health monitoring, 15 (2006) 737.

[43] J. Zhang, J. Liu, R. Zhuang, E. Mäder, G. Heinrich, S. Gao, Single MWNT-glass fiber as strain sensor and switch, 23 (2011) 3392-3397.

[44] D. Lee, H.P. Hong, M.J. Lee, C.W. Park, N.K. Min, A prototype high sensitivity load cell using single walled carbon nanotube strain gauges, 180 (2012) 120-126.

[45] L. Wang, Y. Li, A review for conductive polymer piezoresistive composites and a development of a compliant pressure transducer, 62 (2012) 495-502.

[46] S. Chung, M. Jang, S.B. Ji, H. Im, N. Seong, J. Ha, S.K. Kwon, Y.H. Kim, H. Yang, Y. Hong, Flexible High-Performance All-Inkjet-Printed Inverters: Organo-Compatible and Stable Interface Engineering, 25 (2013) 4773-4777.

[47] J. Ha, S. Chung, M. Pei, K. Cho, H. Yang, Y. Hong, One-step interface engineering for all-inkjet-printed, all-organic components in transparent, flexible transistors and inverters: polymer binding, 9 (2017) 8819-8829.

[48] H. Sirringhaus, T. Kawase, R. Friend, T. Shimoda, M. Inbasekaran, W. Wu, E. Woo, High-resolution inkjet printing of all-polymer transistor circuits, 290 (2000)

2123-2126.

[49] B.S. Cook, J.R. Cooper, M.M. Tentzeris, Multi-layer RF capacitors on flexible substrates utilizing inkjet printed dielectric polymers, 23 (2013) 353-355.

[50] Y. Li, R. Torah, S. Beeby, J. Tudor, An all-inkjet printed flexible capacitor on a textile using a new poly (4-vinylphenol) dielectric ink for wearable applications, in: SENSORS, 2012 IEEE, IEEE, 2012, pp. 1-4.

[51] H. Minemawari, T. Yamada, H. Matsui, J.y. Tsutsumi, S. Haas, R. Chiba, R. Kumai, T. Hasegawa, Inkjet printing of single-crystal films, 475 (2011) 364.

[52] H. Yan, Z. Chen, Y. Zheng, C. Newman, J.R. Quinn, F. Dötz, M. Kastler, A. Facchetti, A high-mobility electron-transporting polymer for printed transistors, 457 (2009) 679.

[53] J.A. Rogers, T. Someya, Y. Huang, Materials and mechanics for stretchable electronics, 327 (2010) 1603-1607.

[54] K.-Y. Chun, Y. Oh, J. Rho, J.-H. Ahn, Y.-J. Kim, H.R. Choi, S. Baik, Highly conductive, printable and stretchable composite films of carbon nanotubes and silver, 5 (2010) 853.

[55] T. Sekitani, T. Someya, Stretchable, large-area organic electronics, 22 (2010) 2228-2246.

[56] D.-H. Kim, J.-H. Ahn, W.M. Choi, H.-S. Kim, T.-H. Kim, J. Song, Y.Y. Huang, Z. Liu, C. Lu, J.A. Rogers, Stretchable and foldable silicon integrated circuits, 320 (2008) 507-511.

[57] D.-H. Kim, J. Song, W.M. Choi, H.-S. Kim, R.-H. Kim, Z. Liu, Y.Y. Huang, K.-C. Hwang, Y.-w. Zhang, J.A. Rogers, Materials and noncoplanar mesh designs for integrated circuits with linear elastic responses to extreme mechanical deformations, 105 (2008) 18675-18680.

[58] S. Gong, D.T. Lai, B. Su, K.J. Si, Z. Ma, L.W. Yap, P. Guo, W. Cheng, Highly Stretchy Black Gold E-Skin Nanopatches as Highly Sensitive Wearable Biomedical Sensors, 1 (2015) 1400063.

[59] J.J. Park, W.J. Hyun, S.C. Mun, Y.T. Park, O.O. Park, Highly stretchable and wearable graphene strain sensors with controllable sensitivity for human motion monitoring, 7 (2015) 6317-6324.

[60] H. Tian, Y. Shu, Y.-L. Cui, W.-T. Mi, Y. Yang, D. Xie, T.-L. Ren, Scalable fabrication of high-performance and flexible graphene strain sensors, 6 (2014) 699-705.

[61] Y. Wang, L. Wang, T. Yang, X. Li, X. Zang, M. Zhu, K. Wang, D. Wu, H. Zhu, Wearable and highly sensitive graphene strain sensors for human motion monitoring, 24 (2014) 4666-4670.

[62] M. Amjadi, K.U. Kyung, I. Park, M. Sitti, Stretchable, Skin-Mountable, and Wearable Strain Sensors and Their Potential Applications: A Review, Adv Funct Mater 26 (2016) 1678-1698. https://doi.org/10.1002/adfm.201504755.

[63] C.L. Choong, M.B. Shim, B.S. Lee, S. Jeon, D.S. Ko, T.H. Kang, J. Bae, S.H. Lee, K.E. Byun, J. Im, Y.J. Jeong, C.E. Park, J.J. Park, U.I. Chung, Highly Stretchable Resistive Pressure Sensors Using a Conductive Elastomeric Composite on a Micropyramid Array, Adv Mater 26 (2014) 3451-3458. https://doi.org/10.1002/adma.201305182.

[64] D. Kang, P.V. Pikhitsa, Y.W. Choi, C. Lee, S.S. Shin, L. Piao, B. Park, K.Y. Suh, T.I. Kim, M. Choi, Ultrasensitive mechanical crack-based sensor inspired by the spider sensory system, 516 (2014) 222-226. https://doi.org/10.1038/nature14002.

[65] Y.J. Liu, W.T. Cao, M.G. Ma, P. Wan, Ultrasensitive Wearable Soft Strain Sensors of Conductive, Self-healing, and Elastic Hydrogels with Synergistic "Soft

and Hard" Hybrid Networks, Acs Appl Mater Inter 9 (2017) 25559-25570. https://doi.org/10.1021/acsami.7b07639.

[66] Y.C. Ding, J. Yang, C.R. Tolle, Z.T. Zhu, A highly stretchable strain sensor based on electrospun carbon nanofibers for human motion monitoring, Rsc Adv 6 (2016) 79114-79120. https://doi.org/10.1039/c6ra16236c.

[67] P. Moyo, J.M.W. Brownjohn, R. Suresh, S.C. Tjin, Development of Fiber Bragg grating sensors for monitoring civil infrastructure, Eng Struct 27 (2005) 1828-1834. https://doi.org/10.1016/j.engstruct.2005.04.023.

[68] T. Lee, Y.W. Choi, G. Lee, P.V. Pikhitsa, D. Kang, S.M. Kim, M. Choi, Transparent ITO mechanical crack-based pressure and strain sensor, 4 (2016) 9947-9953.

[69] B. Park, J. Kim, D. Kang, C. Jeong, K.S. Kim, J.U. Kim, P.J. Yoo, T.i. Kim, Dramatically Enhanced Mechanosensitivity and Signal-to-Noise Ratio of Nanoscale Crack-Based Sensors: Effect of Crack Depth, 28 (2016) 8130-8137.

[70] E. Oh, T. Kim, J. Yoon, S. Lee, D. Kim, B. Lee, J. Byun, H. Cho, J. Ha, Y. Hong, Highly Reliable Liquid Metal-Solid Metal Contacts with a Corrugated Single-Walled Carbon Nanotube Diffusion Barrier for Stretchable Electronics, Adv Funct Mater 28 (2018) 1806014. https://doi.org/ARTN 1806014 10.1002/adfm.201806014.

[71] S. Kim, J. Byun, S. Choi, D. Kim, T. Kim, S. Chung, Y. Hong, Negatively strain-dependent electrical resistance of magnetically arranged nickel composites: application to highly stretchable electrodes and stretchable lighting devices, 26 (2014) 3094-3099. https://doi.org/10.1002/adma.201304686.

[72] J. Lee, S. Chung, H. Song, S. Kim, Y. Hong, Lateral-crack-free, buckled, inkjet-printed silver electrodes on highly pre-stretched elastomeric substrates, J Phys D

Appl Phys 46 (2013) 105305. https://doi.org/Artn 105305
10.1088/0022-3727/46/10/105305.

[73] A. Kim, J. Ahn, H. Hwang, E. Lee, J. Moon, A pre-strain strategy for developing a highly stretchable and foldable one-dimensional conductive cord based on a Ag nanowire network, 9 (2017) 5773-5778.

[74] C.-J. Lee, K.H. Park, C.J. Han, M.S. Oh, B. You, Y.-S. Kim, J.-W. Kim, Crack-induced Ag nanowire networks for transparent, stretchable, and highly sensitive strain sensors, 7 (2017) 7959.

[75] T. Kim, D. Kim, Y. Joo, J. Park, J. Yoon, Y. Hong, Crack propagation design in transparent polymeric conductive films via carbon nanotube fiber-reinforcement and its application for highly sensitive and mechanically durable strain sensors, 28 (2018) 025008.

[76] H.-N. Kim, S.-H. Lee, K.-Y. Suh, Controlled mechanical fracture for fabricating microchannels with various size gradients, 11 (2011) 717-722.

[77] Y.-h. Wu, H.-z. Liu, S. Chen, X.-c. Dong, P.-p. Wang, S.-q. Liu, Y. Lin, Y. Wei, L. Liu, Channel Crack-Designed Gold@ PU Sponge for Highly Elastic Piezoresistive Sensor with Excellent Detectability, 9 (2017) 20098-20105.

[78] Z. Liu, D. Qi, P. Guo, Y. Liu, B. Zhu, H. Yang, Y. Liu, B. Li, C. Zhang, J. Yu, B. Liedberg, X. Chen, Thickness-Gradient Films for High Gauge Factor Stretchable Strain Sensors, 27 (2015) 6230-6237. https://doi.org/10.1002/adma.201503288.

[79] J. Park, I. You, S. Shin, U. Jeong, Material approaches to stretchable strain sensors, 16 (2015) 1155-1163. https://doi.org/10.1002/cphc.201402810.

[80] T. Yamada, Y. Hayamizu, Y. Yamamoto, Y. Yomogida, A. Izadi-Najafabadi, D.N. Futaba, K. Hata, A stretchable carbon nanotube strain sensor for human-motion detection, 6 (2011) 296-301. https://doi.org/10.1038/nnano.2011.36.

[81] Y. Ding, J. Yang, C.R. Tolle, Z. Zhu, A highly stretchable strain sensor based on electrospun carbon nanofibers for human motion monitoring, 6 (2016) 79114-79120.

[82] K.K. Kim, S. Hong, H.M. Cho, J. Lee, Y.D. Suh, J. Ham, S.H. Ko, Highly sensitive and stretchable multidimensional strain sensor with prestrained anisotropic metal nanowire percolation networks, 15 (2015) 5240-5247.

[83] K.H. Kim, N.S. Jang, S.H. Ha, J.H. Cho, J.M. Kim, Highly Sensitive and Stretchable Resistive Strain Sensors Based on Microstructured Metal Nanowire/Elastomer Composite Films, 14 (2018) 1704232.

[84] M.S. Kim, D. Kwon, S. Kim, K. Kim, I. Park, Surface micro-structured, stretchable strain sensor towards biaxial sensitivity and performance enhancement, in: Micro Electro Mechanical Systems (MEMS), 2017 IEEE 30th International Conference on, IEEE, 2017, pp. 1044-1047.

[85] J. Zhou, H. Yu, X. Xu, F. Han, G. Lubineau, Ultrasensitive, stretchable strain sensors based on fragmented carbon nanotube papers, 9 (2017) 4835-4842.

[86] N. Liu, G. Fang, J. Wan, H. Zhou, H. Long, X. Zhao, Electrospun PEDOT: PSS–PVA nanofiber based ultrahigh-strain sensors with controllable electrical conductivity, 21 (2011) 18962-18966.

[87] X. Liao, Q. Liao, Z. Zhang, X. Yan, Q. Liang, Q. Wang, M. Li, Y. Zhang, A Highly Stretchable ZnO@ Fiber-Based Multifunctional Nanosensor for Strain/Temperature/UV Detection, 26 (2016) 3074-3081.

[88] C. Wang, X. Li, E. Gao, M. Jian, K. Xia, Q. Wang, Z. Xu, T. Ren, Y. Zhang, Carbonized silk fabric for ultrastretchable, highly sensitive, and wearable strain sensors, 28 (2016) 6640-6648.

[89] S. Dogru, B. Aksoy, H. Bayraktar, B.E. Alaca, Poisson's ratio of PDMS thin films, 69 (2018) 375-384.

[90] Eunho Oh, Junghwan Byun, Byeongmoon Lee, Sangwoo Kim, Daesik Kim, Jaeyoung Yoon, a.Y. Hong, Modulus-Gradient Conductive Core–Shell Structures Formed by Magnetic Self-Assembling and Printing Processes for Highly Stretchable Via Applications, 3 (2017) 1600517. https://doi.org/10.1002/aelm.201600517.

[91] J. Jeong, S. Kim, J. Cho, D. Kim, Y. Hong, Stretchable Low Resistance Thick Silver Electrode on Poly (dimethylsiloxane) Compliant Elastomeric Substrate, 49 (2010) 05EB09.

[92] T. Sharma, S.-S. Je, B. Gill, J.X. Zhang, Patterning piezoelectric thin film PVDF–TrFE based pressure sensor for catheter application, 177 (2012) 87-92.

[93] Y.R. Jeong, H. Park, S.W. Jin, S.Y. Hong, S.S. Lee, J.S. Ha, Highly stretchable and sensitive strain sensors using fragmentized graphene foam, 25 (2015) 4228-4236.

[94] Y. Kervran, O. De Sagazan, S. Crand, N. Coulon, T. Mohammed-Brahim, O. Brel, Microcrystalline silicon: Strain gauge and sensor arrays on flexible substrate for the measurement of high deformations, 236 (2015) 273-280.

[95] T.-W. Kim, J.-S. Lee, Y.-C. Kim, Y.-C. Joo, B.-J. Kim, Bending Strain and Bending Fatigue Lifetime of Flexible Metal Electrodes on Polymer Substrates, 12 (2019) 2490.

[96] D. Kwon, T.-I. Lee, J. Shim, S. Ryu, M.S. Kim, S. Kim, T.-S. Kim, I. Park, Highly sensitive, flexible, and wearable pressure sensor based on a giant piezocapacitive effect of three-dimensional microporous elastomeric dielectric layer, 8 (2016) 16922-16931.

[97] J. Oh, J.C. Yang, J.-O. Kim, H. Park, S.Y. Kwon, S. Lee, J.Y. Sim, H.W. Oh, J. Kim, S. Park, Pressure insensitive strain sensor with facile solution-based process for tactile sensing applications, 12 (2018) 7546-7553.

Publication List

International Journals

1. **S. Choi**, S. Kim, H. Kim, B. Lee, T. Kim*, and Y. Hong*, “2-D Strain Sensors Implemented on Asymmetrically Bi-axially Pre-strained PDMS for Selectively Switching Stretchable Light-emitting Device Arrays” (paper submitted to *IEEE Sensors*)
2. **S. Choi**, S. Lee, B. Lee, T. Kim*, and Y. Hong*, “Selective crack formation on stretchable silver nano-particle based thin films for customized and integrated strain-sensing system” (paper submitted to *Thin Solid Films*)
3. **S. Choi**, H. Oh, S. Lee, B. Lee, T. Kim*, and Y. Hong*, “Crack-focused phenomenon on inkjet-printed silver strain sensor with high sensitivity for applications in human-machine interactions” (submission in preparation)

i. S. Kim, J. Byun, **S. Choi**, D. Kim, T. Kim, S. Chung, Y. Hong*, " Negatively Strain-Dependent Electrical Resistance of Magnetically Arranged Nickel Composites: Application to Highly Stretchable Electrodes and Stretchable Lighting Devices", Advanced Materials, 26, 3094 (2014)

ii. S. Kim, **S. Choi**, E. Oh, J. Byun, H. Kim, B. Lee, S. Lee, and Y.

Hong*, "Revisit to three-dimensional percolation theory: Accurate ana lysis for highly stretchable conductive composite materials", Scientific Reports, 6, 34632 (2016)

Oral Presentation

1. **S. Choi**, T. Kim, and Y. Hong*, “Hybrid structure of inkjet-printed Ag strain sensor for wearable device applications”, The 5th Internatio nal Conference on Advanced Electromaterials (ICAE 2019), Jeju, Kor ea, November (2019)

Poster Presentation

1. **S. Choi**, S. Kim, J. Byun, Y. Park, and Y. Hong*, "Stress-transition phenomenon in the patterned nickel composite materials for stretchabl e electronic applications," The 14th international Meetings on Informa tion Display (IMID), Daegu, Korea, August (2014)
2. **S. Choi**, S. Kim, T. Kim, B. Lee, and Y. Hong*, "2-D Strain Senso rs with Asymmetrically Pre-stretched Metal Thin Film for Multidimen sionally Stretchable Electronics", The 25th International Workshop on Active-Matrix Flat Panel Display and Devices (AM-FPD18), Kyoto, Japan, July (2018)

국문 초록

최근 개발되고 있는 전자 기기들은 대부분 이전에 비해 인간의 편의와 건강을 목표로 하고 있기 때문에 인간과 기계간의 상호작용의 효율성이 높이기 위해 플렉서블 및 스트레쳐블 분야에 대한 연구의 집중도 및 관심이 고조되어 왔다. 기기의 플렉서블 특성은 인간의 인체와 높은 호환성을 가능하게 하여 부착 및 이식과 같은 형태를 포함한 웨어러블 응용을 가능케 하며, 그렇게 개발된 웨어러블 디바이스는 근육과 관절의 움직임을 측정하거나 다양한 생체신호를 감지함으로써 질병을 예방하고 관리하는 데에 큰 도움을 줄 수 있다. 이를 위해선 고성능의 피부형태에 유사한 센서가 필요하고 이러한 연구들은 기존의 디바이스보다 인간으로 하여금 전자 장치와 보다 편리하게 상호 작용할 수 있는 기회를 제공해왔다. 또한, 이미 상용화된 스마트폰에서는 단순한 터치 센싱 방식을 떠나 고민감도 센서를 탑재하여 훨씬 효율적인 유저 인터페이스를 개발함으로써 사용자로 하여금 스마트기기를 직관적으로 조작할 수 있도록 돕고 있다. 또, 스트레쳐블 기기가 개발됨에 따라 훨씬 더 다양한 유저인터페이스 활용이 가능해 질 것이고 동시에 발생할 해상도 감소와 같은 이슈들에 대처 하기 위해서는 보다 정교하고 내구성이 확보된 센서를 개발하는 것이 중요할 것으로 생각된다. 이러한 응용에 필요한 요인들을 충족시키기 위해서 스트레쳐블 스트레인 센서는 가장 주목받는 기술들

중 하나이며, 인장도를 감지할 수 있는 다양한 메커니즘 중에서도 재료 자체의 물리적 특성차이를 이용하여 유연기판 상의 전도성 필름상에 인장에 따른 크랙을 발생시키는 기술이 대표적이다.

본 학위 논문에서는 신축성이 있는 엘라스토머 기판 상에 나노파티클 기반의 은 박막을 저렴한 비용으로 쉽게 제작할 수 있는 잉크젯 프린팅 기술로 제작함으로써, 크랙 발생 현상에 의한 스트레인 센싱 기술을 보고하고자 한다. 금속 재료가 외부 변형에 의해 쉽게 크랙을 발생시키기 때문에 외부 인장에 따른 고민감도 특성을 얻을 수 있지만, 그만큼 안정성이 열악하다는 단점을 주름 구조와 결합하여 극복하고자 한다. 2장에서는, 안정성을 보장할 수 있는 주름구조의 은 박막 위에 추가적인 은 박막을 패터닝 하여 박막 두께에 따른 크랙 발생 현상으로 고민감도 특성을 가지는 스트레인 센싱 기술을 소개하고자 한다. 또, 잉크젯 프린팅을 이용하여 대면적에서 원하는 위치에 패턴이 용이하다는 장점과 주름구조 은 박막을 스트레쳐블 전극으로 활용하여 사용자의 손의 크기에 따라 커스터마이징이 가능한 통합된 형태의 웨어러블 디바이스를 소개한다. 3장에서는, 은 박막 센서에 이방성 (asymmetric) 주름구조를 형성하여 유연기판 자체의 높은 프아송 비 (Poisson’s ratio) 때문에 발생하는 전기적 간섭현상을 최소화할 수 있는 2축 스트레인 센싱 기술을 소개한다. 또한, 특정 인장 이상에서 민감도를 가지는 센서의 특성과 2차원 스트레쳐블 발광소자 어레이를 활용하여, 스트레쳐블 디스플레이의 인장에 따른 해상도 감지를 보상하기 위한 히든픽셀 데모를 소개하고자 한다. 마지막 4장에서는 기존 은

나노파티클 박막의 인장에 따른 고민감도 특성을 더욱 증폭시키기 위해 수직 패턴을 형성하여, 딱딱한 필름에 센서를 부착하여 매우 작은 변형도 감지 할 수 있는 초 고민감도 센싱 기술을 소개한다. 센서가 부착될 필름의 물리적 특성에 따라 센서의 다양한 활용이 가능하므로, 부착 위치에 상관없이 맥박 측정이 가능한 웨어러블 디바이스와 견고한 디스플레이 스크린의 작은 휨을 감지하는 포스 터치 센싱 기술의 활용 또한 검증한다.